A SELF-STRUCTURING TWO-PORT NETWORK

By

Andrew K. G. Temme

A THESIS

Submitted to
Michigan State University
in partial fulfillment of the requirements
for the degree of

MASTER OF SCIENCE

ELECTRICAL ENGINEERING

2011

ABSTRACT

SELF-STRUCTURING TWO-PORT NETWORK

By

Andrew K. G. Temme

This work explores the capabilities of a self-structuring two-port network. Based on the idea of a self-structuring antenna, a self-structuring two-port network utilizes switches to dynamically reconfigure itself using intelligent search algorithms such as genetic algorithms (GA). This allows for the S-parameters of the self-structuring two-port network to be adjusted to match, ideally, any desired set of S-parameters. A combination of simulations and experiments were carried out to characterize such a network. It was found that the constructed prototype exhibited significant loss of power yet no one mechanism could be identified either through simulations or experiments as the most significant mechanism. Steps were taken in the experimental setup to mitigate the power loss with relatively little improvement. Given the loss of power, the capabilities of the manufactured self-structuring two-port network were investigated using both random and GA based searches. Results from the random search suggested that the lowest losses for the network are over the frequency range of approximately 750 MHz to 1.5 GHz. Random search results suggested that switch combinations exist for matching various types of loads and to create an adjustable attenuator among other applications. Through the use of a GA certain applications were investigated further. Accepting the system power loss, the network was fairly successful in matching arbitrary loads. The network was also used successfully to create an arbitrary attenuator with losses larger than normally observed in the network. Due to the high power loss observed in both simulations and in experiments, further research should be directed to creating a two-port network with lower losses. Doing so would allow for further exploration of this topic.

Soli Deo gloria.

ACKNOWLEDGMENTS

When I made my decision to come to Michigan State University for my undergraduate degree, I knew very little about the EM group. When I made my decision to stay at MSU for graduate school, I knew a great deal about the EM group. Without having attended MSU for my bachelor's degree, there is little chance that I would be attending MSU now or even studying EM at another school. The experiences that the undergraduate program offered me here have shaped my career goals and opportunities. One of the reasons why I attended Michigan State University for my undergraduate degree was the STARR Charitable Foundation Scholarship. Due to the significant impact that the STARR Charitable Foundation Scholarship has had on me and the opportunities afforded to me, I would like express my continued thanks and apprecaition to the anonymous donors. Their financial support has helped bring me to where I am today.

Completion of this thesis has required a large amount of work. I received support from many sources in order to accomplish this.

I would like to first thank my advisor Dr. Edward Rothwell. His has offered guidance and advice since I first came to MSU. As a research advisor, Dr. Rothwell has helped me develop my research abilities and skills as well as improving my technical writing. His guidance has been invaluable throughout this research.

Secondly, I would like to thank Dr. Raoul Ouedraogo for mentoring me since I first joined the Electromagnetics Research Group (EM Group) in the summer of 2008 and helped him on his master's work. He has been a source of information on all things self-structuring and genetic algorithm.

I would like to thank Dr. Rothwell and Dr. Shanker Balasubramaniam for bringing me into the EM Group and giving me an opportunity to work on both computational and experimental EM during my first summer. The EM Group has also been supportive and helpful during my time as a group member and I would like to thank them for this.

Further, I would like to thank Dr. Rothwell, Dr. Shanker, and Dr. Prem Chahal for serving on my thesis committee.

A large thanks goes out to Don VanderLaan for all of his help with LabView. Collin Meierbachtol has been kind enough to offer his LaTeX 2_ε thesis template for use by other students, upon which this thesis typesetting is based. Andrew Prey and Dr. Raoul Ouedraogo were kind enough to review this thesis and provide their comments.

Dr. Jack Ross has been kind enough to provide and help the EM Group with his software genetic algorithm software for the FEKO Suite, GA-FEKO. Your continued support of MSU is much appreciated.

I would also like to thank my family, Hanna Miller, and Kathryn Bonnen for their support (and food) during my research and especially during the writing process.

This work has been supported by a scholarship from the IEEE Antennas and Propagation Society, through a Graduate Office Fellowship, and through a National Science Foundation Graduate Research Fellowship.

Table of Contents

List of Tables viii

List of Figures xii

List of Listings xiii

1 Introduction 1

2 Background and Literature Review 3
- 2.1 Self-Structuring Antennas and Systems . . . 3
  - 2.1.1 Self-Structuring Patch Antenna . . . 5
  - 2.1.2 Automatically Tunable Cavity Resonator System . . . 7
- 2.2 Two-Port Networks . . . 7
- 2.3 Self-Structuring Two-Port Network . . . 10
- 2.4 Power Balance . . . 11

3 Simulations of a Self-Structuring Two-Port Network 14
- 3.1 Initial Investigation and Simulations . . . 14
- 3.2 Power Balance Simulations . . . 15
  - 3.2.1 FEKO Suite 6.1 Upgrade . . . 18
  - 3.2.2 List of Simulations . . . 18
  - 3.2.3 Cavity Simulations . . . 19
  - 3.2.4 Coplanar Simulations . . . 22
  - 3.2.5 Perimeter Post Simulations . . . 27
  - 3.2.6 Switched Shorting Post Simulations . . . 41
- 3.3 Conclusion . . . 41

4 Experimental Investigation 46
- 4.1 Hardware . . . 46
  - 4.1.1 Two-Port Network . . . 46
  - 4.1.2 HP 8753D Network Analyzer . . . 53
- 4.2 Selection of States . . . 54
- 4.3 LabView Software . . . 55
  - 4.3.1 Random Search . . . 56
  - 4.3.2 Standing Wave Ratio . . . 58
  - 4.3.3 Genetic Algorithm . . . 58
- 4.4 Random Search . . . 62
  - 4.4.1 Initial Investigation . . . 62
  - 4.4.2 Matching a Wideband Horn Antenna . . . 71
  - 4.4.3 Power Balance of Self-Structuring Two-Port Network . . . 74
  - 4.4.4 Mitigation techniques . . . 76

4.5 Genetic Algorithm Based Search 78
4.5.1 Optimized transmission 82
4.5.2 Spiral 82
4.5.3 Dipole Antenna Transmission 86
4.5.4 Attenuator 90
4.6 Switch Investigation 91
4.6.1 Individual Switch Properties 91
4.6.2 Switch Removal from Experiment 91

5 Conclusion **104**
5.1 Conclusion 104
5.2 Contributions 105
5.3 Topics and Suggestions for Future Study 105

Appendix **108**

HP 85052D Economy Mechanical Calibration Kit, DC to 26.5 GHz, 3.5 mm **109**

Bibliography **112**

List of Tables

4.1 Pin and port placement 50

4.2 Genetic algorithm search parameters and results. 81

List of Figures

2.1 SSA schematic 4

2.2 Shorting post, pad, and switch. For interpretation of the references to color in this and all other figures, the reader is referred to the electronic version of this thesis. 6

2.3 Automatically tunable cavity resonator. 8

2.4 Prototype self-structuring two-port network. 11

3.1 GA optimized band pass filter centered at f_0=5.005 GHz. 16

3.2 Bandpass filter tunability over 4.90–5.05 GHz 17

3.3 Free cavity report. 20

3.4 Free cavity power balance report. 21

3.5 Lossless cavity report. 23

3.6 Lossless cavity power balance report. 24

3.7 Lossy cavity report. 25

3.8 Lossy cavity power balance report. 26

3.9 no-sides-lossless-cavity report. 28

3.10 no-sides-lossless-cavity power balance report. 29

3.11 no-sides-lossy-cavity report. 30

3.12 no-sides-lossy-cavity power balance report. 31

3.13 post-cavity-lossless report. 32

3.14 post-cavity-lossless power balance report. 33

3.15 post-cavity-lossless-walls report. 34

3.16 post-cavity-lossless-walls power balance report. 35

3.17 post-cavity-lossy report. 37

3.18 post-cavity-lossy power balance report. 38

3.19 post-cavity-lossy-15 report. 39

3.20 post-cavity-lossy-15 power balance report. 40

3.21 post-cavity-lossy-walls report. 42

3.22 post-cavity-lossy-walls power balance report. 43

3.23 rings-reduced report. 44

3.24 rings-reduced power balance report. 45

4.1 Prototype self-structuring two-port network. Reprint of Figure 2.4. 47

4.2 Material parameters of the circuit board used to create the self-structuring two-port network prototype provided by Taconic. 48

4.3 Schematic view of self-structuring two-port. 49

4.4 Genetic algorithm flow chart. 60

4.5 Experimental setup for initial random search experiment. 62

4.6 Random search results, S_{11} magnitude, `5-20-21-2001-combine`. 63

4.7 Random search results, S_{11} phase, `5-20-21-2001-combine`. 64

4.8 Random search results, S_{12} magnitude, `5-20-21-2001-combine`. 65

4.9 Random search results, S_{12} phase, `5-20-21-2001-combine`. 66

4.10 Random search results, S_{21} magnitude, `5-20-21-2001-combine`. 67

4.11 Random search results, S_{21} phase, `5-20-21-2001-combine`. 68

4.12 Random search results, S_{22} magnitude, `5-20-21-2001-combine`. 69

4.13 Random search results, S_{22} phase, `5-20-21-2001-combine`. 70

4.14 Wideband horn antenna matching experimental setup. 71

4.15 Random search of possible states and original unmatched antenna performance. 72

4.16 Random search zoomed in. 73

4.17 Maximum and minimum observed power balances. 74

4.18 Average observed power balances. 75

4.19 Copper covered self-structuring two-port network. 77

4.20 Best S_{21} and S_{11}. 79

4.21 Difference between maximum transmission and minimum reflection. 80

4.22 Optimized transmission with 50 Ω loads, 750 MHz to 1.0 GHz 83

4.23 Optimized transmission with 50 Ω loads, 1.4GHz to 1.5 GHz 84

4.24 Spiral antenna used for input impedance matching experiments. 85

4.25 Experimental setup schematic for spiral antenna measurements and optimization. 86

4.26 Spiral antenna transmission optimization results at 1.4 GHz to 1.5 GHz. . . 87

4.27 Spiral antenna system transmission, 1.9 GHz to 2.2 GHz 88

4.28 Experimental setup schematic for dipole antenna measurements and optimization. 88

4.29 Dipole antenna throughput results, dataset `7-8-2010-155PM-v`. 89

4.30 20 dB attenuator optimization results. 90

4.31 Switch testing microstrip setup. 92

4.32 S-parameters of an opened relay switch. 93

4.33 S-parameters of a closed relay switch. 94

4.34 Power balance of a relay switch. 95

4.35 S-parameters for state 0x00000000. 96

4.36 S-parameters with switches unsoldered from shorting posts. 97

4.37 Power balance for switches unsoldered from shorting posts. 98

4.38 Difference in power balance for between open state and unsoldered switches. 99

4.39 Limited frequency range for the difference in power balance for between open state and unsoldered switches. 100

4.40 S-parameters with no switches connected to the two-port network. 102

4.41 Power balance with no switches connected to the two-port network. 103

Listings

4.1 Sample configuration file, `5-26-2009-1152AM-v-config.txt`. 58

Chapter 1

Introduction

This thesis presents a self-structuring two-port network that is capable of being adjusted to perform as various two-port devices including matching networks, filters, and attenuators. Such a network is based upon the principles of a self-structuring antenna.

The primary goal of this thesis is to explore the capabilities of a self-structuring two-port network. This thesis chronicles the work carried out by the author while exploring and experimenting with a manufactured self-structuring two-port network. The research was carried out with radio frequency (RF) applications in mind but applications certainly go beyond just transmitters and antennas. Perhaps the application furthest from RF is for power factor correction in power distribution systems. Within the realm of RF applications, this work has implications in numerous areas. Currently there is a very strong interest in reconfigurable filters, especially using microelectromechanical systems (MEMS) technology. A MEMS implementation of a self-structuring two-port network is desirable due to the demand for small, multi-frequency radio systems in cellphones and other devices. Section 2.2 further discusses the current state of research in the MEMS field further. Besides a MEMS implementation, a self-structuring two-port network is desirable in situations when an RF system is working under changing conditions. The ability to adjust to these changes without a technician present is very advantageous. The author's work in this thesis serves as a

investigation into the operation and capabilities of a self-structuring two-port network while lying the foundation for others to implement application specific designs.

Chapter 2 of this thesis presents a more thorough examination of self-structuring antennas and their influence on this work followed by a discussion of two-port devices and a brief look at reconfigurable two-port devices. Finally, the self-structuring two-port network is presented for the reader.

Chapter 3 contains results from simulations of the network. Prior work performed by a visiting scholar who first investigated the network is discussed, followed by results from further simulations. Much of the work done in the new simulations focuses on system losses.

Experimental results are presented and discussed in Chapter 4. First the prototype unit is fully presented, followed by results from a random search of possible states. Next, results from genetic algorithm based searches are presented. The chapter concludes with experiments investigating system losses.

A conclusion and topics for future work are presented in Chapter 5.

An appendix is provided that describes how calibration kits may be downloaded to the HP 8753D network analyzer and how new kits may be defined.

Throughout this thesis, certain types of figures are used repeatedly. One such figure is a plot of S parameters. A two-port network has four S parameters: $S_{11}, S_{21}, S_{12}, S_{22}$. Because of their physical meaning, these are often paired as S_{11} and S_{22}, and S_{12} and S_{21}. S_{xx} parameters describe how the complex voltage reflected back at a port while S_{xy} parameters describe how the complex voltage transmitted from port y to port x. S parameters are most often plotted following these pairings in dB and degrees. Finally, simulations results typically include a plot of efficiency versus frequency. Efficiency in this case is defined based on power radiated over power delivered to the antenna. In this case, the antenna is the two-port network.

Chapter 2

Background and Literature Review

2.1 Self-Structuring Antennas and Systems

A self-structuring antenna (SSA) is a type of antenna that is able to adapt to changes in the environment as well as to change performance characteristics such as radiation pattern or input impedance. An SSA is made up of wire segments or patches (collectively known as an antenna template) with numerous switches placed in between the segments, a sensor, and a controller with a search algorithm [1, 2]. Figure 2.1 shows a typical self-structuring antenna.

Switches are used to electrically connect or disconnect pieces of the antenna template, thereby changing properties of the antenna. In the context of an SSA, a state is defined as a particular permutation of opened and closed switches.

Self-structuring antennas have been investigated in numerous conference papers, journal articles, and theses [1–16]. A thorough review of SSAs as an antenna class and an exploration of possible search techniques are presented in [4, 6] (a review of the somewhat related topic of frequency-reconfigurable antennas is presented in [17]). Topics of particular interest to this thesis are self-structuring patch antennas [11] and automatically tunable cavity resonator systems [15].

Figure 2.1: Schematic diagram of a self-structuring antenna.

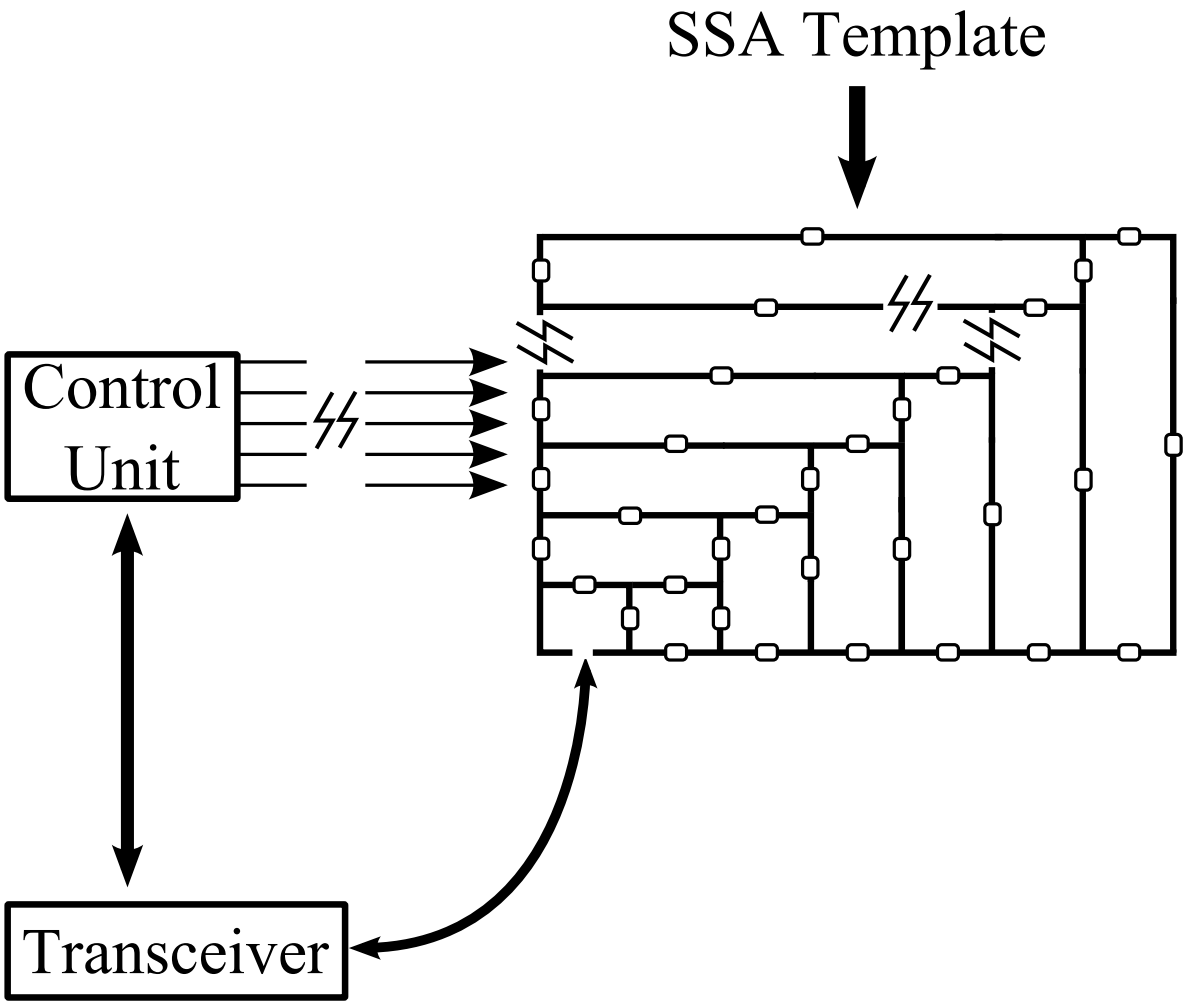

2.1.1 Self-Structuring Patch Antenna

It has been shown in previous research that shorting posts may be used to adjust the operating frequency of a patch antenna [18–21], allow multi-frequency operation [20, 22, 23], adjust the input impedance [23] and/or reduce the size of the patch [20, 24–28]. Authors utilize various approaches to the analysis of these effects. Cavity model theory was one of the first techniques used [22], followed by an extension of nonuniform transmission line theory [19]. Finally analytic methods were dropped due to complexity while computational methods increased in popularity [24, 29]. Effectively the shorting posts are used to adjust the fields in the substrate between the patch and the ground plane. Multiple posts allow more degrees of freedom in how the fields are effected and thereby more degrees of freedom to control the behavior of the antenna [25].

A self-structuring patch antenna is presented in [10, 11]. This patch uses an array of switch-controlled shorting posts to control the performance and characteristics of the patch antenna. All posts are permanently connected to the surface of the patch. When a switch is opened, the shorting post is not connected to the ground plane. When a switch is closed, the shorting post is connected to the ground plane through the switch, effectively behaving like a shorting post used in other research [18–28] to allow, for example, adjustment of the operating frequency or multi-frequency operation.

Figure 4.4 in [11] shows the shorting pin soldered to a disk pad isolated from the ground plane by an annular slot. Figure 2.2 shows a similar setup used in the self-structuring two-port network with the addition of a perimeter shorting post.

As in other patches that utilize shorting posts, the cavity fields are perturbed by the posts, especially when the posts are connected to the ground plane. Unlike most other patches [18–31], the SSA patch has a large number of shorting posts, 32 posts in [14]. Typically other patches have shorting posts that are placed after careful analysis and design in order to effect the fields in a certain manner; see [21]. The SSA patch in [14] has a large number of posts which results in an extremely large number of switch states, i.e. 2^{32} states. This makes

Figure 2.2: Photograph of shorting pin soldered to a disk pad isolated from the ground plane by an annular slot. The switch, control wires and a perimeter shorting post are also seen. For interpretation of the references to color in this and all other figures, the reader is referred to the electronic version of this thesis.

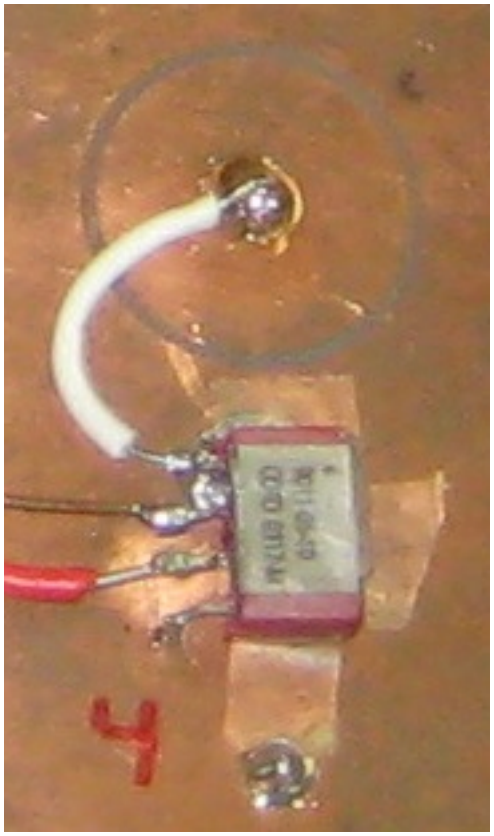

analysis impractical, so posts are placed based on patterns, symmetry (or antisymmetry), experience, and a limited analysis of certain states.

2.1.2 Automatically Tunable Cavity Resonator System

The extent to which a cavity may be tuned using SSA principles was investigated in [15]. In this paper twenty-six "L" shaped wires with segments of various lengths and orientations were placed inside of a cavity extending away from one wall. These were then connected to the cavity wall through switches. Figure 1 of [15] shows a schematic drawing of the automatically tunable cavity resonator system and Figure 2.3 shows the prototype resonator placed inside of an anechoic chamber for testing. It was shown that it is possible to change the resonant frequency of the cavity by selecting different states without changing the physical dimensions of the cavity or by using other existing tuning methods. It was also shown that the cavity could be retuned to the original resonant frequency if the cavity fields were perturbed by an object that was placed into the cavity.

The combination of the SSA patch and tunable cavity resonator concepts points towards the idea of creating a general self-structuring two-port network using on a copper clad substrate.

2.2 Two-Port Networks

Typical two-port devices include matching networks, filters, attenuators, and phase shifters. There has been extensive research done on making these devices reconfigurable. One of the main driving forces behind this research has been the need for mobile devices to operate at multiple frequencies. Early two-port devices used varactors and potentiometers [32], whereas recently microelectromechanical systems (MEMS) have been heavily used [33–40]. Two commonly researched devices are the matching network and the filter.

Matching networks are used to transfer the maximum power possible when an impedance

Figure 2.3: Automatically tunable cavity resonator system placed inside of an anechoic chamber for testing.

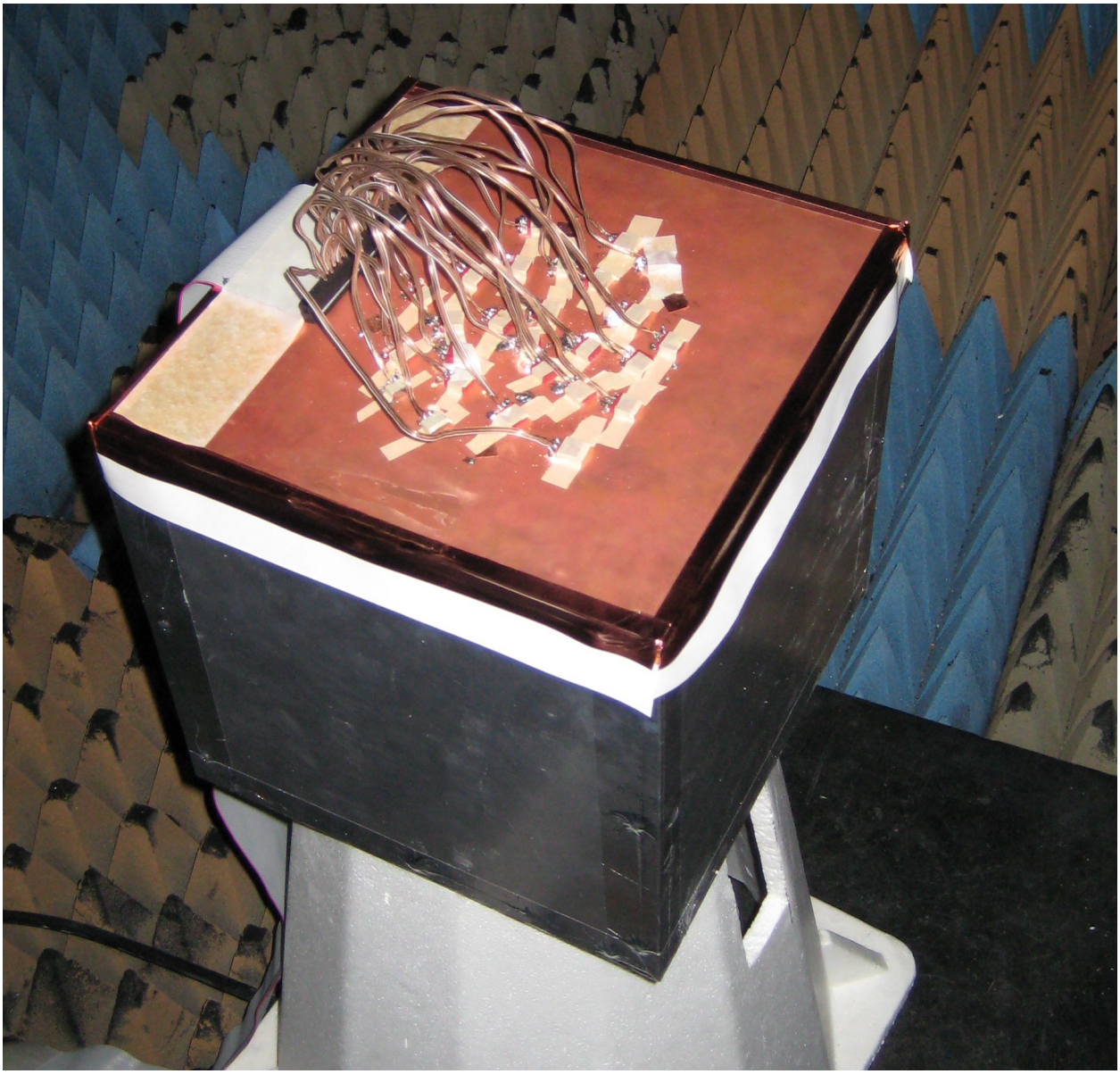

mismatch exists. Maximum power is transferred when a port presents an impedance that is the complex conjugate of the load attached to said port.

A matching network may take various forms. When impedances are known, resistors, capacitors, and inductors may be used provided that the frequency is within the operating range of these devices. Another option is to use transmission lines to transform an impedance or to use tuning stubs attached to another transmission line. Both discrete components and transmission lines have been implemented in adjustable value configurations, e.g. varactors and sliding loads. This allows for tunable matching networks to be created [34–38, 41–43]. These are commonly found in applications where loads are often changed or effected by outside factors, or when the input impedance of an antenna varies significantly across an operating band.

Currently most MEMS based matching networks use MEMS switches to place tuning stubs or capacitors in shunt with a transmission structure, usually a coplanar waveguide or slow wave structure [33–39, 41–47]. Some devices use other MEMS elements such as varactors.

Filters are typically adjusted in a similar manner as above when used at the microstrip or smaller scale. Various valued components are switched into and out of the circuit to achieve the desired results [32, 40, 48–56]. Often the type of filter (low-pass, high-pass, or band-pass) is not able to be changed; instead, the center frequency, bandwidth, and shape of the filter are the adjustable parameters. Recent work is beginning to make switching between types of filters possible without discretely building each type of filter [54–56].

Before MEMS came into widespread use, a common approach was to use a dual-mode microstrip filter [48]. A band-pass filter is demonstrated in [48] that utilizes the degenerate modes found in a dual-mode microstrip to tune the filter. Figure 1 of [48] shows the layout of the filter. This filter uses a meandered loop with equivalent sides to form a resonator. The key to the filter is the small square of metal added to the top-right, inside corner of the resonator as shown in the figure. By adjusting the size of the added metal, i.e. adjusting d,

the amount of coupling between degenerate modes may be varied. This leads to variations in mode splitting which creates the band-pass filter. The filter presented in [48] makes use of modal interaction which may play a role in the operation of self-structuring patch antennas and self-structuring two-port networks. A downside to this filter, however, is that it is not reconfigurable.

The work presented in [56] allows for one structure to be reconfigured and tuned as either a bandstop or band-pass filter. The circuit in [56] makes use of mutual coupling between two cavities and the impedance transformation properties of transmission lines. By asymmetrically tuning the cavities, the coupling can effectively be changed to switch the filter from a bandstop to band-pass filter and vice-versa. Tuning of a cavity is achieved by mechanically deforming the cavity using a piezoelectric actuator. An exploded view of the filter is shown in Figure 7 of [56]. This paper along with [53] are two of the few papers to utilize cavity perturbation to affect the response of a filter at this scale or smaller. Cavity perturbation is used in a self-structuring two-port network to effect transmission characteristics. A self-structuring two-port network is advantageous over the filters presented in [53, 56] as the network could be switched to other devices as needed whereas the filters in [53, 56] will always be filters.

2.3 Self-Structuring Two-Port Network

A self-structuring two-port network is based on an extension of SSA principles. The goal is to use the reconfigurable nature of this two-port to create various types of two-port devices.

Using a design similar to an SSA patch antenna, the two-port adds a second port to the patch structure and permanently connected shorting posts around the perimeter . Using thirty-two switched controlled posts, there are 2^{32} or 4,294,967,296 possible states.

2.4 shows a prototype self-structuring two-port network. On the right is port one, on the left is port two, and at the top is the ribbon cable used to control the switches. Switch control

Figure 2.4: Prototype self-structuring two-port network.

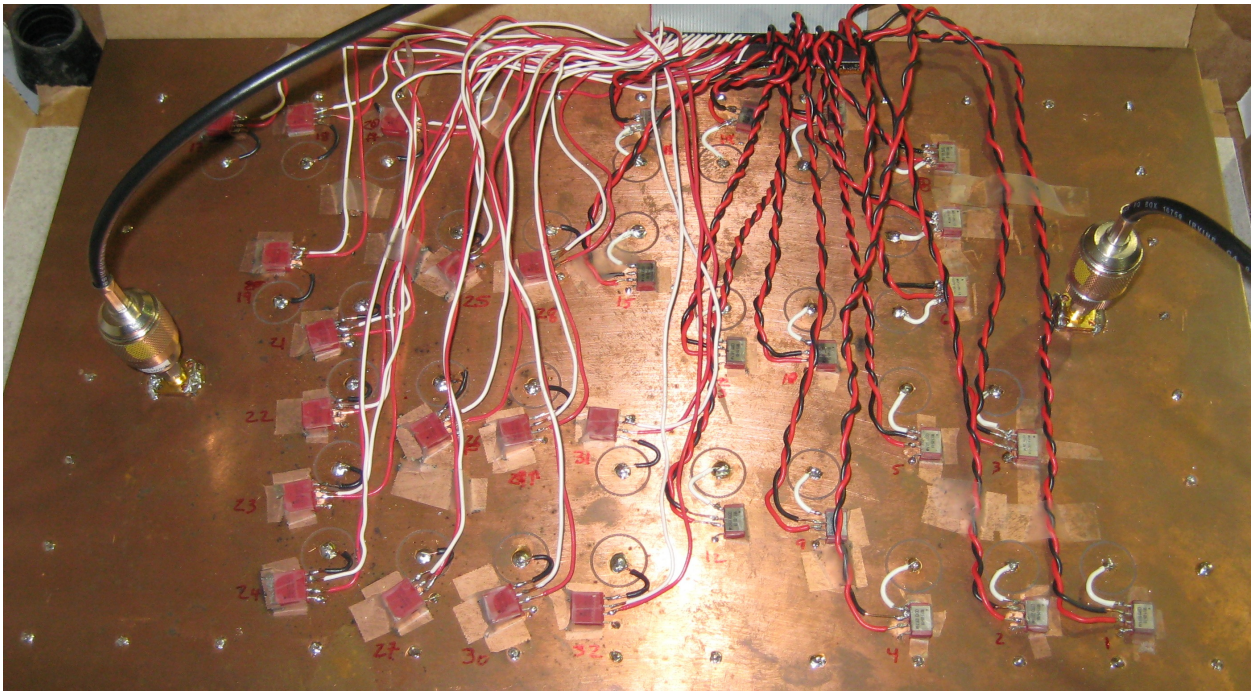

and shorting post operation is the same as in the self-structuring patch antenna prototype. The switches can be seen laid out on the top of the network with control cables running to the middle two pins of each switch. One side of the switch is connected to the top surface of the network while the other side of the switch connects to a shorting post. The shorting post is soldered to a piece of the top surface which has a ring of copper removed from around it. Finally, perimeter shorting posts can be seen along the perimeter of the network. These are used to keep power from radiating out of the sides, thereby acting like an antenna.

2.4 Power Balance

When a matching network presents a matched load at all ports, the maximum power will be transferred to or from the matching network. What is not taken into account in this description is how much power is lost in the network, known as the insertion loss of the network. It is possible that given a matching network that is too lossy, less power would be

delivered to the load than when no matching network is used. In order to determine how much power is being lost in a matching network, the power balance of the network should be examined. Power balance is a way to express the percentage of input power lost by the network.

Networks may be active, lossless or lossy with regard to power balance. Insertion loss quantifies the difference between power received at the load and the source power. It is expressed as a positive number when power is absorbed.

Take a_n and b_n as the amplitudes of the waves entering and exiting port n of a microwave network, respectively. The average power entering a port is given by $P_i = \frac{1}{2}a_n a_n^*$ and the average power leaving a port is given by $P_o = \frac{1}{2}b_n b_n^*$. If power is applied to port 1, then the average source power is the sum of power entering and leaving, i.e. reflected from, port 1. Regarded input power as positive, then the power leaving port 1 is a negative quantity. The average source power is then given by

$$P_{src} = \frac{1}{2}(a_1 a_1^* - b_1 b_1^*). \tag{2.1}$$

According to the conservation of energy, power entering a system must equal the sum of power lost in and power leaving the system,

$$P_{src} = P_{out} + P_{lost}. \tag{2.2}$$

For a two-port network with power applied to port 1, $P_{out} = \frac{1}{2}b_2 b_2^*$. Substituting this expression into Equation 2.2 and dividing by $P_{in} = \frac{1}{2}a_1 a_1^*$ gives

$$\frac{\frac{1}{2}(a_1 a_1^* - b_1 b_1^*)}{\frac{1}{2}a_1 a_1^*} = \frac{\frac{1}{2}b_2 b_2^*}{\frac{1}{2}a_1 a_1^*} + \frac{P_{lost}}{P_{in}}. \tag{2.3}$$

S-parameters are defined as

$$S_{mn} = \left.\frac{b_m}{a_n}\right|_{a_k=0,\ k\neq n} \tag{2.4}$$

where m and n may be equal. Equation 2.3 can therefore be written as

$$1 - S_{11}S_{11}^* = S_{21}S_{21}^* + \frac{P_{lost}}{P_{in}}. \tag{2.5}$$

Equation 2.5 is called the power balance equation and is generally given as an inequality [57]

$$1 - S_{11}S_{11}^* \geq S_{21}S_{21}^*. \tag{2.6}$$

If a system is lossless, then

$$\mathrm{S_{21}S_{21}^* + S_{11}S_{11}^* = 1}. \tag{2.7}$$

An active network, such as an amplifier, may appear to be lossless or have gain, i.e. the inequality in (2.6) may be switched to a less than or equal to sign. This is due to an external power source that is not typically included in the power balance equation.

In this work the term power balance is used to describe the term $-P_{lost}/P_{in}$ in the equation $-P_{lost}/P_{in} = S_{11}S_{11}^* + S_{21}S_{21}^* - 1$. In some cases, it may be expressed as a percentage given by $-(-P_{lost}/P_{in}) \times 100\%$. Throughout this thesis, power balance is calculated as $|\mathrm{S_{11}}|^2 + |\mathrm{S_{21}}|^2 - 1$ or equivalently $\mathrm{S_{11}S_{11}^* + S_{21}S_{21}^* - 1}$. The exact definition used is typically included in the label of the ordinate axis. Using this definition, a net power loss results in a value between minus one and zero while a net power gain results in a value greater than zero.

Chapter 3

Simulations of a Self-Structuring Two-Port Network

In 2007, Chien-Hsien (Jay) Lee was a visiting scholar from National Taiwan University in the Electromagnetics Research Group at Michigan State University (MSU). As his research project, Lee began studying the self-structuring two-port network. He designed a circuit based on Lynn Greetis' self-structuring patch antenna [10, 11] and conducted simulations in order to find suitable post placements and evaluate the performance of the network as a filter. Acceptable results from simulations led to the construction of a prototype unit. Experimental results showed high system losses, hence further simulations were undertaken by the author to evaluate the performance of the prototype.

3.1 Initial Investigation and Simulations

Simulations of the two-port network were carried out using FEKO Suite 5.2, a commercial method of moments EM solver provided by EM Software and Systems [58]. The genetic algorithm (GA) optimizer GA-FEKO [59] was used to optimization switch states.

A design similar to a patch SSA was first simulated. In order to keep the network from radiating, shorting posts were placed around the perimeter of the network. These posts

essentially create the side walls of a cavity. Lee then investigated appropriate board size and thickness, various methods of feeding the network, and the placement of the switch-controlled shorting posts. An infinite ground plane was used so that the half-space Green's function could be used thereby reducing computational complexity. This made the use of a genetic algorithm for optimization practical.

A major goal of Lee's research was to learn how the frequency response of the network could be adjusted or tuned. This mainly took the form of searching for various types of filter responses. Searches were performed using either random searches or genetic algorithm based searches. Figure 3.1 shows the response of the circuit configured as a band pass filter, found using a GA, centered at f_0=5.005 GHz. This center frequency may be moved or tuned across a range of frequencies by changing the switch state, as demonstrated by Figure 3.2, over the band 4.90 GHz to 5.05 GHz.

3.2 Power Balance Simulations

As discussed in Section 2.4, the experimental setup exhibited an unexpectantly high power loss, even after various mitigation techniques were applied. A new series of simulations was carried out in an attempt to better understand the loss mechanisms involved in this project. These simulations were run in a newer version of the FEKO Suite than previously empoyed and used a finite ground plane. As the objective was to investigate power losses in the experimental system, the physical and material properties from the constructed self-structuring two-port were used, see Section 4.1.1 for specific values. The increased computational complexity of this model was acceptable because optimization was unnecessary. While short solution times were not required, extremely long solution times were undesired as well. As such, the medium density mesh included in CAD FEKO was used.

Figure 3.1: GA optimized band pass filter centered at f_0=5.005 GHz.

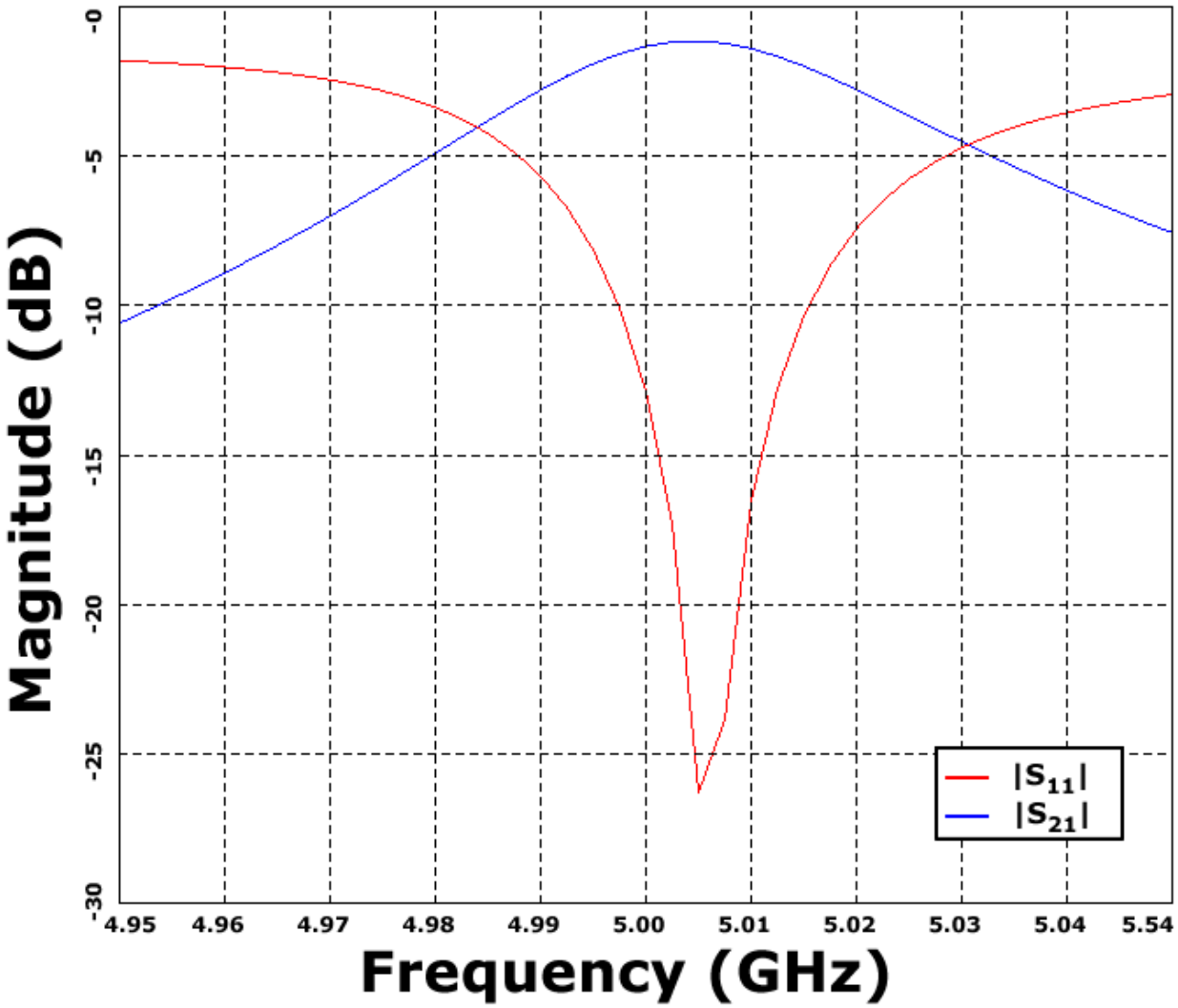

Figure 3.2: Demonstration of the ability to tune the center frequency of a bandpass filter over the frequency range of 4.90 GHz to 5.05 GHz.

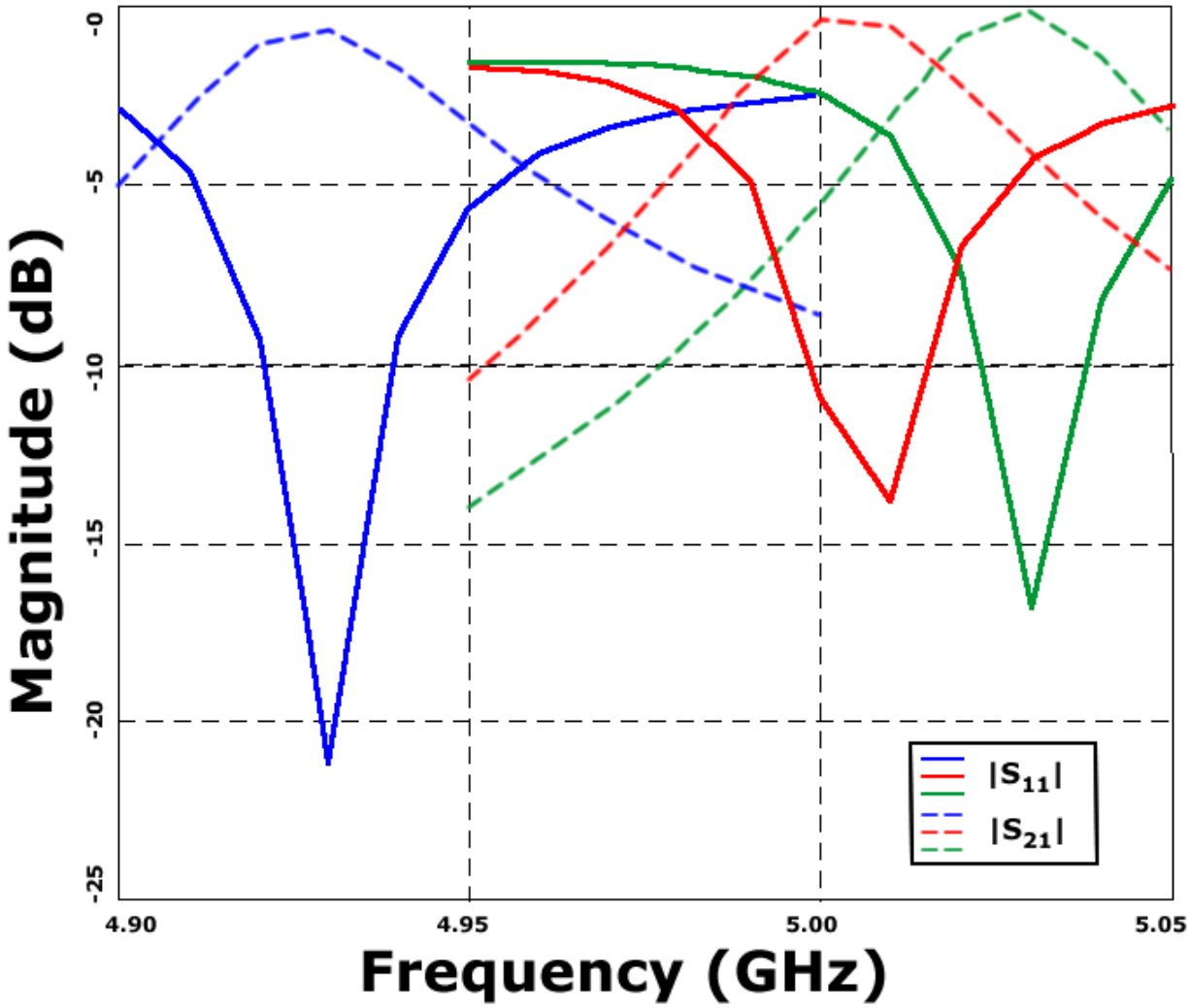

3.2.1 FEKO Suite 6.1 Upgrade

Previous simulations were carried out in FEKO Suite 5.2. While learning FEKO, the author noticed that when simulating cavities and patch antennas, antenna efficiency was larger than one hundred percent. This was observed in multiple simulations including the patch antenna example included with FEKO Suite 5.2. This example, when run in FEKO Suite 6.1, provided acceptable results. It is suspected that something in the configuration of the solver used in version 5.2 was changed since the time that Lee ran the GA optimization simulations.

The author visited the EM Software and Systems booth at the 2011 IEEE APS/URSI conference in Spokane, WA. After discussing this problem with them, FEKO Suite 6.1 and a trial license were obtained. Besides changes in the computational engine, other changes included a redesign of CAD FEKO, the GUI based model input program. This allowed for the creation of models and simulations without the direct editing of a card file. It should be noted that card files may still be used in the new version.

3.2.2 List of Simulations

Below is a brief description of the simulations run to investigate power losses in the experimental setup. All simulations were calculated at twenty-six frequencies between 700 MHz and 1.5 GHz (32 MHz step) except in `post-cavity-lossy-15` as noted. TLY5 is the name of the Taconic circuit board used to construct the experimental network, see Section 4.1.1.

- `free-cavity` - PEC cavity with a free space interior
- `lossless-cavity` - PEC cavity with a lossless TLY5 interior
- `lossy-cavity` - Copper cavity with a lossy TLY5 interior
- `no-sides-lossless-cavity` - PEC top and bottom with a lossless TLY5 dielectric
- `no-sides-lossy-cavity` - Copper top and bottom with a lossy TLY5 dielectric

- `post-cavity-lossless` - PEC top and bottom with a lossless TLY5 dielectric and perimeter shorting posts
- `post-cavity-lossless-walls` - PEC cavity with a lossless TLY5 interior and perimeter shorting posts
- `post-cavity-lossy` - Copper top and bottom with a lossy TLY5 dielectric and perimeter shorting posts
- `post-cavity-lossy-15` - Copper top and bottom with a lossy TLY5 dielectric and perimeter shorting posts at thirteen frequency points between 1.5 GHz and 1.884 GHz (32 MHz steps)
- `post-cavity-lossy-walls` - Copper cavity with a lossy TLY5 dielectric and perimeter shorting posts
- `rings-reduced` - Copper cavity with a lossy TLY5 dielectric, perimeter shorting posts, and sixteen switched shorting posts

3.2.3 Cavity Simulations

Three cavities were simulated to investigate the properties of a cavity having the same dimensions (42 x 27 x 0.5 cm) as the self-structuring two port network. All cavities had two ports placed in the same locations as on the constructed two port network. The first cavity simulated, `free-cavity`, consists of PEC walls and a free space interior. Results from this simulation are shown in Figures 3.3 and 3.4. One can see that the cavity demonstrates reciprocity as do all simulations. Seen in the plots for efficiency and power balance are non-realistic values (negative efficiencies and net power gain). These values, or errors, are on the order of hundredths of a percent. These errors are most likely numerical artifacts because of the relatively small active power. Even with these errors, it is easy to see that power is maintained in the system as expected.

Figure 3.3: Free cavity report.

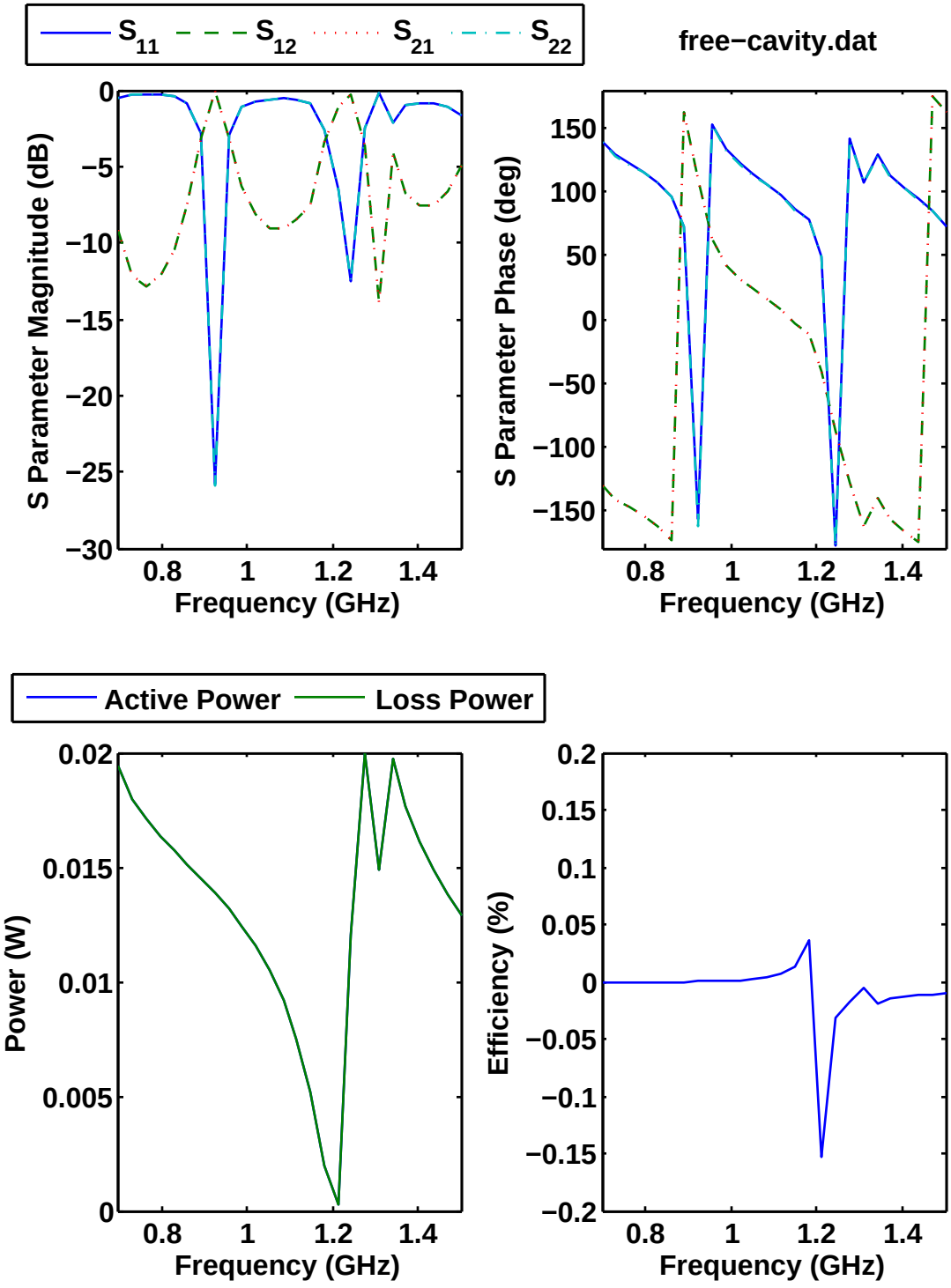

Figure 3.4: Free cavity power balance report.

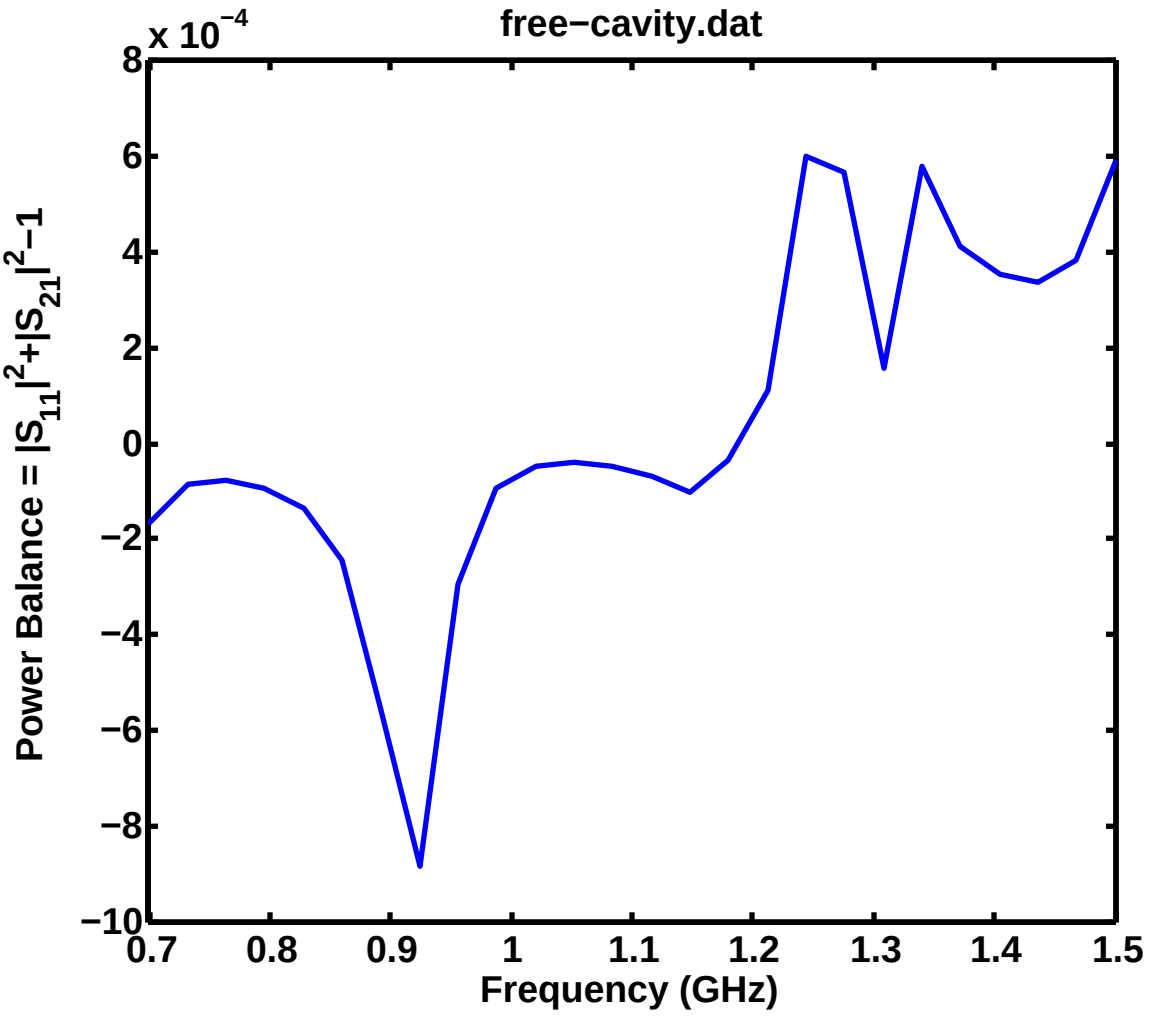

The second cavity, `lossless-cavity`, had PEC walls and a lossless TLY5 interior dielectric with a relative permittivity of $\epsilon_r = 2.2$. Results from this simulation are shown in Figures 3.5 and 3.6. The graph of antenna efficiency shows that no power is lost due to radiation. Figure 3.6 shows that no power is lost. Again though, there are errors in the calculations as the power balance is larger than 0, representing a net power gain.

The third cavity, `lossy-cavity`, was designed to have system losses. It consisted of 17.78 μm thick, i.e. 1/2 oz, Copper walls on all six sides and a lossy TLY5 interior dielectric with a relative permittivity of $\epsilon_r = 2.2$ and a loss tangent of $\delta = 0.0010$. Results from this simulation are shown in Figures 3.7 and 3.8. Here one is able to see that the simulations exhibit no unrealistic values. This improvement can most likely be attributed to the added loss. A technique used early on in computational electromagnetics was to add small amounts of loss in order to account for slight divergences in the solution. It is possible that the two previous simulations were causing problems for the FEKO solver, for which the loss helped in this case. This is plausible because the FEKO solver in FEKO Suite 5.2 had significant error for the same and simpler cavity simulations. Very little power was lost in this simulation due to radiation; however, at some frequencies up to twenty-five percent of the power was lost. While it is expected that some power would be lost, this amount is more than expected. Examination of the output files revealed that most of the power was lost in the dielectric and metal, but a primary loss mechanism was not pinpointed.

3.2.4 Coplanar Simulations

In order to show how much power is lost through the sidewalls, the sidewalls were removed from the cavities. This is important to evaluate in order to determine the effectiveness of the perimeter shorting posts.

Only two simulations with TLY5 dielectric were used for this new set of simulations and for the remaining simulations. The two TLY5 dielectric models from the previous section were modified for use in these simulations. As mentioned above, the four side walls of each

Figure 3.5: Lossless cavity report.

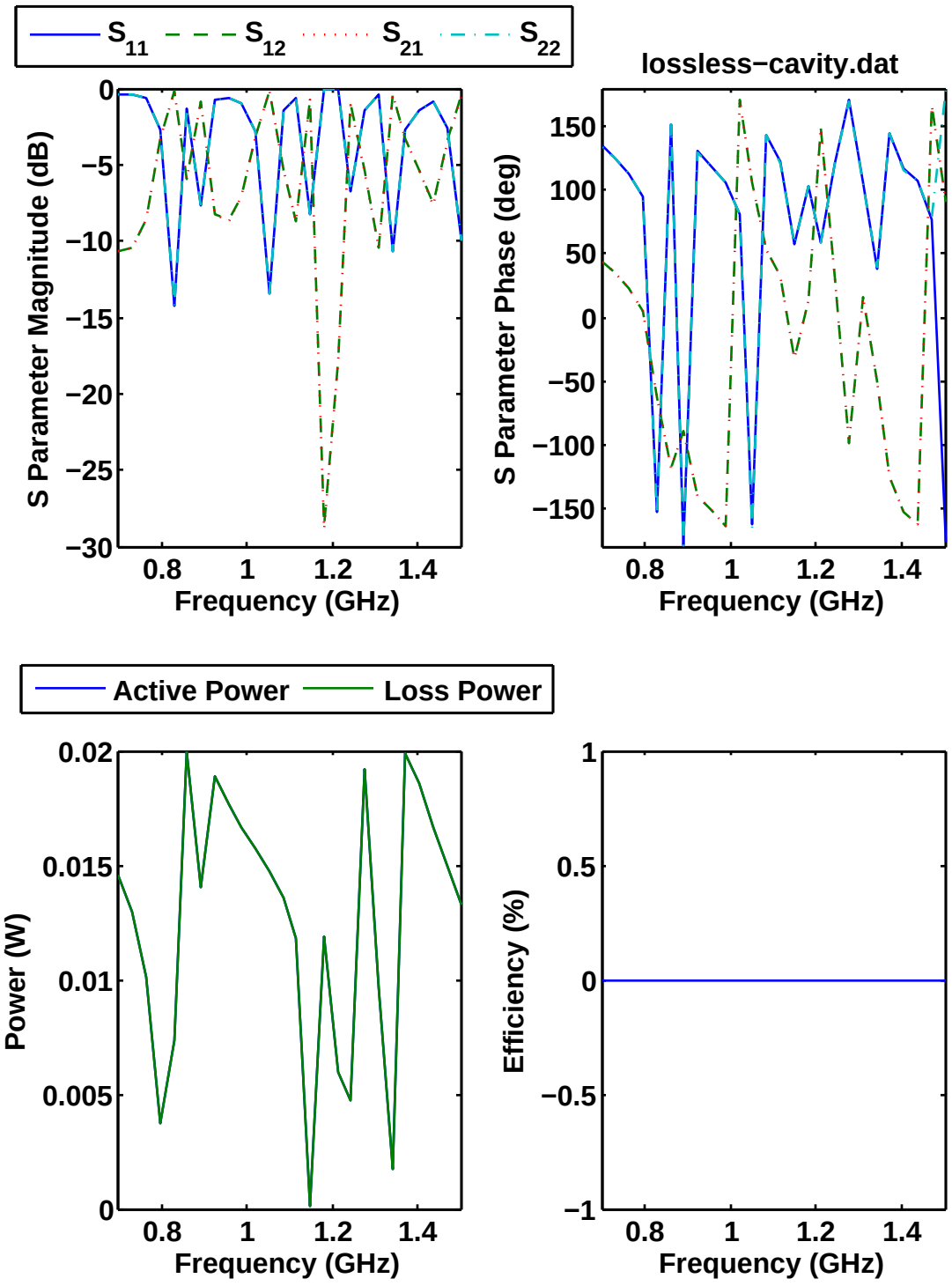

Figure 3.6: Lossless cavity power balance report.

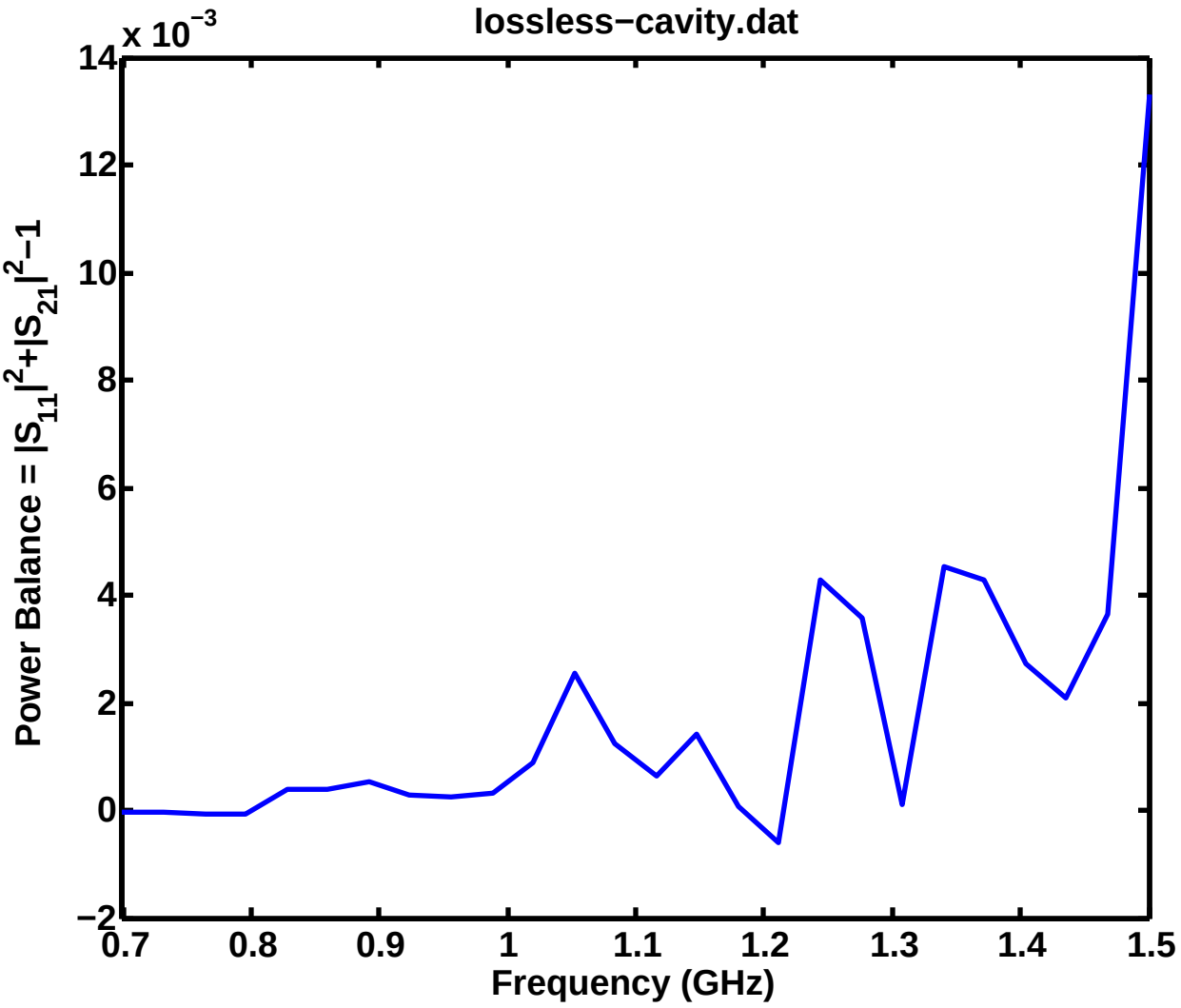

Figure 3.7: Lossy cavity report.

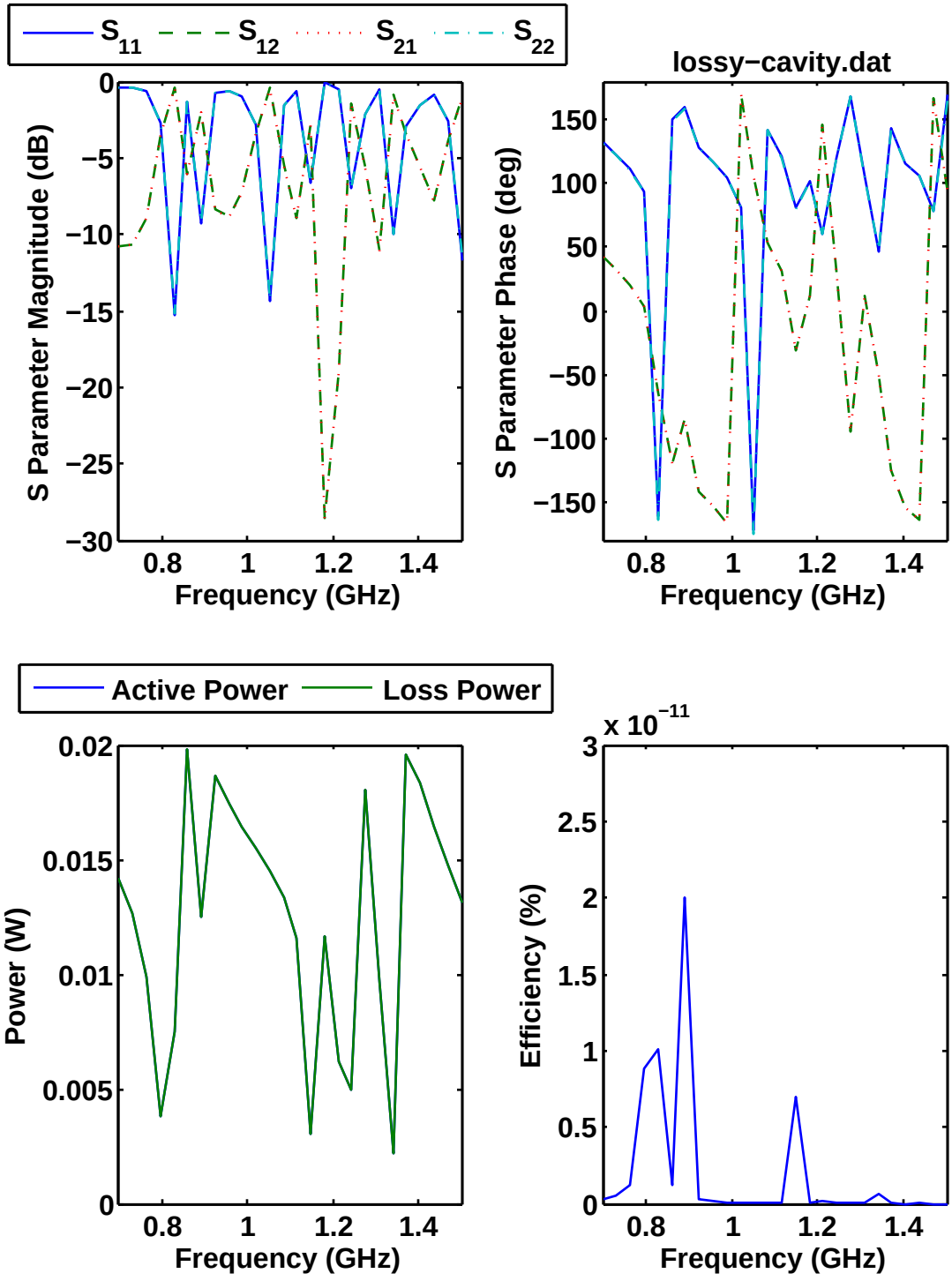

Figure 3.8: Lossy cavity power balance report.

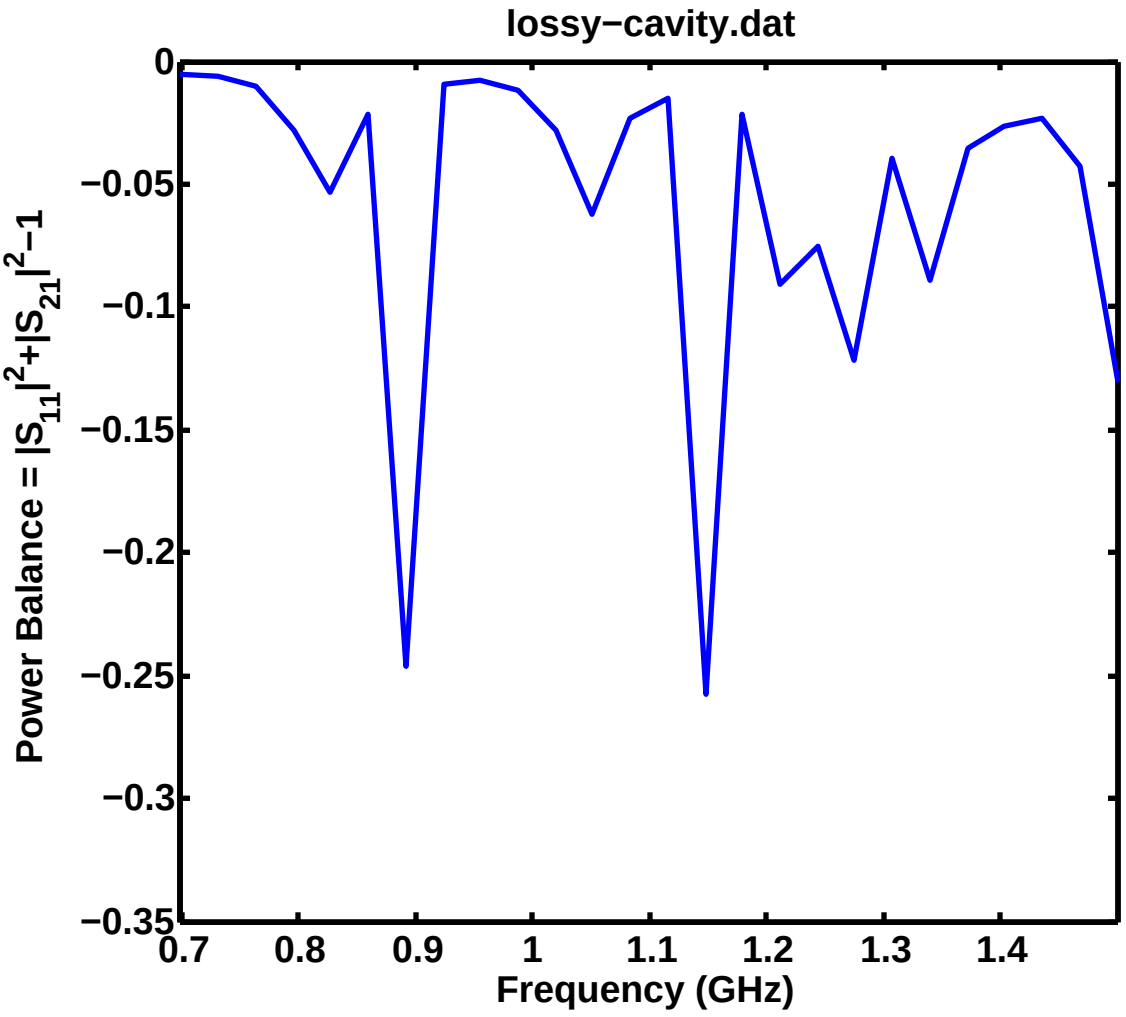

cavity were removed to create a coplanar structure. All other parameters and geometries remained unchanged.

Figures 3.9 and 3.10 show the results for the lossless dielectric simulation, `no-sides-lossless-cavity`. Unlike the results presented in the last section, the active and loss power are noticeably different. Looking at the plot of efficiency shows that at four frequencies, over twenty percent of the delivered power is radiated, and at one of those four frequencies, over sixty-five percent is radiated. Figure 3.10 shows that at almost all frequencies, over ten percent of the power is lost.

The results from the lossy simulation, `no-sides-lossy-cavity`, are shown in Figure 3.11 and 3.12. While the results vary from the lossless case, the behavior is similar. As the power loss is similar in both simulations, one can see that without walls, the primary loss mechanism is radiation. This same observation was made by Lee and resulted in the two port network having perimeter shorting posts.

3.2.5 Perimeter Post Simulations

The thirty-eight perimeter shorting posts were added to the lossless and lossy TLY5 cavity and coplanar simulations. In addition, the lossy TLY coplanar simulation was run at frequencies above 1.5 GHz. Together, these simulations demonstrated the effectiveness of the shorting posts and point towards loss mechanisms other than radiation.

Figures 3.13 and 3.14 show the results from a lossless TLY5 coplanar simulation with perimeter shorting posts, `post-cavity-lossless`. It is easily seen that power is lost due to radiation and other loss mechanisms. Figures 3.15 and 3.16 show the results from a lossless TLY5 cavity simulation with perimeter shorting posts. In this simulation, one sees behavior similar to that of the `lossless-cavity` simulation. There is essentially no radiated power while the overall power balance is almost zero. Here, errors in the numerical solver cause power generation.

Figures 3.17 through 3.20 show the results from a lossy TLY5 coplanar simulation with

Figure 3.9: no-sides-lossless-cavity report.

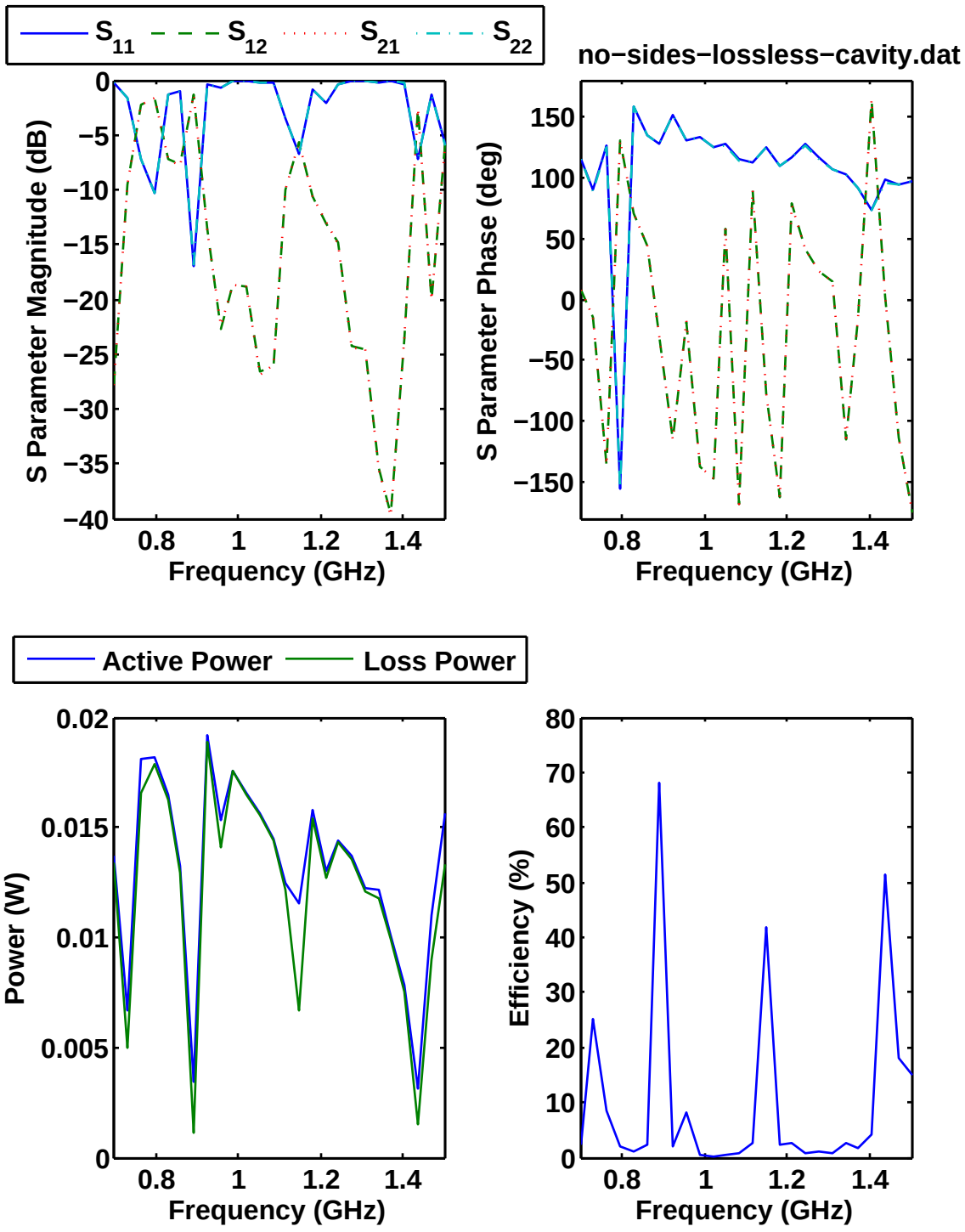

Figure 3.10: no-sides-lossless-cavity power balance report.

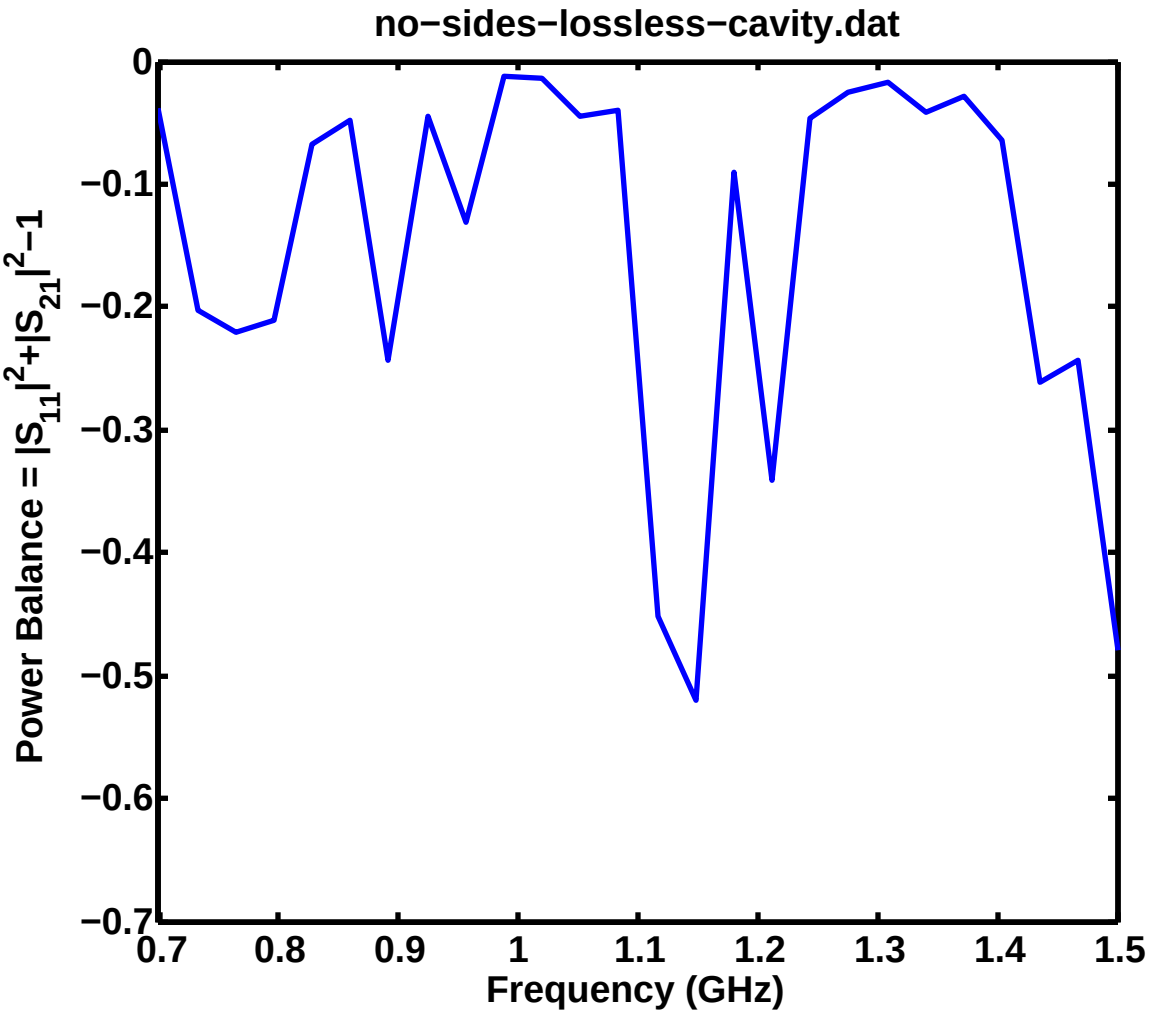

Figure 3.11: no-sides-lossy-cavity report.

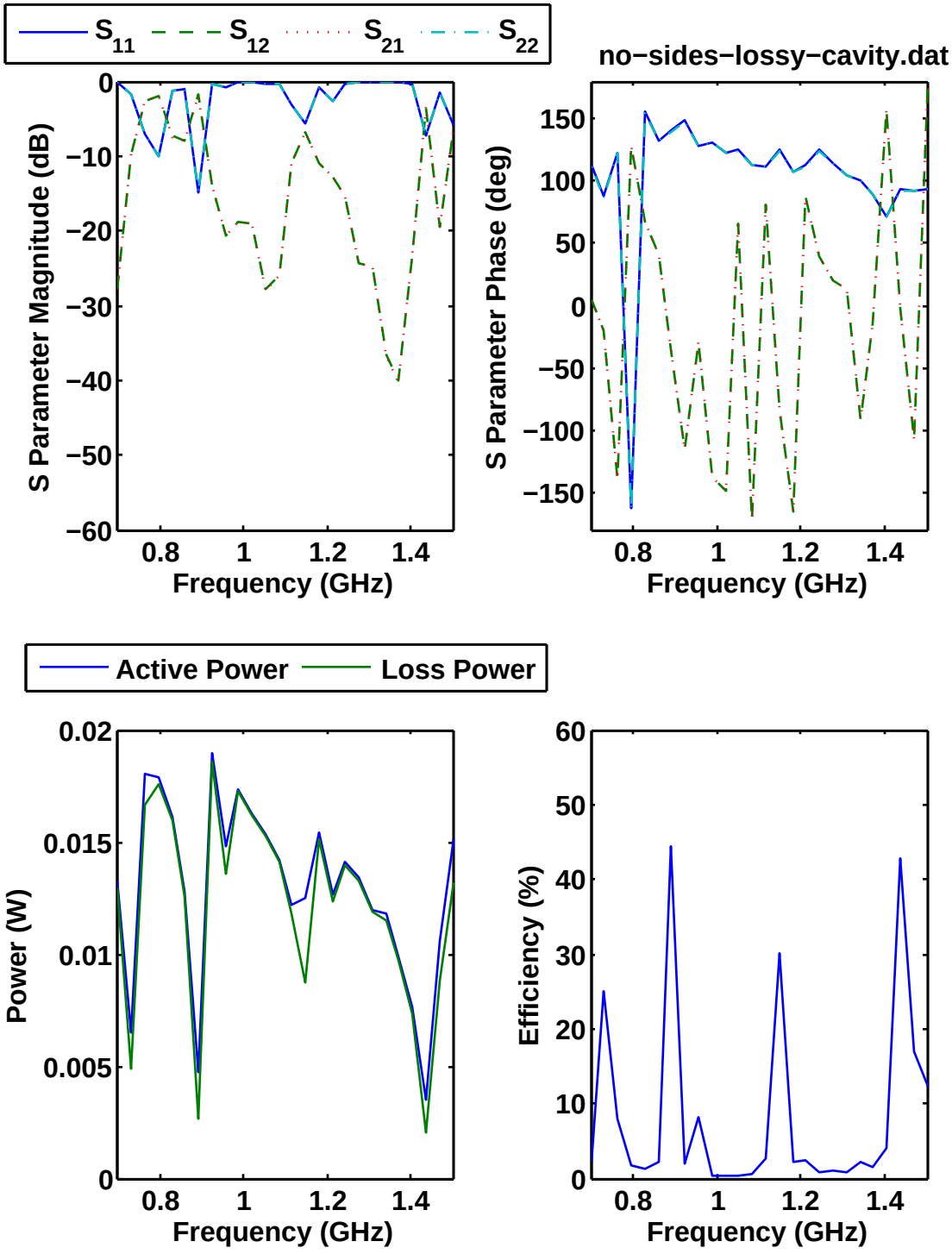

Figure 3.12: no-sides-lossy-cavity power balance report.

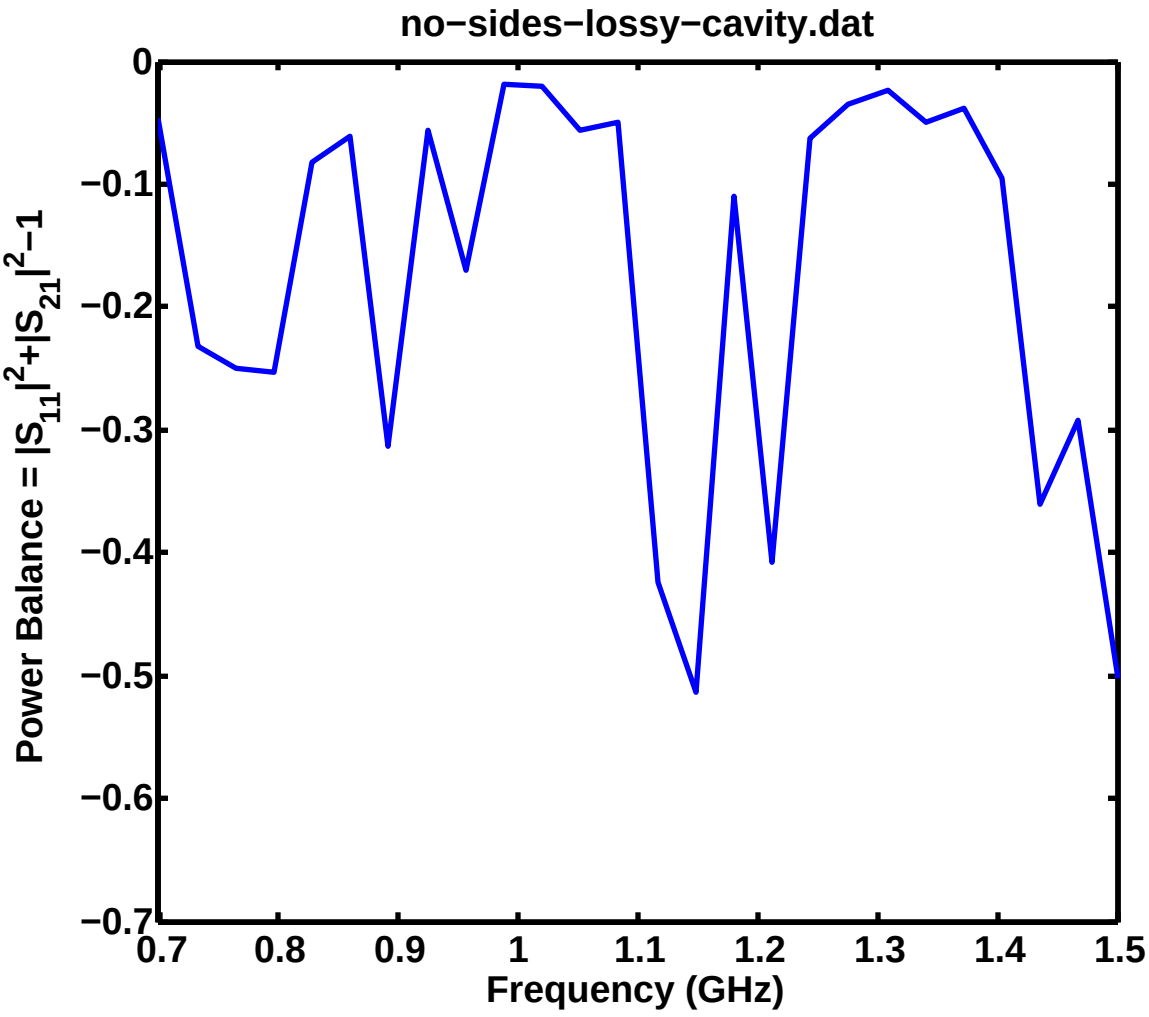

Figure 3.13: post-cavity-lossless report.

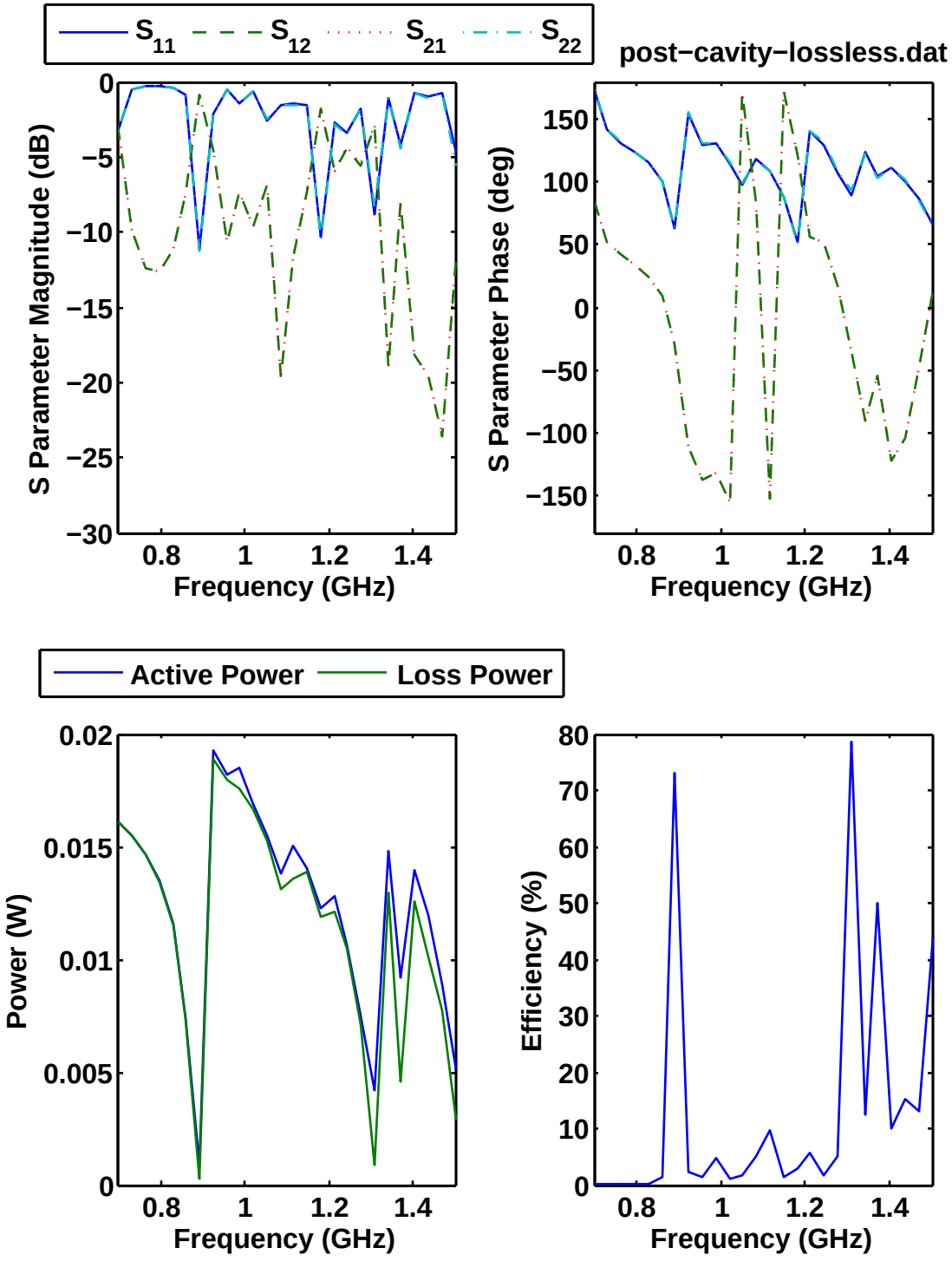

Figure 3.14: post-cavity-lossless power balance report.

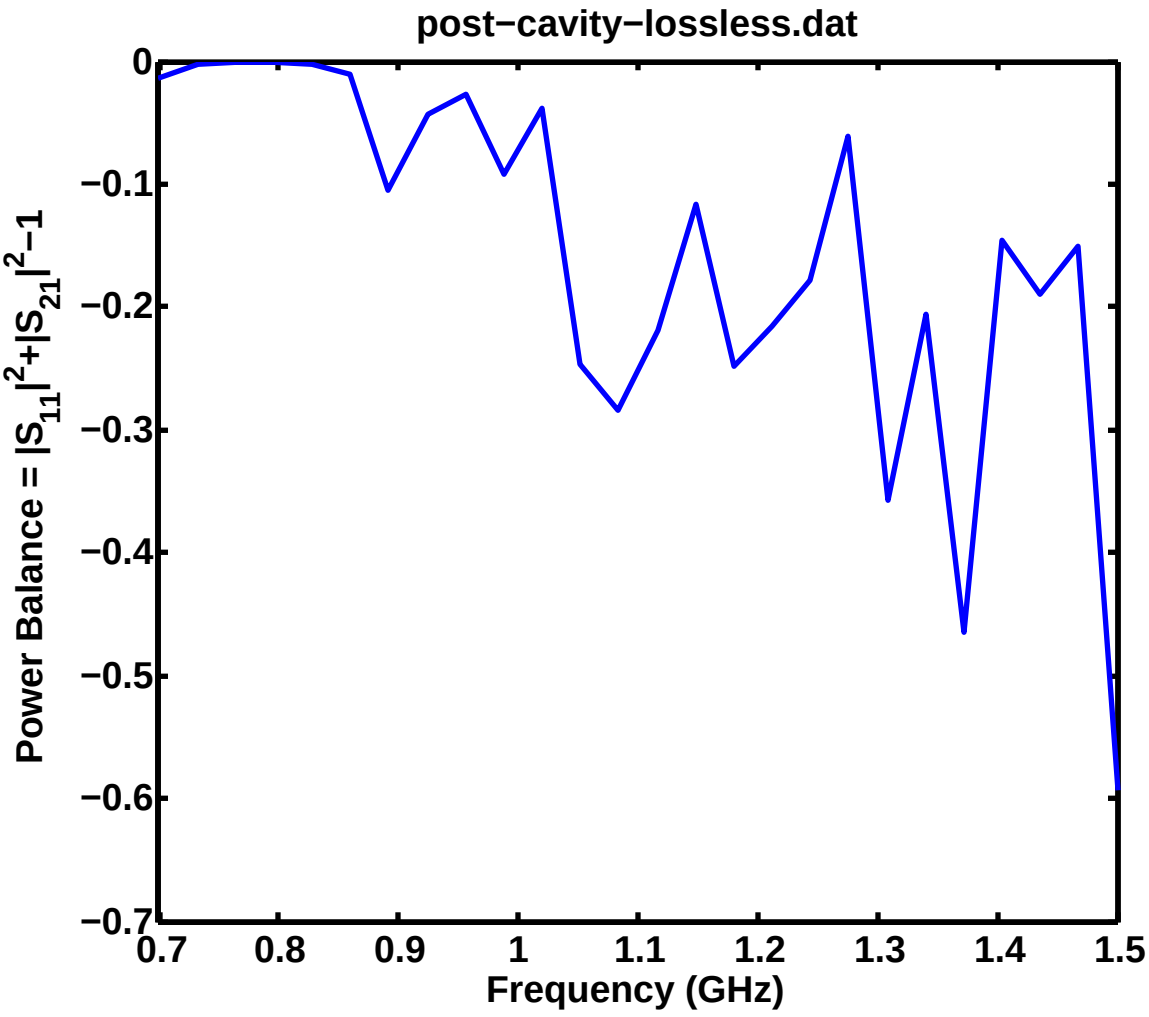

Figure 3.15: post-cavity-lossless-walls report.

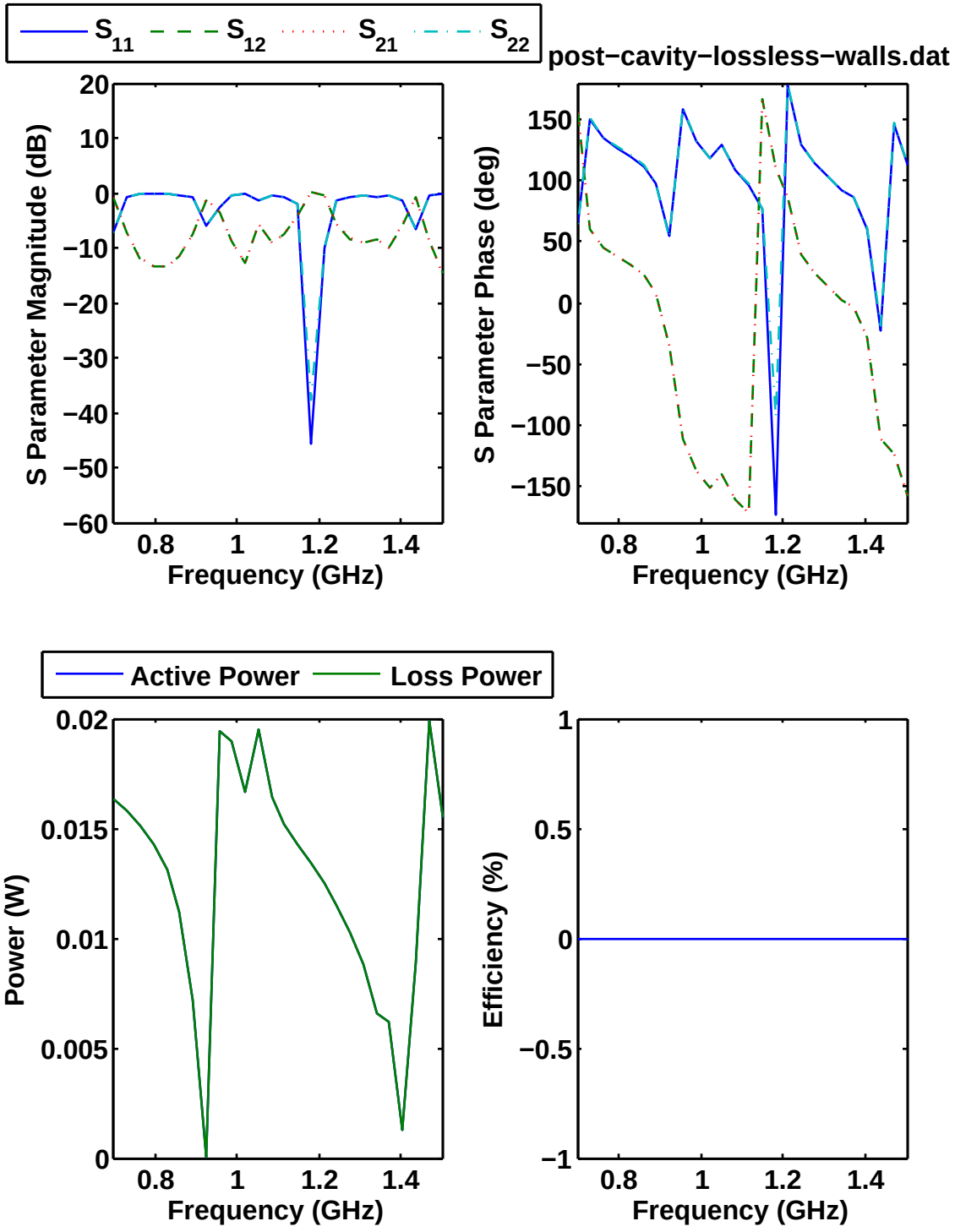

Figure 3.16: post-cavity-lossless-walls power balance report.

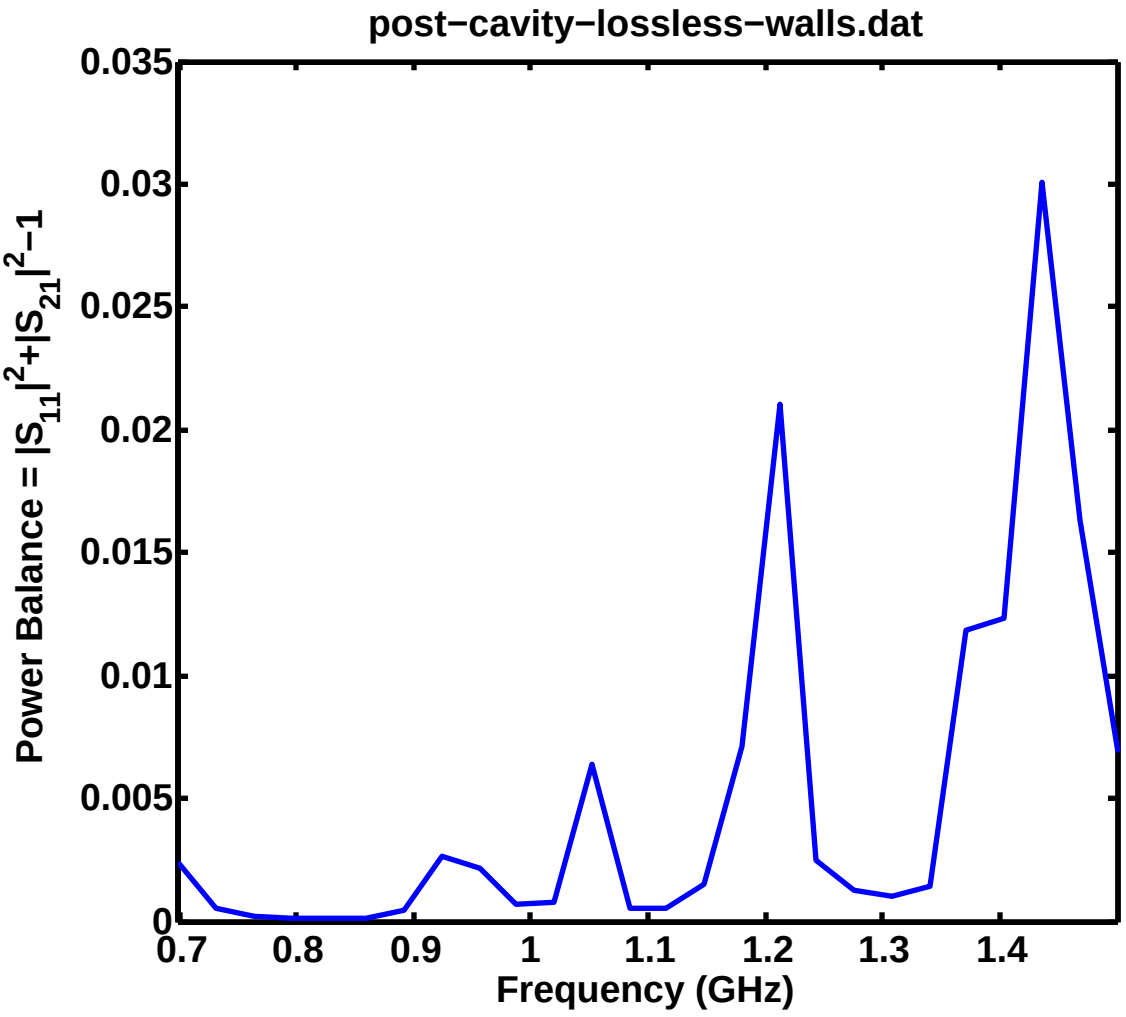

perimeter shorting posts, `post-cavity-lossy`. The first two figures cover the usual frequency range while the last two figures show an extended range from 1.5 GHz to 1.8 GHz. As expected, the system exhibits loss from both radiation and other loss mechanisms. The perimeter shorting posts appear to behave less like a wall as the distance between shorting posts becomes significantly greater than a wavelength. A higher overall power loss is noted suggesting that in general power loss increases with frequency. This behavior is no surprise as this is typical with most materials.

Figures 3.21 and 3.22 show the results from a lossy TLY5 cavity simulation with perimeter shorting posts, `post-cavity-lossy-walls`. Due to the addition of walls to form a cavity, the radiation efficiency has decreased to almost zero. Power loss is reduced but still present. These results suggest that the perimeter shorting posts only effect power loss through radiation.

Figure 3.17: post-cavity-lossy report.

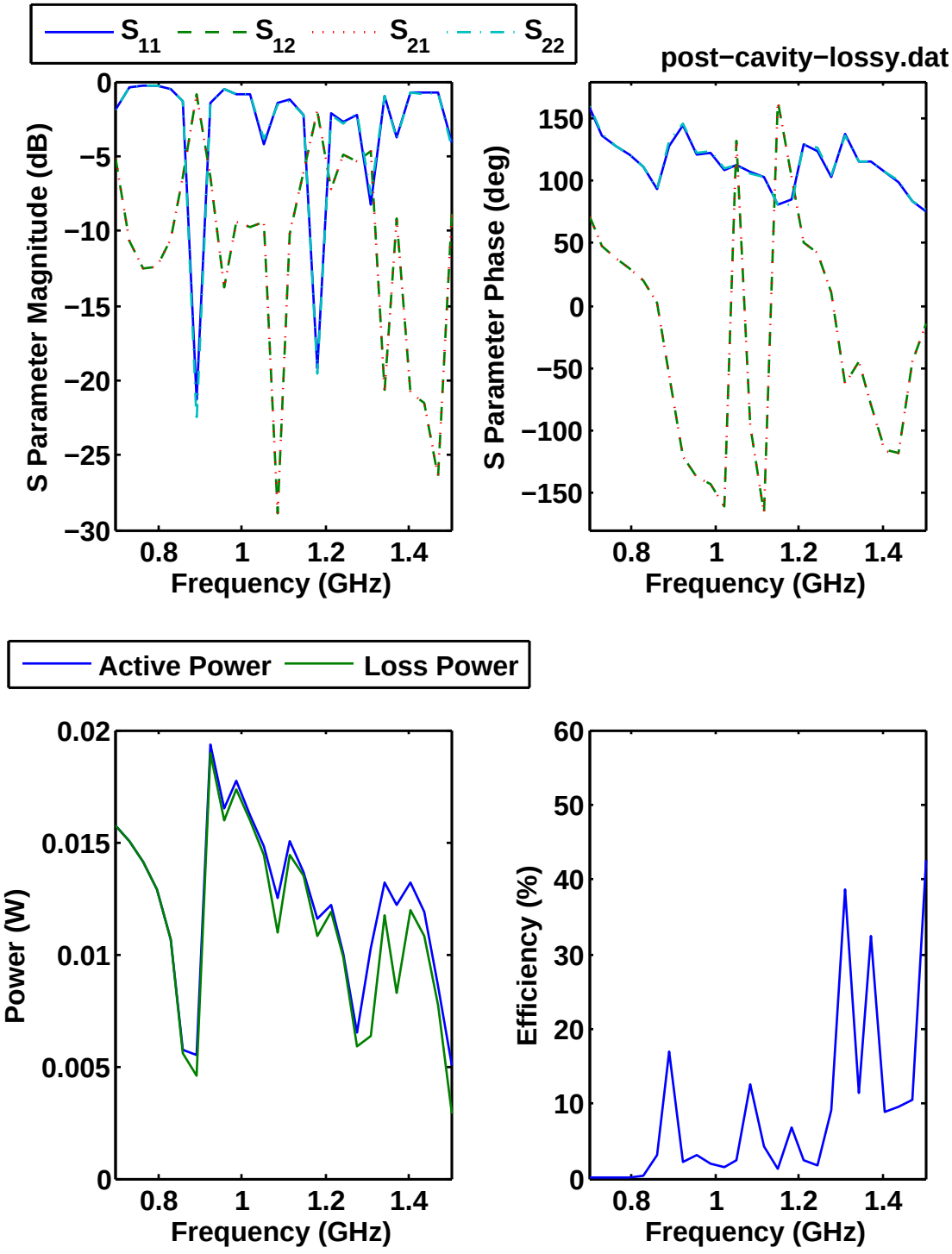

Figure 3.18: post-cavity-lossy power balance report.

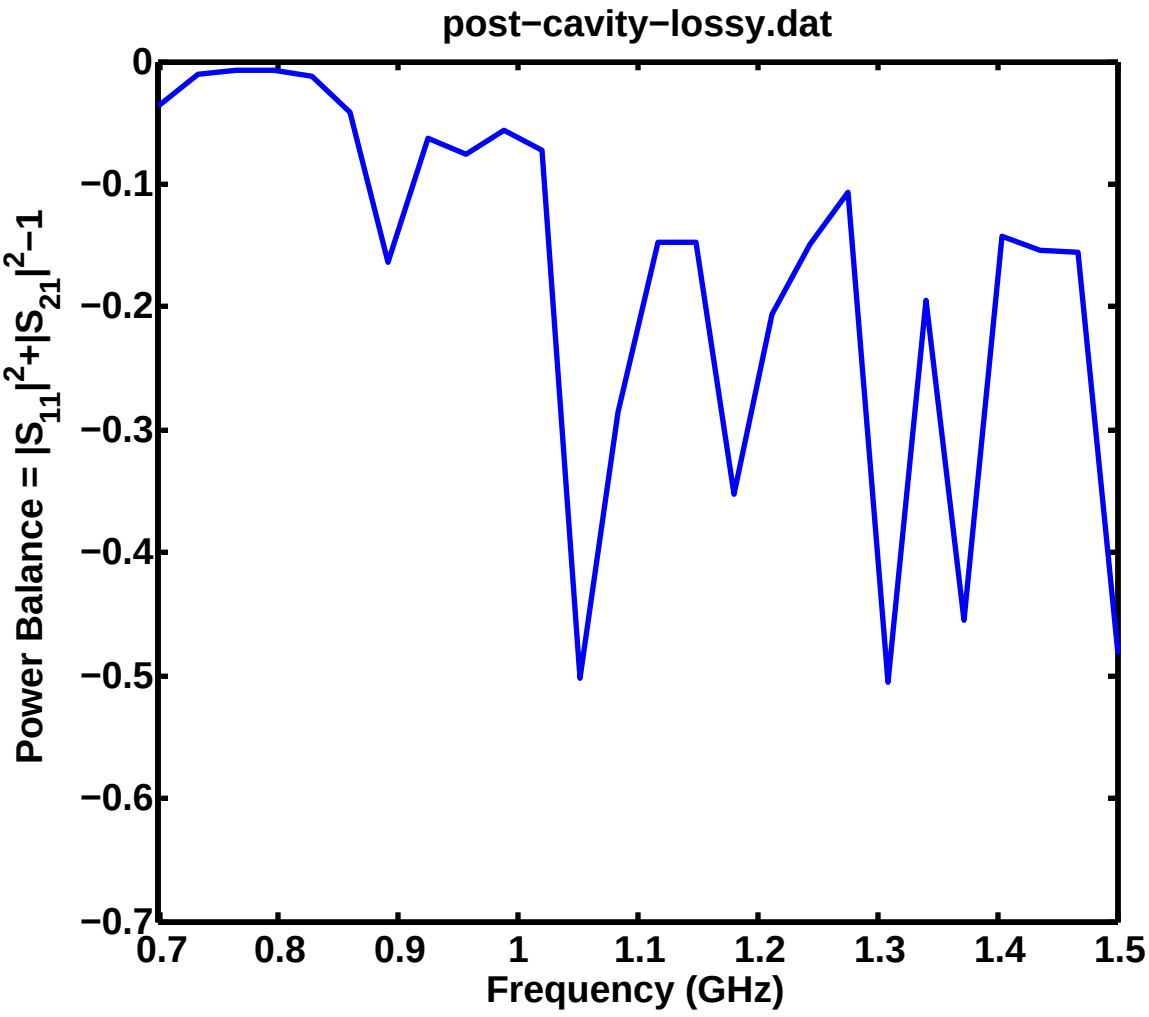

Figure 3.19: post-cavity-lossy-15 report.

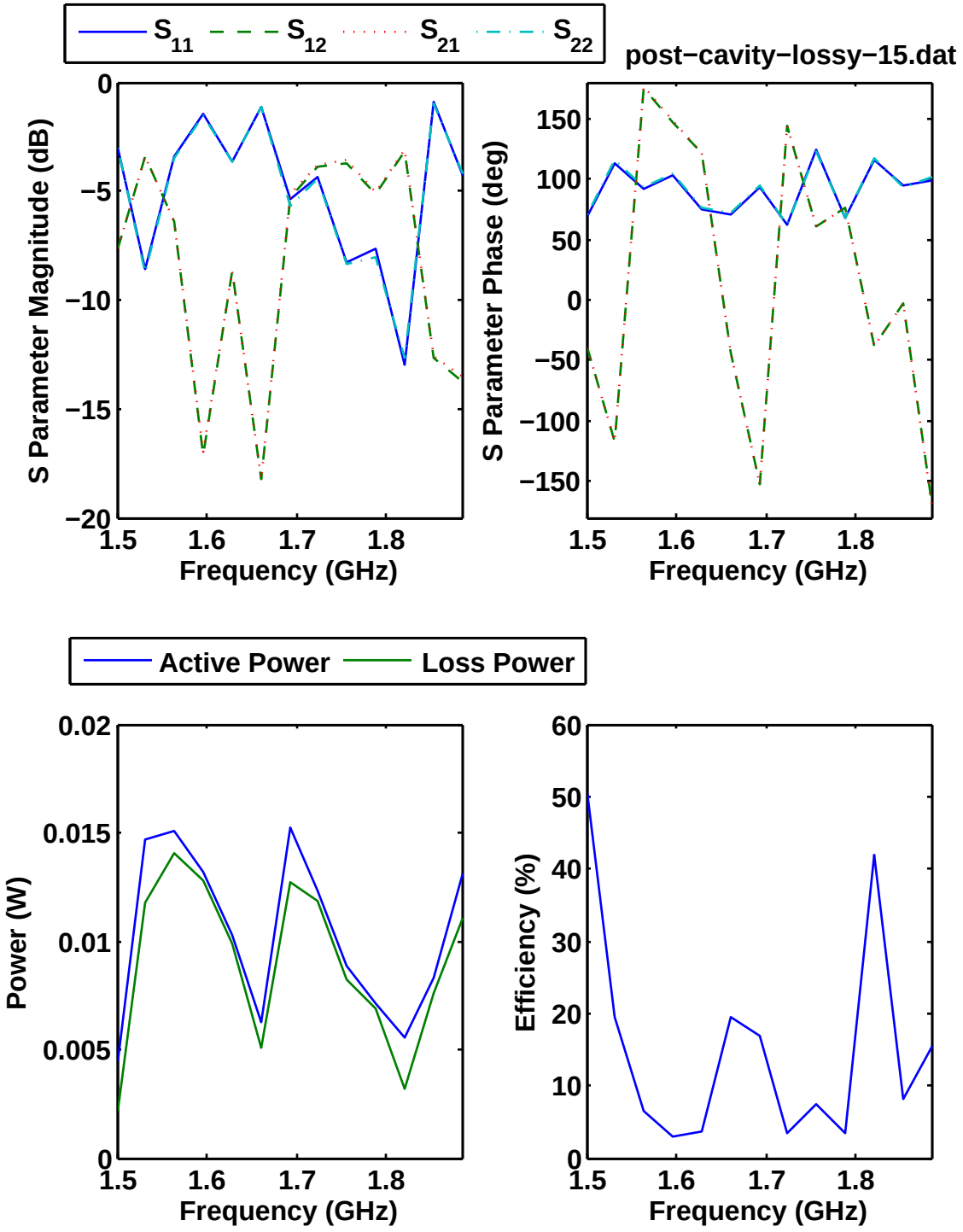

Figure 3.20: post-cavity-lossy-15 power balance report.

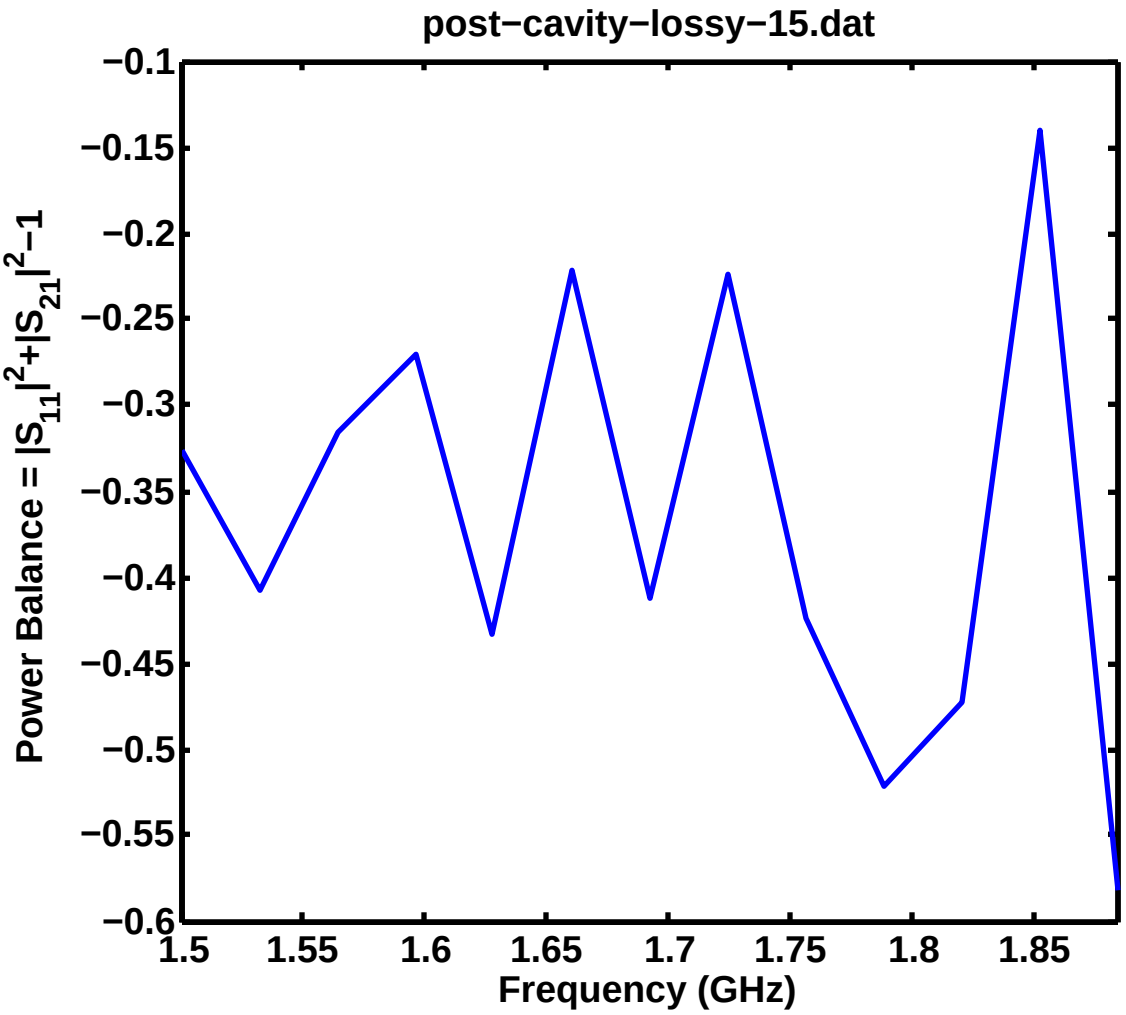

3.2.6 Switched Shorting Post Simulations

Finally a simulation, `rings-reduced`, was run that involved sixteen of the thirty-two switched shorting posts. The posts and annular rings were simulated with no switch, effectively simulating an all open state. Material properties and geometry were the same as in `post-cavity-lossy`. Only sixteen posts could be simulated due to computational costs. Figures 3.23 and 3.24 show the results from this simulation. These results suggest a decrease in power loss as compared to prior simulations. Further, it demonstrates that, especially in comparison to radiated loss from the sides of a coplanar two port network, the annular rings contribute very little to the power loss.

3.3 Conclusion

Various simulations were carried out to study the self-structuring two-port network. Initial simulations consisted of lossless materials and an infinite ground plane. The goal was to explore the capabilities of the network in a timely manner. These simulations also provided guidance when it came time to manufacture a self-structuring two-port network. Results from these initial simulations demonstrated the ability to create a filter with a tunable center frequency.

New simulations were carried out after unsatisfactory performance of the manufactured self-structuring two-port network during experiments. The goal of these simulations was to determine sources of significant power loss. Actual physical dimensions and material properties were used in an attempt to model the constructed network. Overall, no one loss mechanism was identified as significant. Perimeter shorting posts and copper tape around the edges was shown to be effective at reducing radiated power. Radiation from the rings around the shorting posts was not significant. These simulations suggested that while dielectric losses were present, they were not sufficient to cause the losses observed in experiments.

Figure 3.21: post-cavity-lossy-walls report.

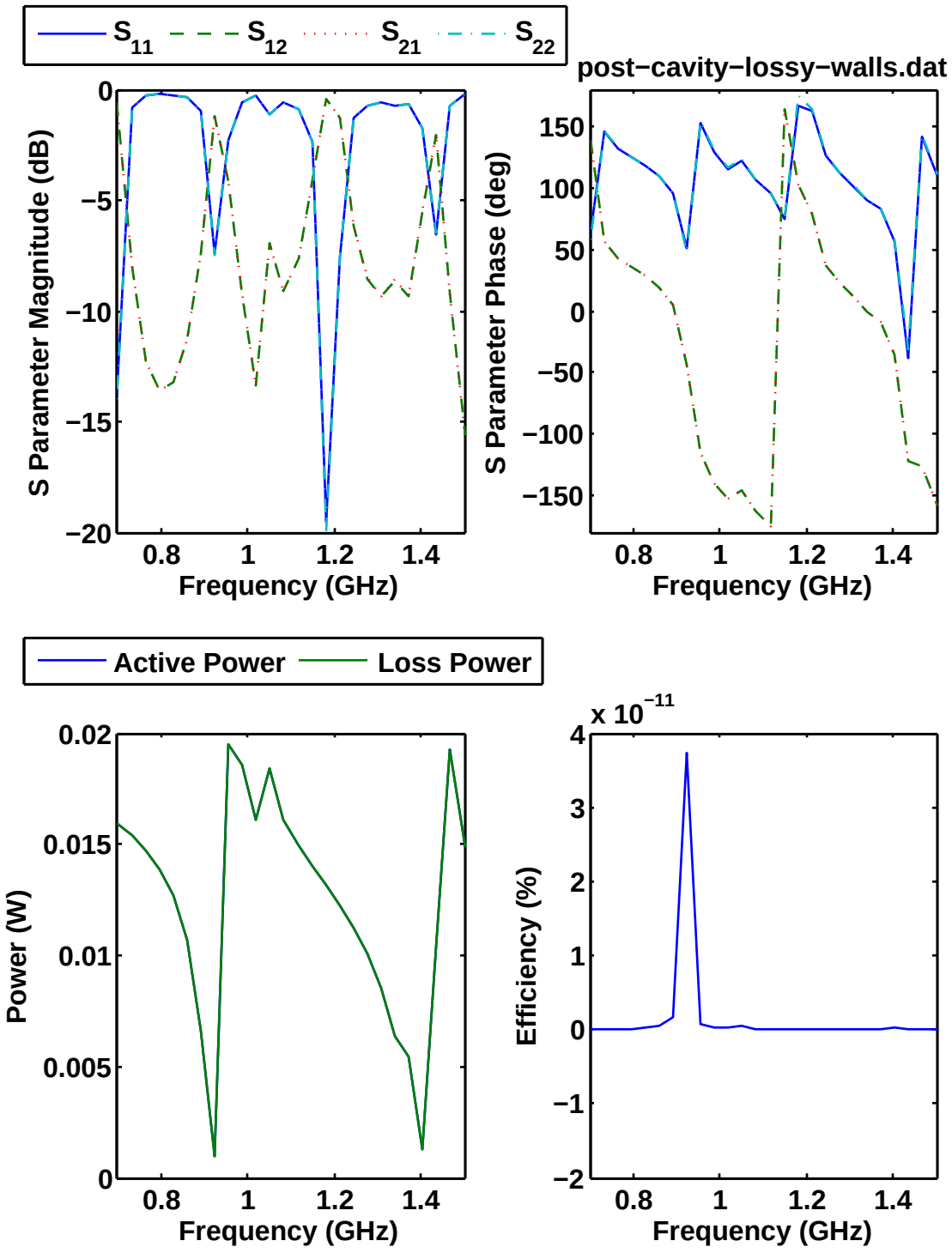

Figure 3.22: post-cavity-lossy-walls power balance report.

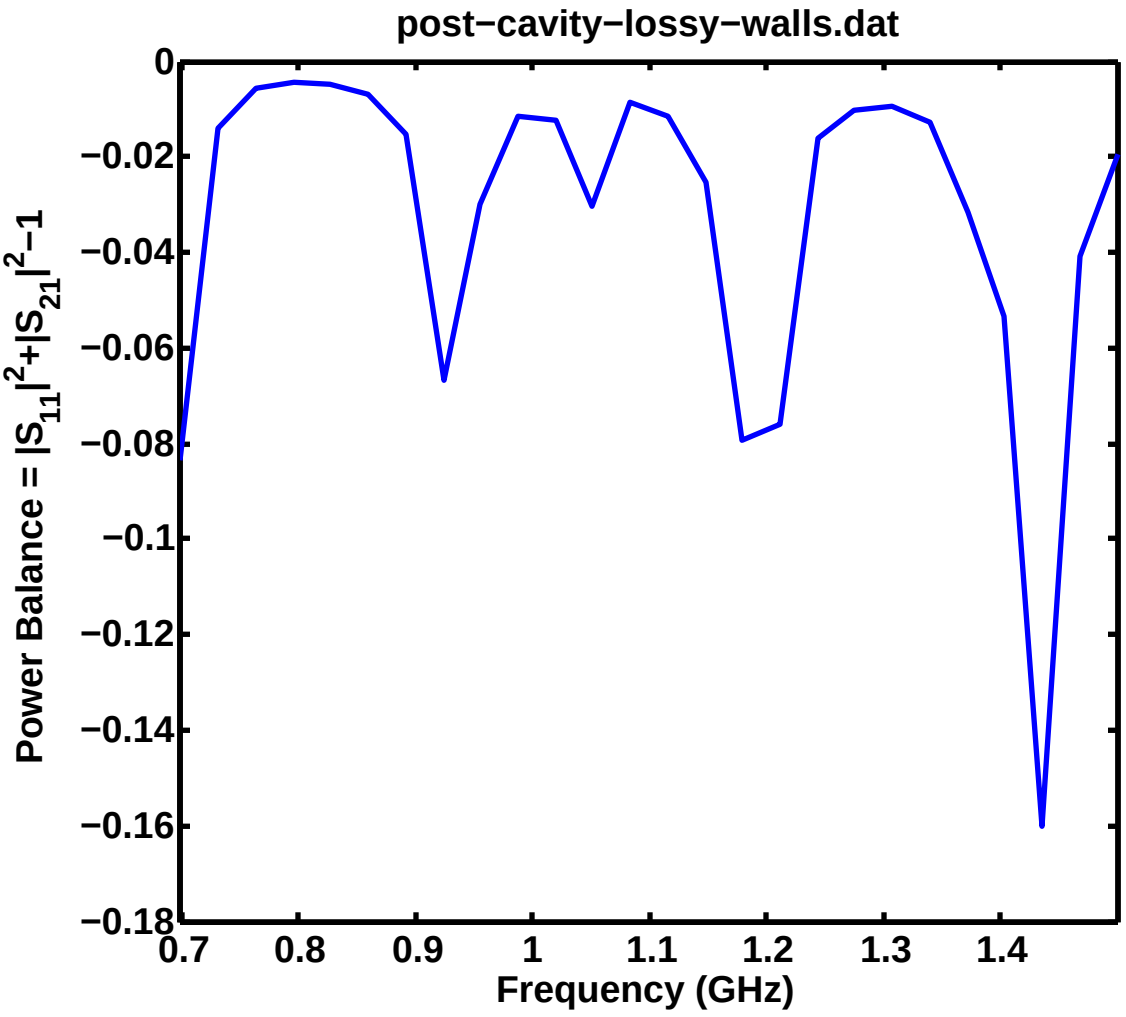

Figure 3.23: rings-reduced report.

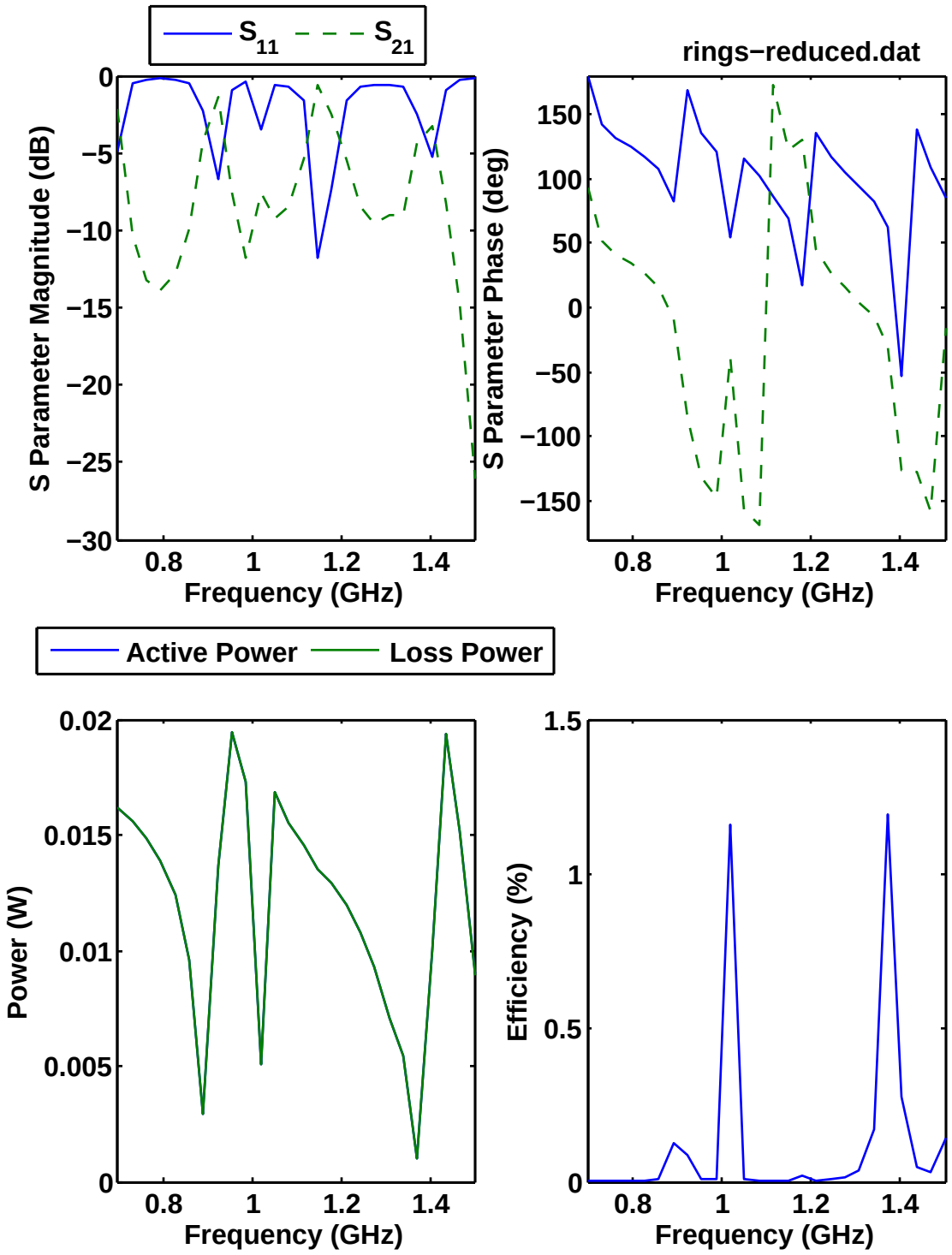

Figure 3.24: rings-reduced power balance report.

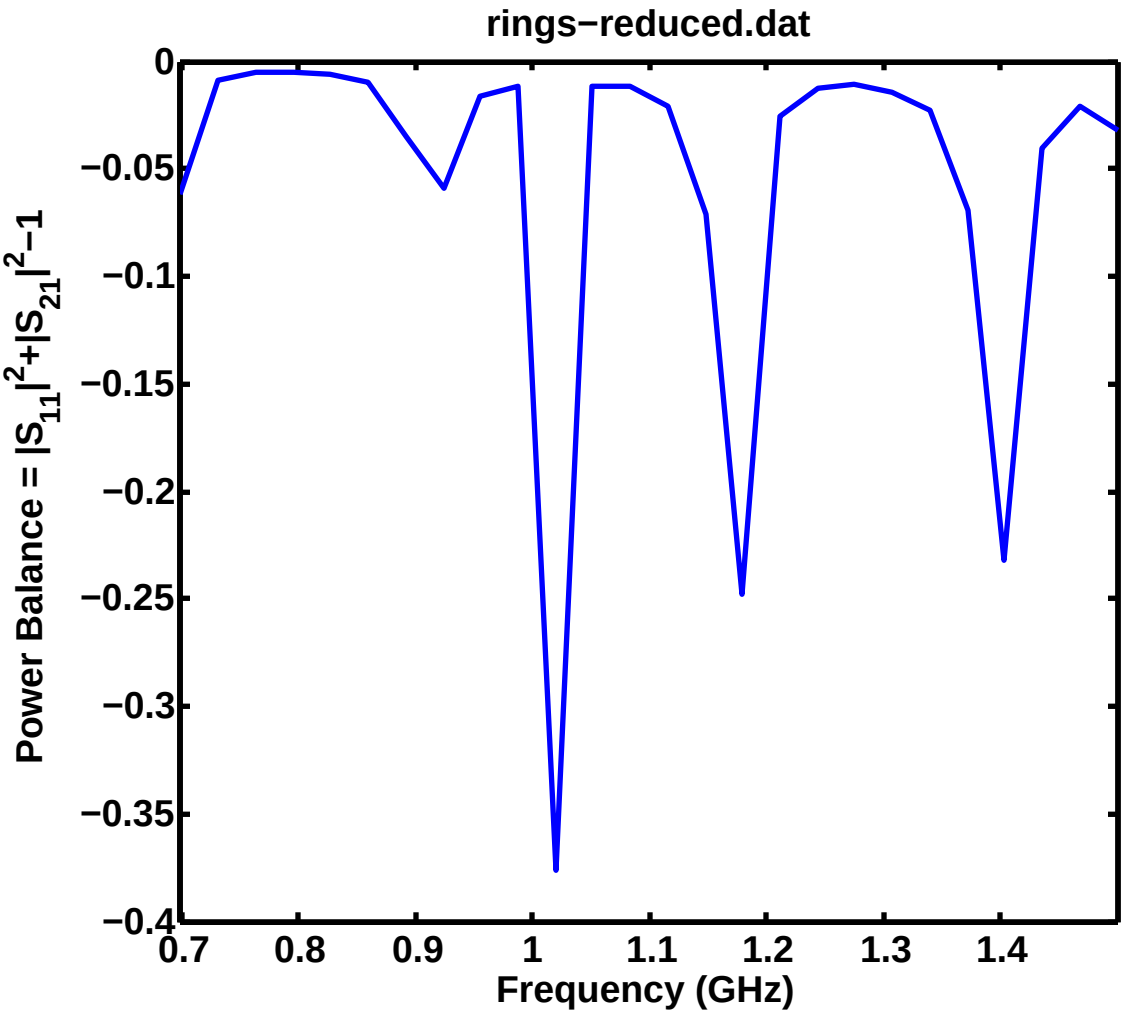

Chapter 4

Experimental Investigation

A prototype self-structuring two-port network was constructed and used to experimentally explore the network as a two-port device. The initial investigation was a random search of a small percentage of the possible switch configurations. Genetic algorithm based searches were then used to explore the characteristics of the network. Results from this stage of experimentation suggested a high-loss network. Mitigation was performed to reduce radiation losses. Random and genetic algorithm searches were carried out post-mitigation. Continued power loss points to an inefficient two-port network.

4.1 Hardware

Before leaving MSU, Chien-Hsien Lee manufactured the two-port network used in the experiments for this thesis. Its construction is described below. A photograph of the completed prototype is shown in Figure 2.4, reprinted here as Figure 4.1 for the reader's convienence.

4.1.1 Two-Port Network

The self-structuring two-port network was constructed on a 42 x 27 x 0.5 cm Taconic TLY-5 double-sided circuit board (relative permittivity, ϵ_r, of 2.20, dissipation factor, δ_t, of 0.0010).

Figure 4.1: Prototype self-structuring two-port network. Reprint of Figure 2.4.

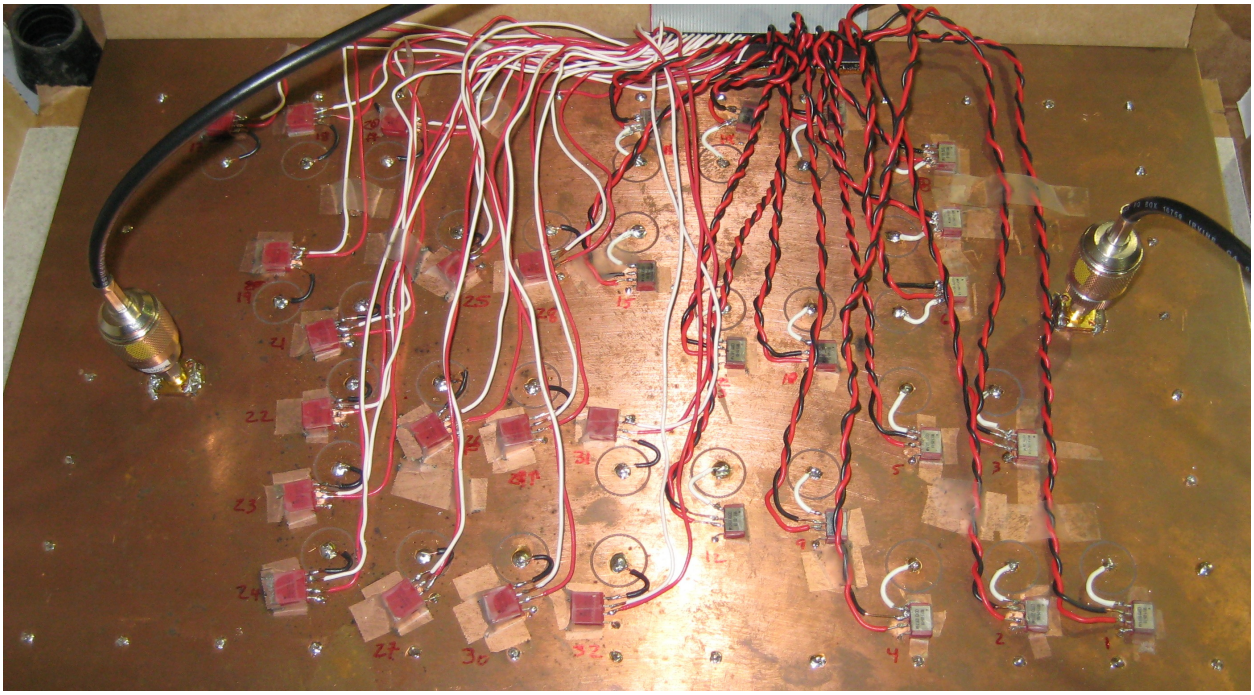

A copy of the letter stating the parameters of the board is shown in Figure 4.2.

Figure 4.3 is a schematic of the network. A 36 x 21 cm rectangle centered on the board was subdivided into a 3 x 3 cm grid. Thirty-eight perimeter shorting posts were placed around the outside of this rectangle at grid intersections. Throughout the rectangle, thirty-two switch controlled shorting posts were placed on the grid along with two SMA female panel mount connectors. Using the perimeter post in the bottom left corner of Figure 4.1 as the origin, Table 4.1 gives the coordinates of each post and port.

Figure 4.2: Material parameters of the circuit board used to create the self-structuring two-port network prototype provided by Taconic.

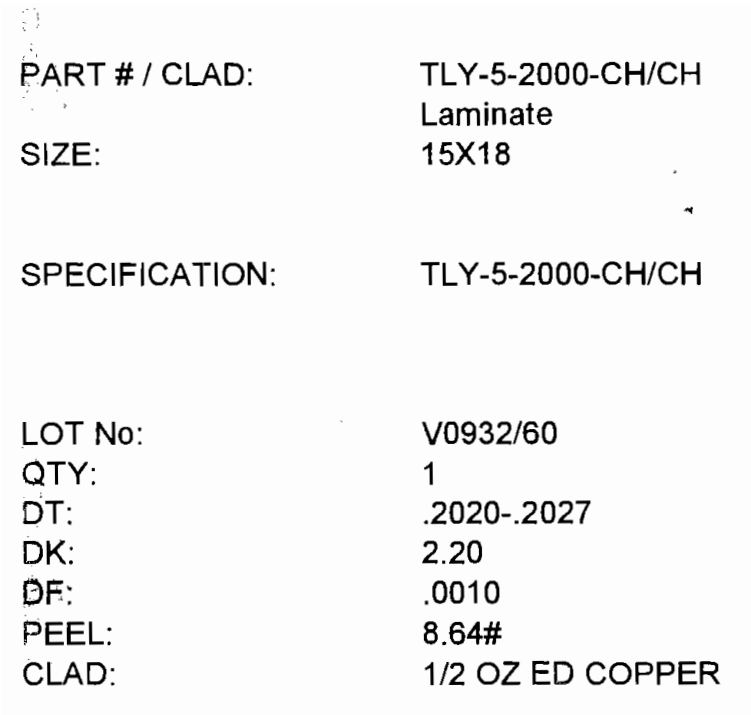

PART # / CLAD:	TLY-5-2000-CH/CH Laminate
SIZE:	15X18
SPECIFICATION:	TLY-5-2000-CH/CH
LOT No:	V0932/60
QTY:	1
DT:	.2020-.2027
DK:	2.20
DF:	.0010
PEEL:	8.64#
CLAD:	1/2 OZ ED COPPER

Figure 4.3: Schematic view of self-structuring two-port.

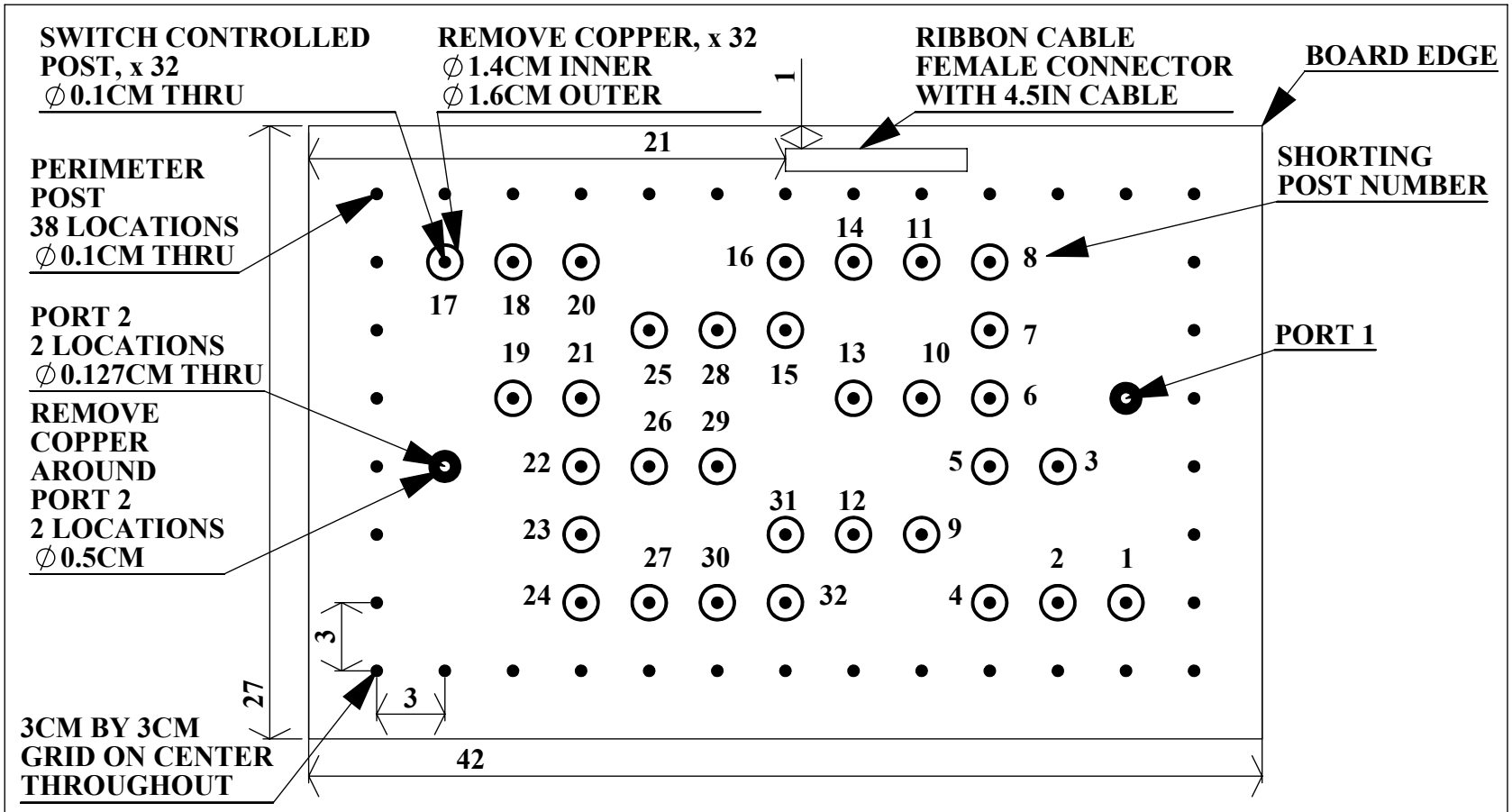

ITEM	QTY.
TACONIC TLY-5 DOULBE SIDED BOARD	1
SMA FEMALE PANEL MOUNT	2
COTO 5V REED RELAY SWITCH	32
THROUGH-HOLE VIA	70

DIM: CM	DATE: 4 APR 2011	SELF-STRUCTURING TWO-PORT NETWORK
		DWG. BY: ANDREW TEMME
		SCALE: 1:3 / SHEET 1 OF 1

Table 4.1: Pin and port placement taking the bottom left perimeter pin as the origin.

Element	x (cm)	y (cm)	Element	x (cm)	y (cm)
Bottom, Left Corner of Board	-3	-3			
Perimeter Post 1	0	0	Port 1	33	12
Perimeter Post 2	0	3	Port 2	3	9
Perimeter Post 3	0	6	Switched Post 1	33	3
Perimeter Post 4	0	9	Switched Post 2	30	3
Perimeter Post 5	0	12	Switched Post 3	30	9
Perimeter Post 6	0	15	Switched Post 4	27	3
Perimeter Post 7	0	18	Switched Post 5	27	9
Perimeter Post 8	0	21	Switched Post 6	27	12
Perimeter Post 9	3	21	Switched Post 7	27	15
Perimeter Post 10	6	21	Switched Post 8	27	18
Perimeter Post 11	9	21	Switched Post 9	24	6
Perimeter Post 12	12	21	Switched Post 10	24	12
Perimeter Post 13	15	21	Switched Post 11	25	18
Perimeter Post 14	18	21	Switched Post 12	21	6
Perimeter Post 15	21	21	Switched Post 13	21	12
Perimeter Post 16	24	21	Switched Post 14	21	18
Perimeter Post 17	27	21	Switched Post 15	18	15
Perimeter Post 18	30	21	Switched Post 16	18	18
Perimeter Post 19	33	21	Switched Post 17	3	18
Perimeter Post 20	36	21	Switched Post 18	6	18
Perimeter Post 21	36	18	Switched Post 19	6	12
Perimeter Post 22	36	15	Switched Post 20	9	18
Perimeter Post 23	36	12	Switched Post 21	9	12
Perimeter Post 24	36	9	Switched Post 22	9	9
Perimeter Post 25	36	6	Switched Post 23	9	6
Perimeter Post 26	36	3	Switched Post 24	9	3
Perimeter Post 27	36	0	Switched Post 25	12	15
Perimeter Post 28	33	0	Switched Post 26	12	26
Perimeter Post 29	30	0	Switched Post 27	12	3
Perimeter Post 30	27	0	Switched Post 28	15	15
Perimeter Post 31	24	0	Switched Post 29	15	9
Perimeter Post 32	21	0	Switched Post 30	15	3
Perimeter Post 33	18	0	Switched Post 31	18	6
Perimeter Post 34	15	0	Switched Post 32	18	3
Perimeter Post 35	12	0			
Perimeter Post 36	9	0			
Perimeter Post 37	6	0			
Perimeter Post 38	3	0			

Each port had a 0.127 cm diameter hole drilled for it. All posts, perimeter and switch-controlled, had 0.1 cm diameter holes drilled for them. An annular ring of copper with an inner diameter of 1.4 cm and width of 0.1 cm was removed from around each switch-controlled shorting post on the top surface of the device. This was done in order to isolate the post from the rest of the surface.

Coto 5 V reed relay switches were used to control the switched posts. Switches were affixed to the network using clear tape. Typical time required to mechanically close a switch is 350 μs and 100 μs to open [60]. The two inside pins on each relay are the control pins and the two outside pins are the switched pins. Switches are not polarized. Each pad and associated switch are covered with electrical tape. Control wires are potted about one inch from the switch. Dow Corning 748 noncorrosive silicone sealant (McMaster-Carr #74915A654) was used as the potting compound. The entire top side of the network is covered with copper tape in an effort to minimize radiation. See Section 4.4.4 for more details.

Placed on the bottom side of the circuit in each corner is a rubber foot. For most experiments, the network was kept in a shallow cardboard box lid. This was done for ease of transportation, setup, and storage. An extra layer of insulation was included for protection from test equipment and surfaces.

Switch control is accomplished through a National Instruments PCI-DIO-96 digital input/output (DIO) board. The board has ninety-six DIO spread connections across two 50-pin ribbon cables. Pins 49 and 50 on each cable are +5 V_{DC} and ground, respectively. Each DIO pin can supply 2.5 mA; however, each switch requires 250 mA. To supply this current, Toshiba TD62783APG source driver chips are used. Each chip is capable of simultaneously driving eight outputs. The cable carrying pins 1 – 50 is connected to a circuit board which has an external power supply and four source driver chips. The outputs of these drivers are connected to the network through a 4.5 in long, 64-pin ribbon cable which carries a signal and ground for each switch. This short cable is split in half with a ferrite on each

half and then one large ferrite around the entire cable. The ribbon cable's connector is glued to the edge of the network, female side up so that the control wires for each switch can be plugged into the connector as seen in the top of Figure 4.1.

Mechanical problems often arise in the connection between the ribbon cable and the switches. The most common problems are the following: one or both control wires for a switch may come out of the connector, the control pins on the switches may break, or the wires need re-soldered to the switches. Often, attempting to fix one problem will cause another one of these problems. These mechanical problems have been observed by the author with all SSA prototypes at MSU that utilize ribbon cable control and/or discrete Coto switches. Another common problem exhibited by most prototypes is a relatively short lifetime for the ribbon cable connectors, both male and female. Often times, the plastic side walls of the male connectors will break and the pins will become bent after repeated connections. This is due to the difficulty in connecting and disconnecting ribbon cables. Female connectors are difficult to assembly and crimp properly leading to the connector not staying together. Caution must be exercised when working with ribbon cables.

Future investigations should consider using different connectors and control methods to reduce mechanical failures in experiments.

Mechanical problems on the network board were mitigated in two ways. First, control wires were mechanically potted near the switches to provide strain relief and to protect the switch pins. Second, control wires were hot glued to the ribbon cable connector after verifying that the switch was operational. The switches were checked again after all control wires were hot glued.

A few words regarding the Dow Corning sealant used as the potting compound are offered. Setting time is one problem; working time is around 1 hr, with complete curing occurring in approximately 24 hrs. This relatively lengthy time means that whatever is being potted must be able to support itself or have a support system during this period. Hot glue, on the other hand, requires only a few seconds or tens of seconds of support. The downside of hot

glue is that it does not adhere to copper tape well. The Dow Corning sealant was selected for multiple reasons including being non-corrosive, non-conductive, giving off few fumes, its ability to bond to all materials of interest, and having a relatively low cost-to-volume ratio.

There are multiple methods used to check for proper switch operation. The simplest check is to listen for the switches to operate. The next check should be performed routinely, especially after an experiment has been moved or any control cables adjusted. Each switch is turned on (either individually or all at once) and the output voltage measured. When operating properly, the voltage should be between 3.50 V and 3.75 V, optimally 3.64 V for the constructed control board and network. If the output is 5 V, there is most likely an open circuit somewhere. The first place to check is the connection between the ribbon cable and the switch control wires. Then the switch pins should be checked. If the output is 0 V, disconnect DC power and look for a short. Leaving power applied may cause the driver to heat up considerably. This leads to another testing procedure which is to check the drivers for high heat. When functioning properly, the drivers should not feel warm.

Over the past three years of working with the Toshiba driver chips, there has only been one time that a chip quit functioning. In this case the defective output would always be at 5 VDC with no current to operate the switch. It was determined to be malfunctioning after switching the orientation of the output ribbon cable (i.e. pin 32 became pin 1) and also after switching SSA devices.

4.1.2 HP 8753D Network Analyzer

Measurements were taken using an HP 8753D network analyzer controlled by a National Instruments USB-to-GPIB converter (product name: NI GPIB-USB-HS). The analyzer was calibrated using an HP 85052D Economy Mechanical Calibration Kit (DC to 26.5 GHz, 3.5 mm) for most experiments. The calibration table for this calibration kit is not readily available in a format usable by the HP 8753D. Using VNA Cal Kit Manager [61], the calibration table for the HP 8510C was edited and then downloaded to the network analyzer.

Appendix 5.3 contains the procedures for editing and downloading the cal kit table to the HP 8753D.

When adapters of various types were used in the same experiment, such as when connecting to a large horn antenna having an N-type connector, the analyzer was calibrated using the 3.5 mm cal kit and then an SMA-to-N type connector attached to the port requiring it. The effect of this adapter is assumed to be negligible. Using existing cal kit definitions and VNA Cal Kit Manager, it is possible to create a cal kit for an SMA connection on one cable and an N type connection on the other cable.

4.2 Selection of States

States for random testing are determined from a state file, not a dynamic random number generator. The state file is parsed sequentially for as many states as needed. The file used throughout the research for this thesis consisted of one hundred thousand unique states that were generated by a National Institute of Standards and Technology (NIST) random number generator. The file begins with states for all switches open, all closed, and each switch closed individually and then has the one hundred thousand random states. Overall, there are one hundred thousand thirty four states in the file, stored as a text file with each state on a line. Each state is encoded as a thirty-two character long string of 0's and 1's. States are read like a binary number with switch 32 corresponding to the left most bit and switch 1 corresponding to the right most bit.

A file of random states is used instead of a random number generator for multiple reasons. First, it lends repeatability to experiments. While each experiment is not random when compared to others, the states used are random. Second, using a NIST generated list ensures a statistically random sample. Third, a set file reduces programming complexity as states do not have to be generated. Finally one is able to use the random state file as a means to associate results with states since the random state file is static. The random state file has

only three repeated states: `0x5D124738`, `0xCFBF5D29`, and `0xF013B91A`. Repeated states can be found using the terminal command `sort` *`file-name`* `| uniq -d`.

4.3 LabView Software

Data accquisition and experiment control were carried out using software written in National Instruments' (NI) LabView environment [62]. LabView allows for easy interface between NI hardware and many other devices using various protocols. The ECE shop at MSU has developed numerous LabView applications for use in the teaching labs. Because of this and the availability of an NI USB-to-GPIB adapter, LabView was selected for this project.

LabView is programmed by creating a block diagram of the program. Blocks essentially represent functions with data being passed between blocks by wires. This design philosophy encourages programs that use a parallel flow instead of a sequential flow.

LabView provides many ready-to-use blocks for both common and uncommon tasks, e.g. plotting. Program development in LabView requires a change in mindset and forces the programmer to change his normal programming style. In addition, proper layout of a program in LabView can be difficult to achieve as the "automatic cleanup" feature often makes the program more difficult to follow. It is often difficult to get an overview of a large LabView program because LabView programs are represented as having three dimensions (height, width, and depth) where in a traditional program such as FORTRAN, C++, or Matlab the program really only has a length. The depth of a LabView program is often displayed in structures such as conditional loops. Only one condition can be displayed at a time. As is common in almost all languages, data types can be confusing at first. While attempting to remove this confusion, LabView has created its own problems with data types.

LabView's strongest attribute is the large, local library of functions available to the user that in other languages would have to be written by the programmer or sought out in a remote code library. Interfacing with various hardware devices is somewhat simplified in LabView.

Also fairly straightforward is data import and export. Mathematical processing of data can be cumbersome, however, as anything beyond simple arithmetic requires a complicated implementation.

Another strength of LabView is the debugging process. LabView provides many ways to track data through a program, provides breakpoints, and very thorough "syntax" checking. The LabView integrated development environment (IDE) gives the user immediate feedback on type mismatches and improperly connected wires.

While the IDE provides helpful debugging features, these features are probably the only helpful thing about the IDE. There is no way to zoom in or out on a block diagram in order to get an overview of the program. Rearranging the block diagram via cut-and-paste or drag-and-drop is implemented, but functionally does not work. Insertion of blank space for visual reasons or for development reasons is extremely difficult. Formatting or layout of the block diagram for ease of reading, programming, and understanding is difficult if not properly done from the beginning.

LabView has great potential; however, programming anything beyond a very basic application involves many hurdles, most notably the IDE itself. Future research should consider using Matlab or another programming language.

The newly acquired Agilent ENA E5071C has Microsoft Visual Basic installed natively. Future data acquisition and automation will most likely be carried out in Visual Basic.

The various programs created using LabView to run experiments are described below.

4.3.1 Random Search

The first program created performs a random search experiment. Using the NIST generated random number pool, the program sets a switch state and then records the measured S-parameters before setting the next state.

To begin, the user configures the network analyzer through the software. Parameters that may be adjusted include start and stop frequency, number of points, averaging, IF

bandwidth, power level, communications time-out, and the GPIB address of the network analyzer.

Next the user selects the NIST random pool file to be used and the folder to which data should be saved. The user then enters how many random states to read from the beginning of the file, the amount of time allowed for the switches to settle before a reading is taken, and the type of experiment. Experiments may be one of three types: setup, testing, or valid. Setup and testing are used for debugging purposes while a valid type experiment is used when data is to be recorded and stored. Finally, the user may enter any annotations regarding the experiment.

Besides running experiments, the user may configure the network analyzer and then enter a state and take a reading for that state. This allows for data from individual states to be selectively gathered.

Once the program is started, the current iteration number and state are displayed. The state is shown as a binary number and also using a series of thirty-two LED type indictors. A progress bar shows the percentage of the experiment which has been completed. At the bottom of the window, the magnitude and phase for measured S-parameters are displayed.

When an experiment is run, the software creates a folder for that experiment. This folder will be a subdirectory of either a folder titled "Valid" or "Other" depending on if the experiment is setup as a valid experiment or either a setup or testing experiment, respectively. These directories are placed in the folder selected when setting up the experiment. The folder for each experiment is titled *mm-dd-yyyy-*{*v,s,t*} where *mm-dd-yyyy* is the date on which the experiment was started and the suffix tells the type of experiment: valid, setup, or testing. Within the folder, data files have the same prefix. Appended to this prefix is either `-config, -freq, -s`*xx*, or `-swr`. Each of these files stores the experiment configuration, the frequency list, S-parameter data (*xx* tells which parameter), or standing wave ratio (SWR) data, respectively. Each line of an S-parameter file stores the data for one state. Each data point has a real and imaginary value separated by a comma. Data points are then separated

Listing 4.1: Sample configuration file, `5-26-2009-1152AM-v-config.txt`.

```
Date: 5/26/2009                                                    1
Time: 11:52 AM                                                     2
Number of States: 1                                                3
Start (Hz):     7.000000000000000E+08                              4
Stop (Hz):     1.500000000000000E+09                               5
Num Points: 26                                                     6
Avg Factor: 1                                                      7
IF BW (Hz):     3.000000000000000E+03                              8
Power (dBm):     1.000000000000000E+01                             9
Settle Time (ms): 30                                               10
VISA Timeout (ms): 30000                                           11
Annotations:                                                       12
Antenna to t-line to  caled port.  No 2 port network.              13
Finish Time: 5/26/2009 11:52 AM                                    14
```

by commas. If S-parameter data is imported into Excel as a `.csv` file, there will be twice the number of columns as frequency points and the same number of rows as states. Frequency files are a comma separated list of frequency points stored on one line.

Listing 4.1 lists an example configuration file. This file contains entries that describe the configuration of the network analyzer, start and end dates and times, and any annotations that were made by the user.

4.3.2 Standing Wave Ratio

A variation of the above program was created to evaluate the SWR observed when using the two-port network. The program measures S_{11}, calculates the SWR and stores both the S_{11} and SWR data.

4.3.3 Genetic Algorithm

To find an optimized state for the self-structuring two-port network, a genetic algorithm (GA) was implemented in LabView. This program was based on the random search program. As such, a great deal of the interface, configuration, and output files are the same.

A genetic algorithm uses the evolutionary principle of survival of the fittest to find an optimized solution. The GA used in this thesis were guided primarily by [63] and previous work done at MSU by Raoul Ouedraogo in [13, 16]. Figure 4.4 is a flowchart of the GA used in this thesis. This GA minimizes the cost function rather than maximizing the fitness.

Figure 4.4: Genetic algorithm flow chart.

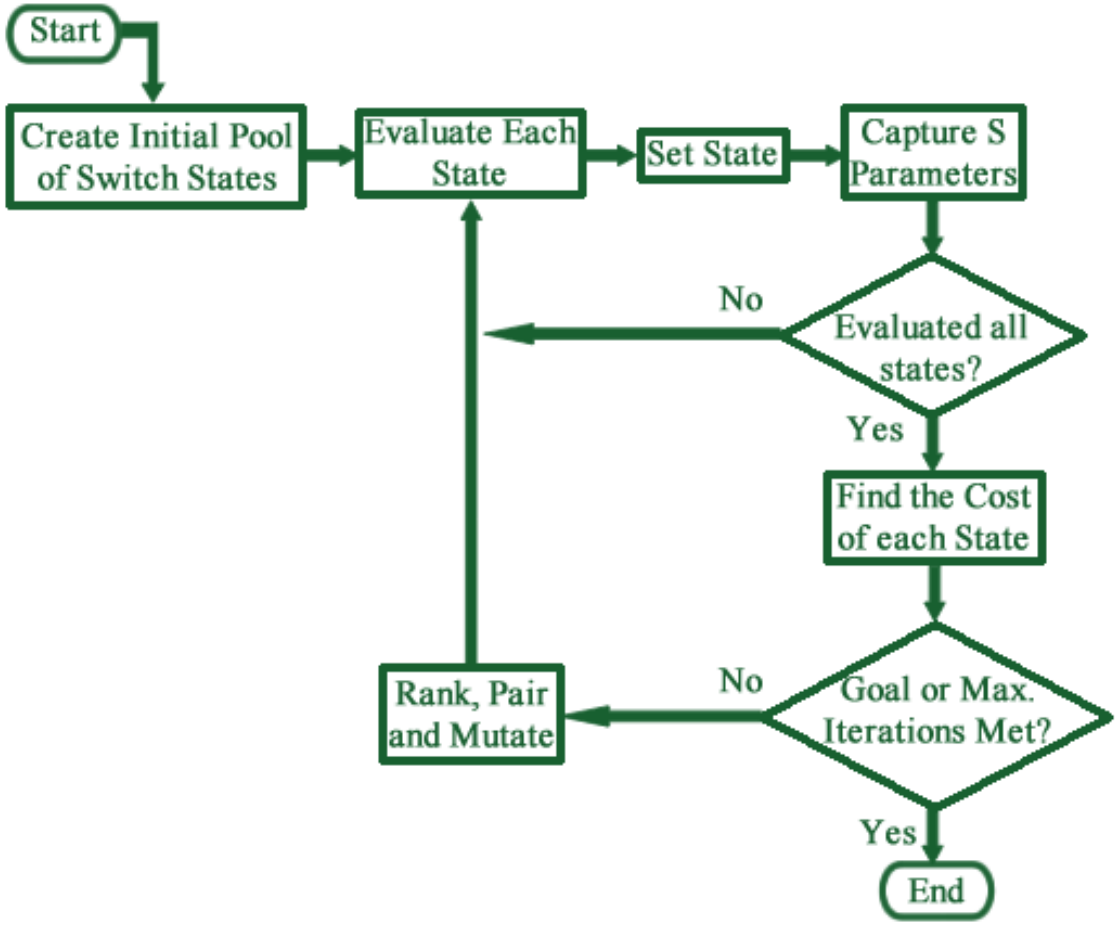

Initially the user configures the network analyzer. Once configured, the program allows the user to set parameters for the experiment and for the genetic algorithm. Currently genes are only paired using random pairing. Future versions may include pairing methods such as top-to-bottom; roulette wheel-weighted random; roulette wheel-cost weighted; and tournament selection.

The first version of this program only optimized at one frequency. The second version is able to optimize at multiple frequencies. When multiple frequencies are desired, the user selects which frequencies to optimize, enters a goal value for each frequency in dB and indicates whether the final value is to be lower than, higher than, or equal to the goal value.

The cost function must be edited in the block diagram because of the limitations of LabView. The cost function, $f_C(\cdot)$, is given by

$$fc(S_{xy,1}, S_{xy,2}, ..., Sxy,n) = \begin{cases} \sum_{i=1}^{n} S_{xy,i} - g_i, & \text{if } dir_i = -1 \\ \sum_{i=1}^{n} \left| S_{xy,i} - g_i \right|, & \text{if } dir_i = 0 \\ \sum_{i=1}^{n} g_i - S_{xy,i}, & \text{if } dir_i = +1 \end{cases} \tag{4.1}$$

where $x, y \in \{1, 2\}$, $S_{xy,i}$ is the S-parameter at the i^{th} frequency, n is the number of frequencies to be optimized, g_i is the goal at the i^{th} frequency, and dir_i is the direction for optimization at the i^{th} frequency. If $dir_i = -1, 0, +1$, then the value is optimized to be less than, equal to, or greater than the goal, respectively.

GA experiments output an additional file with the suffix `-states.txt`. This is a list of evaluated states in an order that corresponds to the order of results in other files for that experiment.

Figure 4.5: Experimental setup for initial random search experiment.

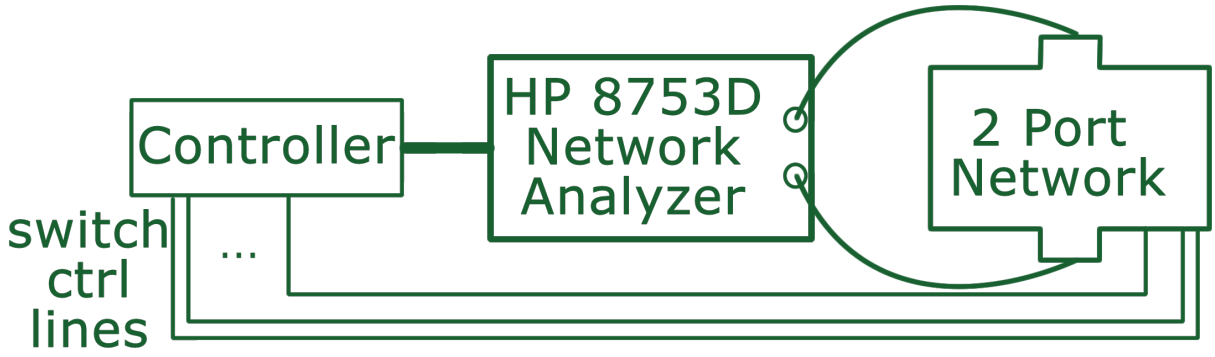

4.4 Random Search

Initial experiments used a random search to explore the capabilities of the two-port network. This random search consisted of setting a switch state and recording the S-parameters before moving onto another state.

4.4.1 Initial Investigation

Characterization of the self-structuring two-port network began by measuring all four S-parameters for thirty thousand states at twenty-six frequencies between 700 MHZ and 1.5 GHz, i.e. in 32 MHz steps. Switches were allowed to settle for 30 ms before S-parameter measurements were taken. The experimental setup is schematically shown in Figure 4.5. This experiment is stored as dataset `5-20-21-2011-combine`.

Figure 4.6 through Figure 4.13 show plots of magnitude and phase for all four S-parameters. Each frequency point from each state is plotted as a '+'. One can see that most states have an insertion loss greater than 10 dB. In the middle of the measured frequency band, $|S_{11}|$ and $|S_{22}|$ of -20 dB were easily reached while at either end of the band it was difficult to reach -10 dB. Phase values ranged from -180° to $+180^\circ$ for all S parameters except for S_{11} where the phase primarily ranged from -180° to 0°.

Figure 4.6: Random search results, S_{11} magnitude, `5-20-21-2001-combine`.

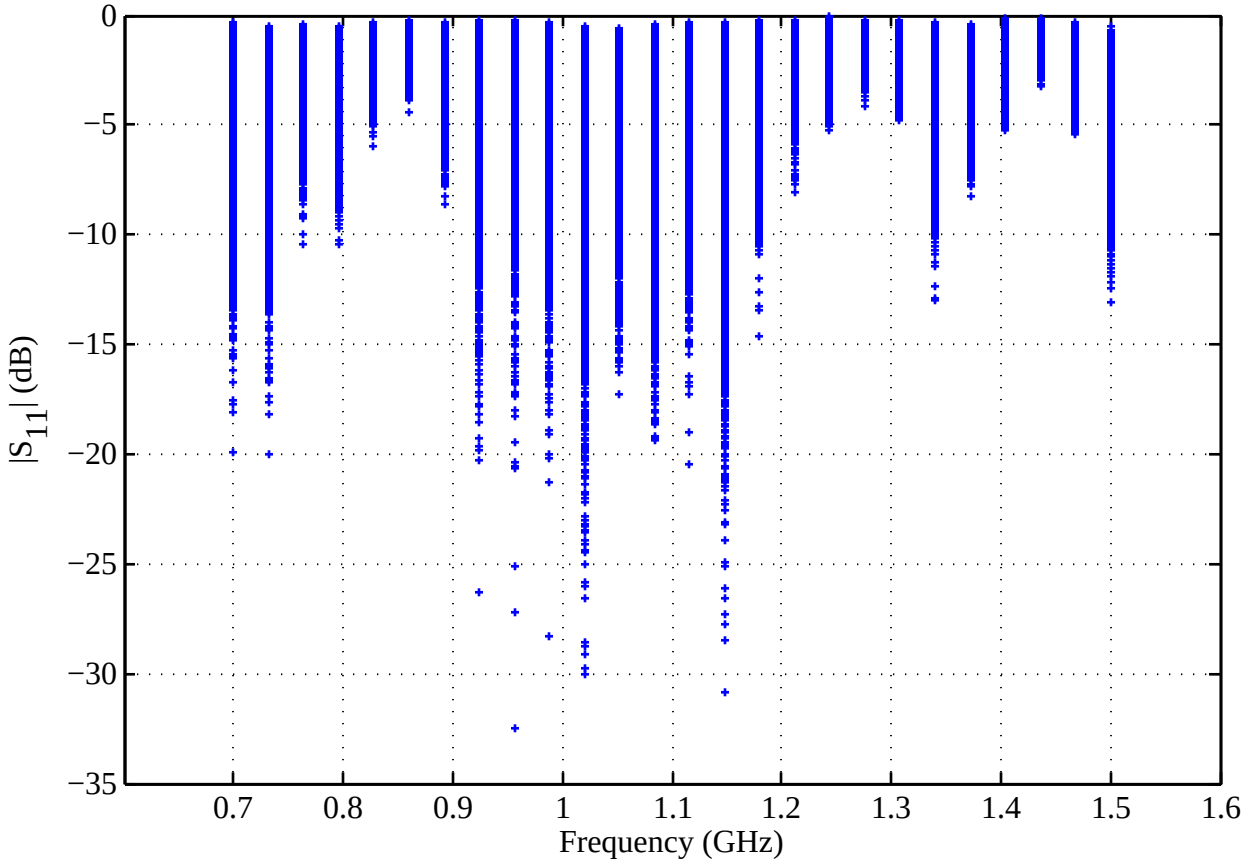

Figure 4.7: Random search results, S_{11} phase, `5-20-21-2001-combine`.

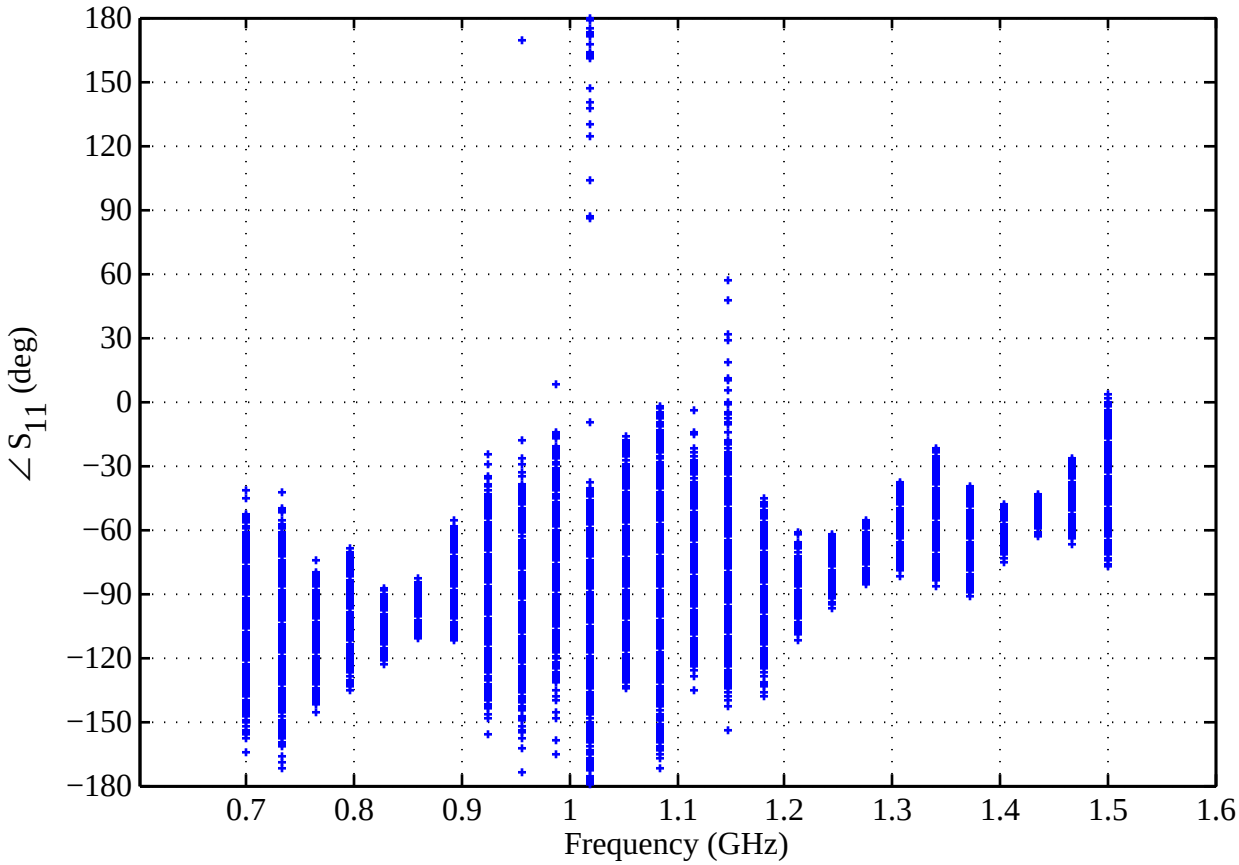

Figure 4.8: Random search results, S_{12} magnitude, `5-20-21-2001-combine`.

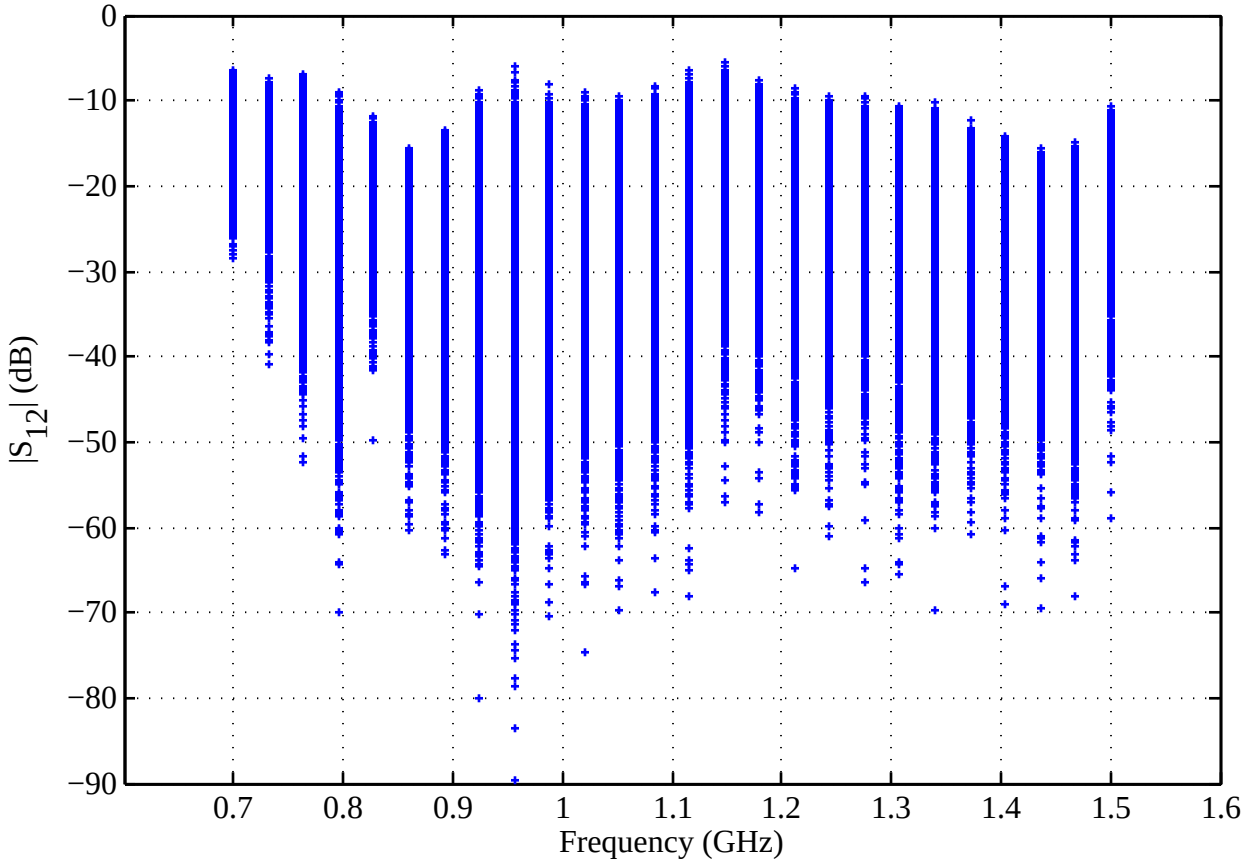

Figure 4.9: Random search results, S_{12} phase, `5-20-21-2001-combine`.

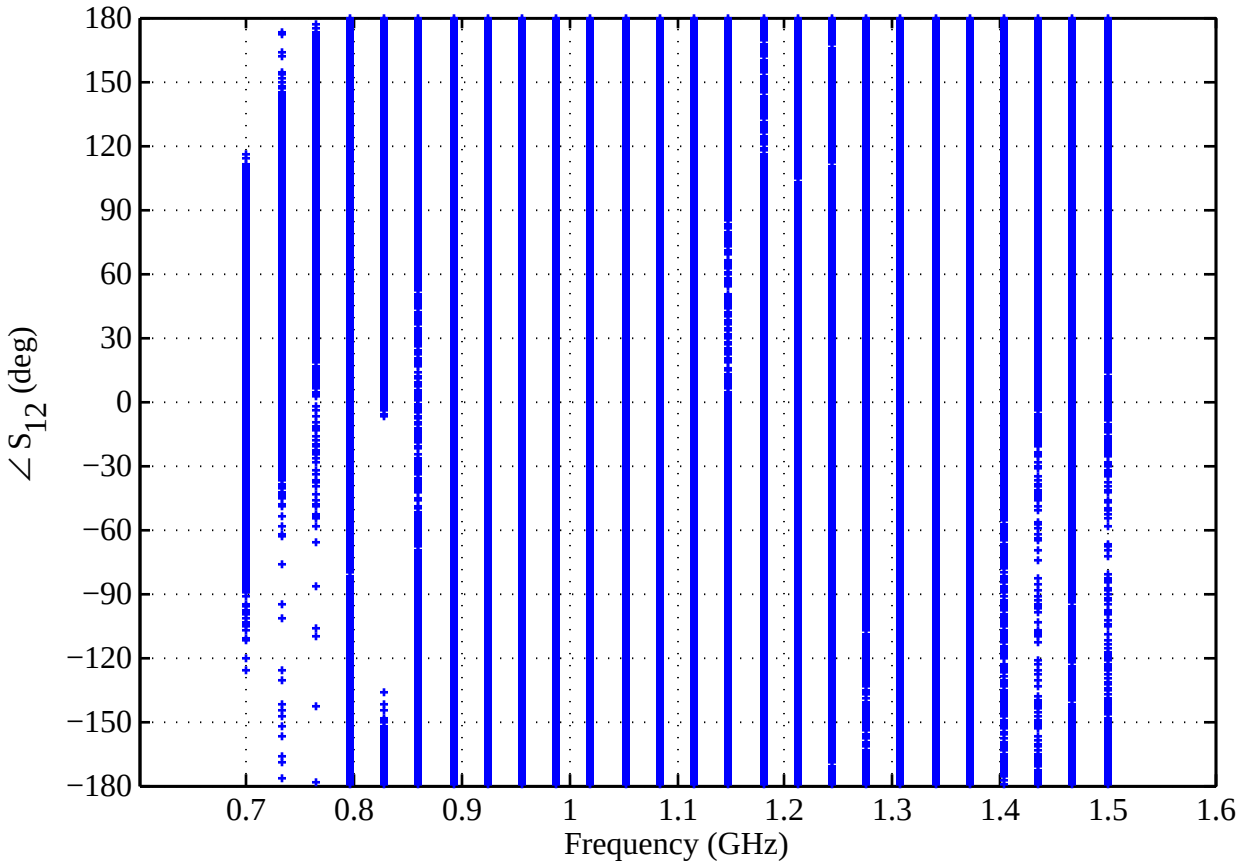

Figure 4.10: Random search results, S_{21} magnitude, `5-20-21-2001-combine`.

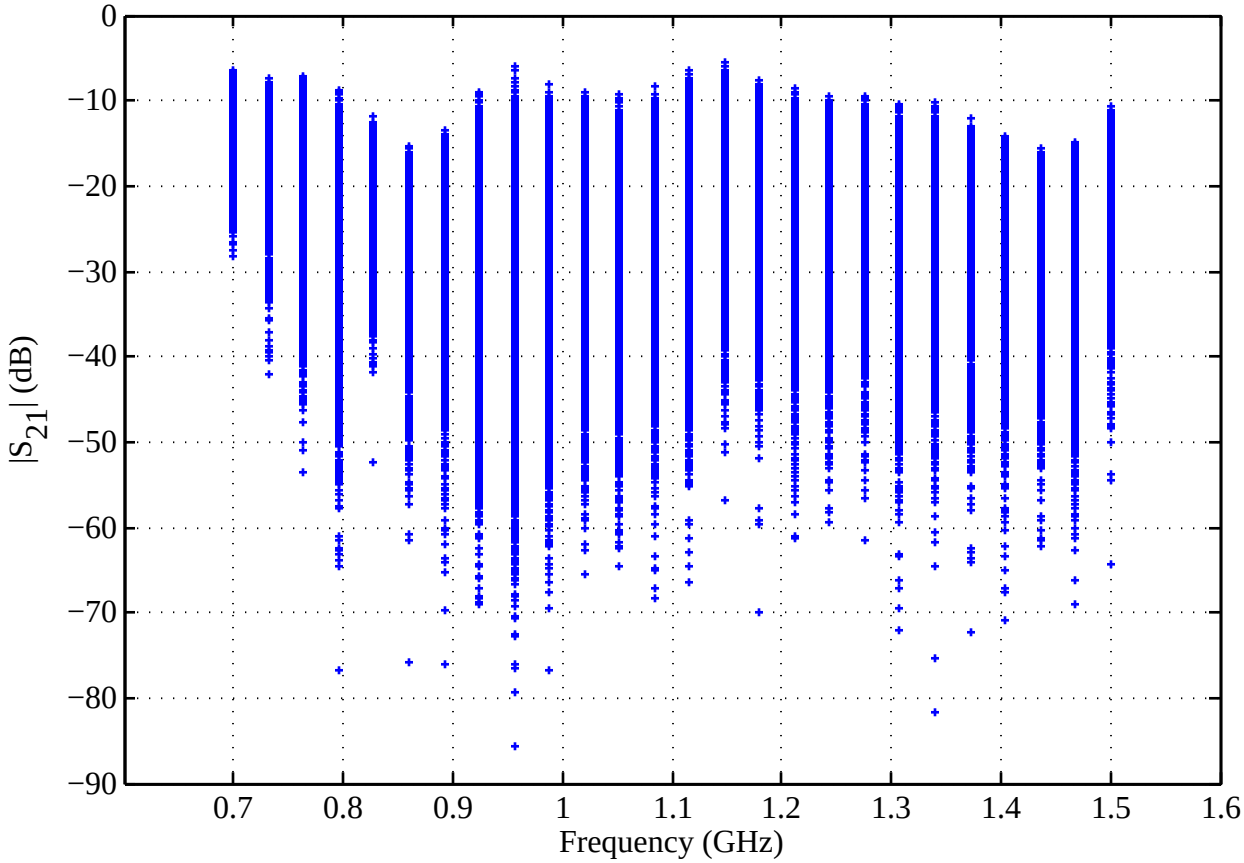

Figure 4.11: Random search results, S_{21} phase, `5-20-21-2001-combine`.

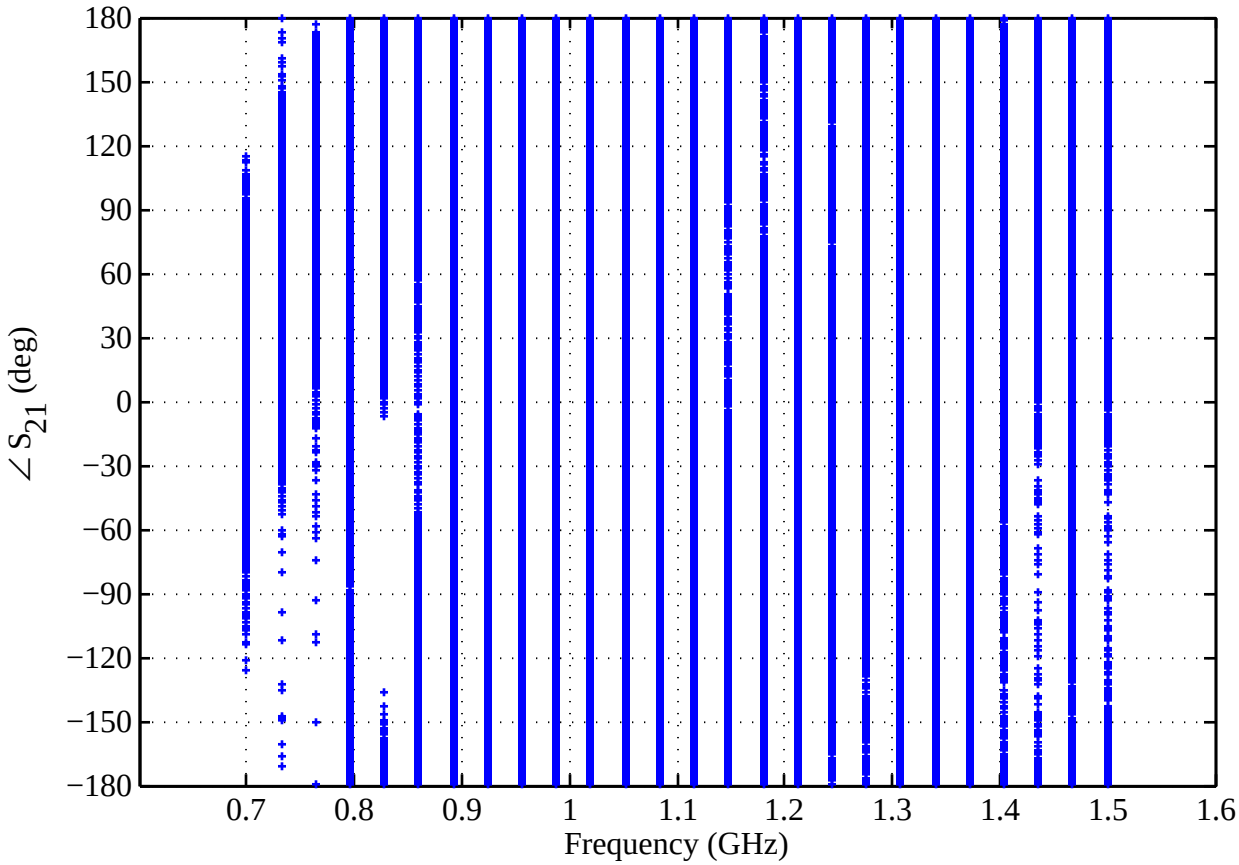

Figure 4.12: Random search results, S_{22} magnitude, `5-20-21-2001-combine`.

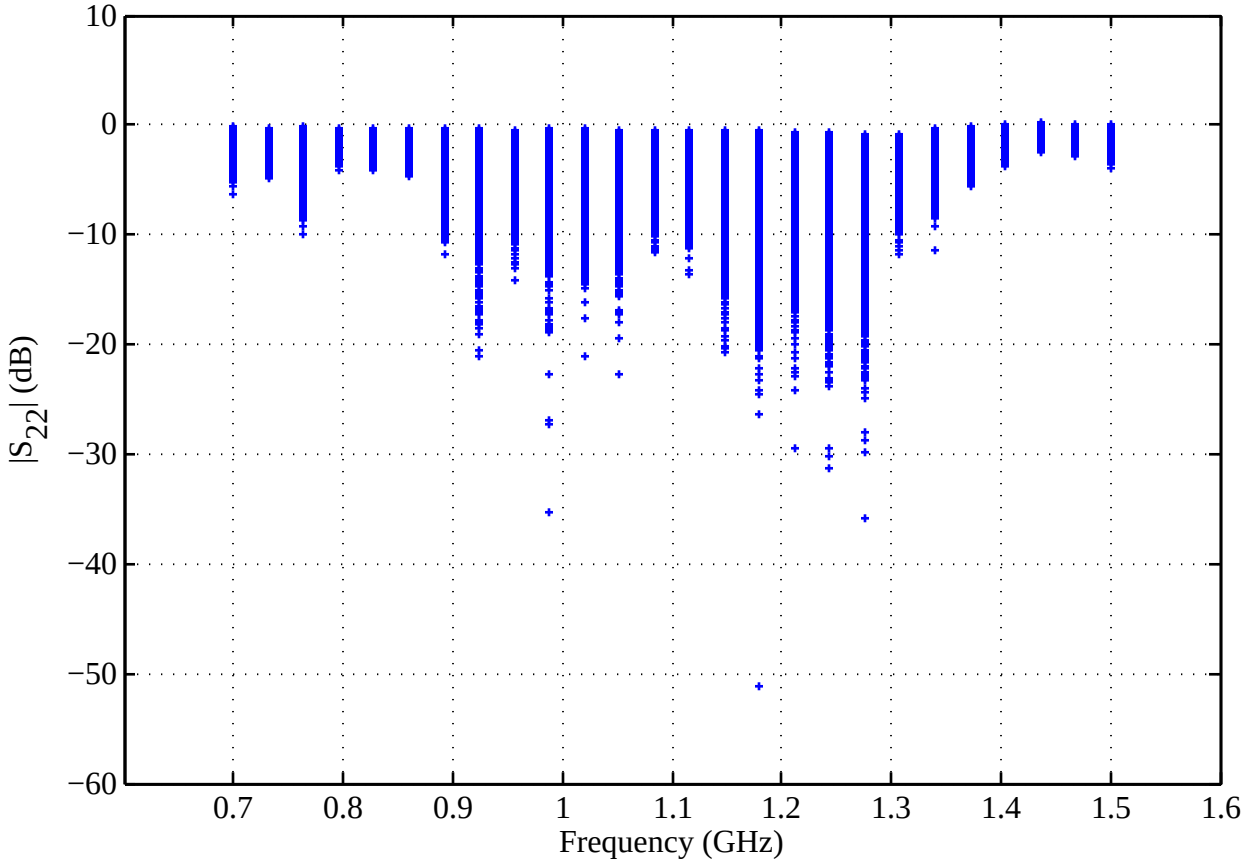

Figure 4.13: Random search results, S_{22} phase, `5-20-21-2001-combine`.

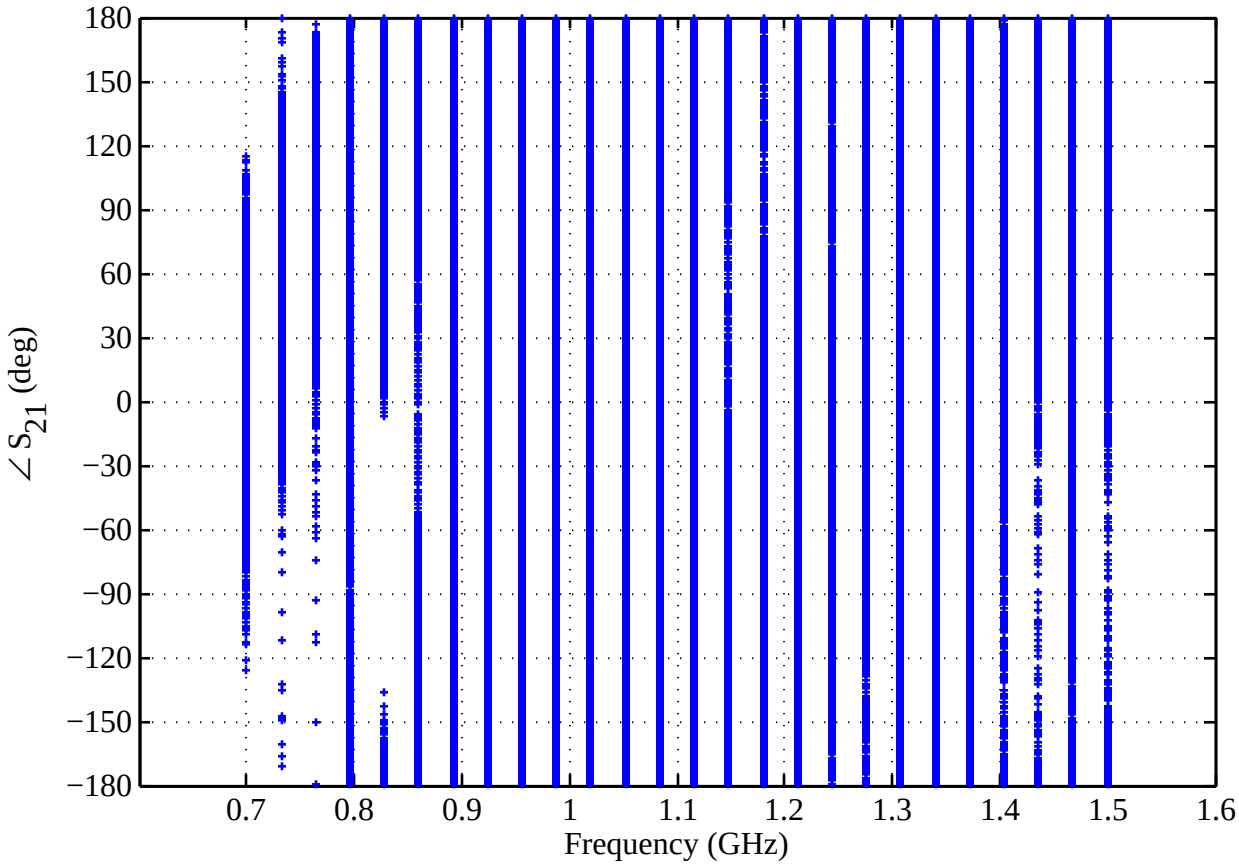

Figure 4.14: Wideband horn antenna matching experimental setup.

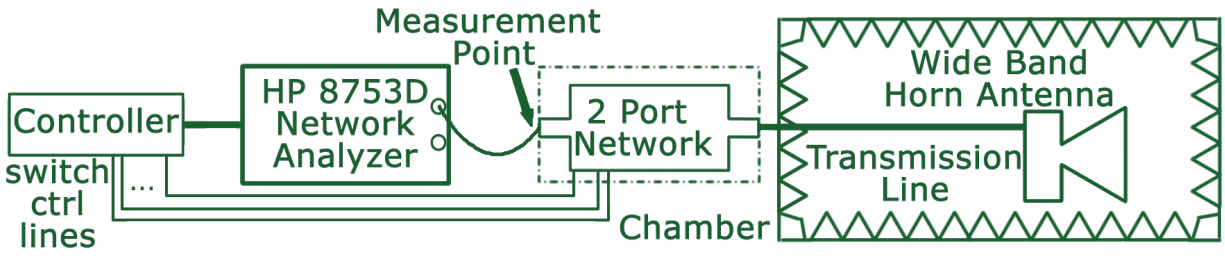

4.4.2 Matching a Wideband Horn Antenna

One possible use for a self-structuring two-port network is as a matching network. In order to explore using the network as a matching network, a American Electronic Laboratories' wideband, 500 MHz to 6 GHz, horn antenna was connected to port 2 of the self-structuring two-port network while the network analyzer was connected to port 1. The LabView random search program was used to explore all one hundred thousand states in the NIST generated pool in addition to each switch operated by itself and all switches open and closed together for a total of 100,034 states or 0.0023% of all possible states. Data was taken at twenty-six frequencies between 700 MHz and 1.5 GHz in 32 MHz steps. Switches were allowed to settle for 30 ms. The experimental setup is shown in Figure 4.14.

Figure 4.15 shows the SWR of the wideband horn antenna without the self-structuring two-port network as a solid red line, data set `5-26-1152AM-v`, and the SWR for all explored states as blue '+'s, data set `5-25-2009-1123AM-v`. Figure 4.16 only shows SWR values between one and eight. The majority of states produce an SWR that is higher than the original SWR of the antenna. It is also clearly seen that there are many states that produce an SWR below that of the unmatched antenna expect at 1.43 GHz. These results seem very promising at first glance; however, the data only shows how much power is reflected back to the analyzer from the input of the matching network. What is not known from this data is how much power is making it to the antenna versus being lost by the self-structuring two-port network.

Figure 4.15: Random search of possible states and original unmatched antenna performance.

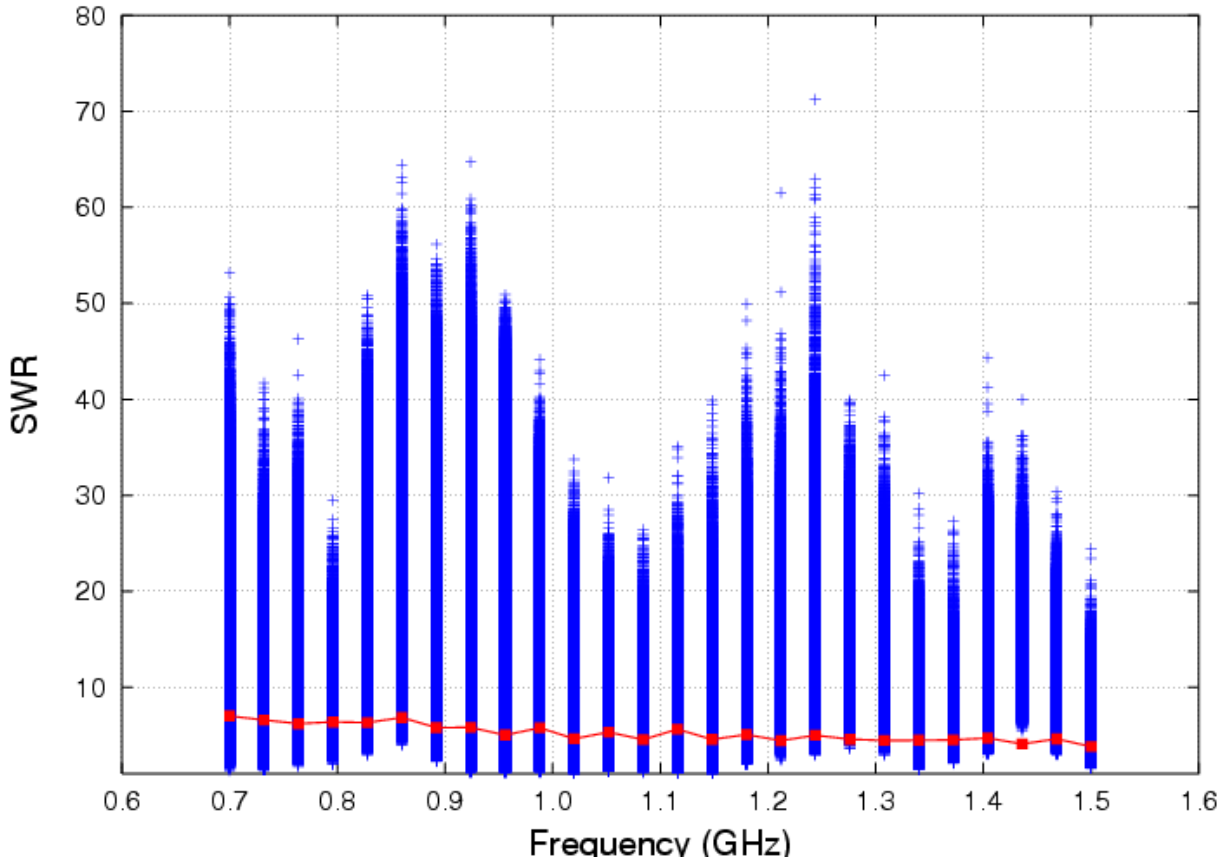

Figure 4.16: Random search zoomed in.

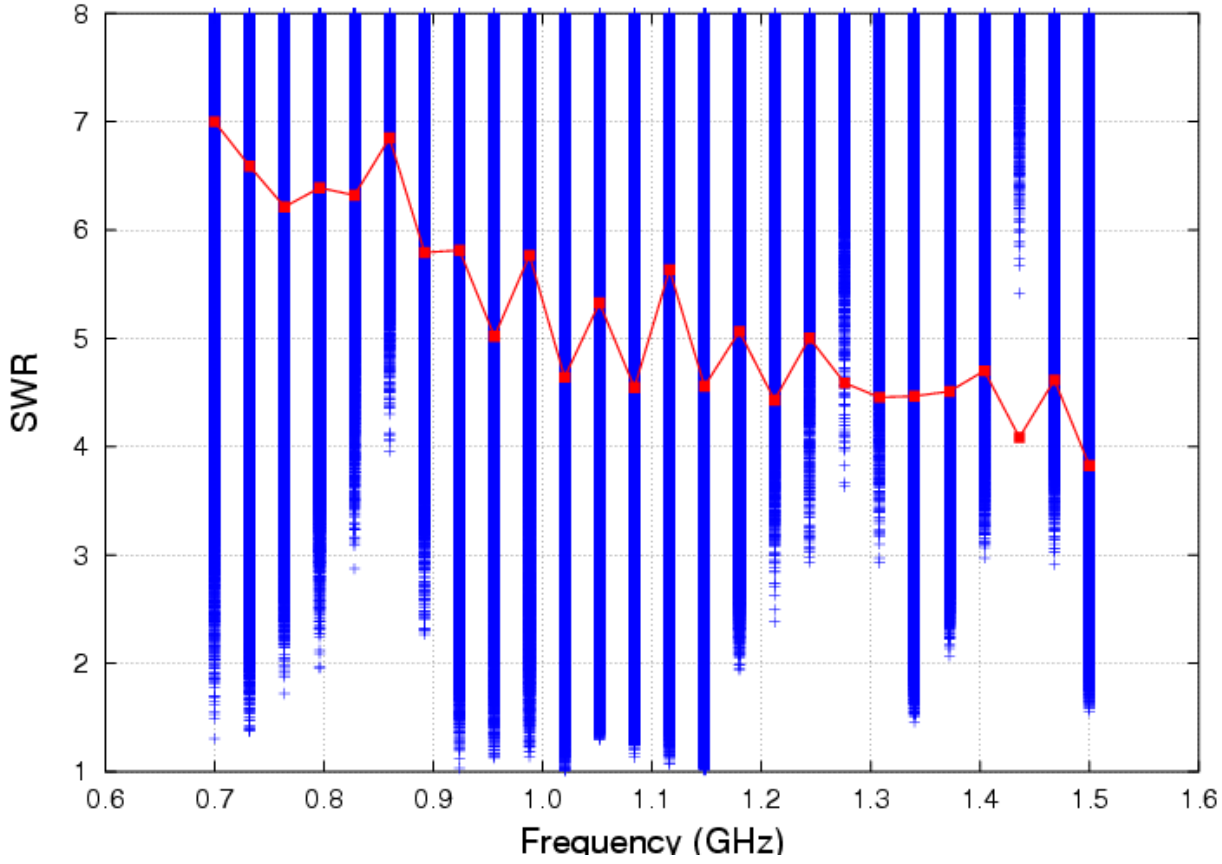

Figure 4.17: Maximum and minimum observed power balances.

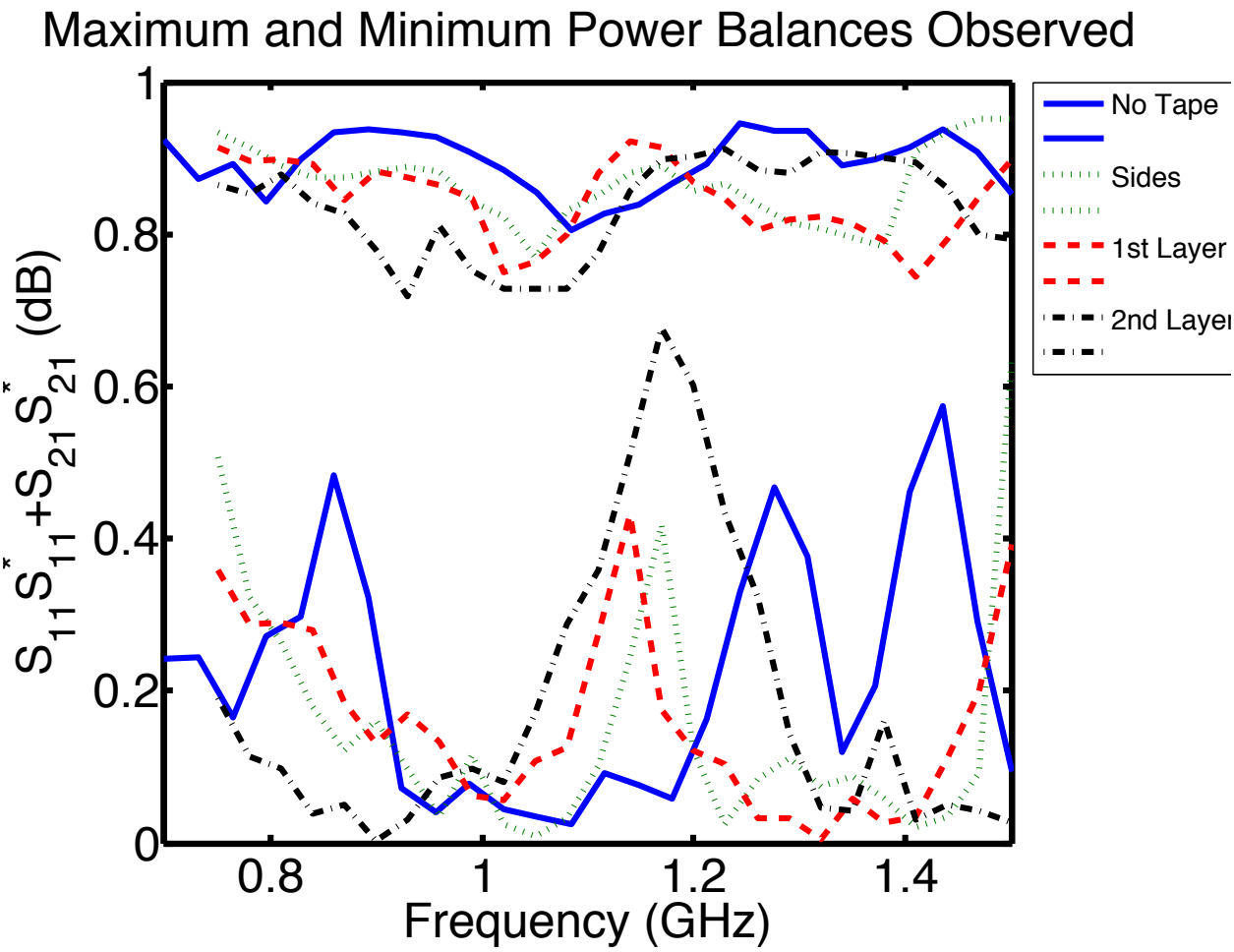

4.4.3 Power Balance of Self-Structuring Two-Port Network

The power balance for the self-structuring two-port network was calculated for each state in the initial random search dataset, dataset `5-20-21-2011-combine`. It should be noted that in this case, the power balance is calculated as $S_{11}S_{11}^{*} + S_{21}S_{21}^{*}$ giving values of zero for complete loss and one for no loss. Figure 4.17 shows the maximum and minimum values for this data set and Figure 4.18 shows the average values for this dataset as solid blue lines. The minimum and maximum values are the extremes for all measured points at each frequency, independent of other values from the same state. The other data series plotted in these figures will be discussed in Section 4.4.4.

Figure 4.18: Average observed power balances.

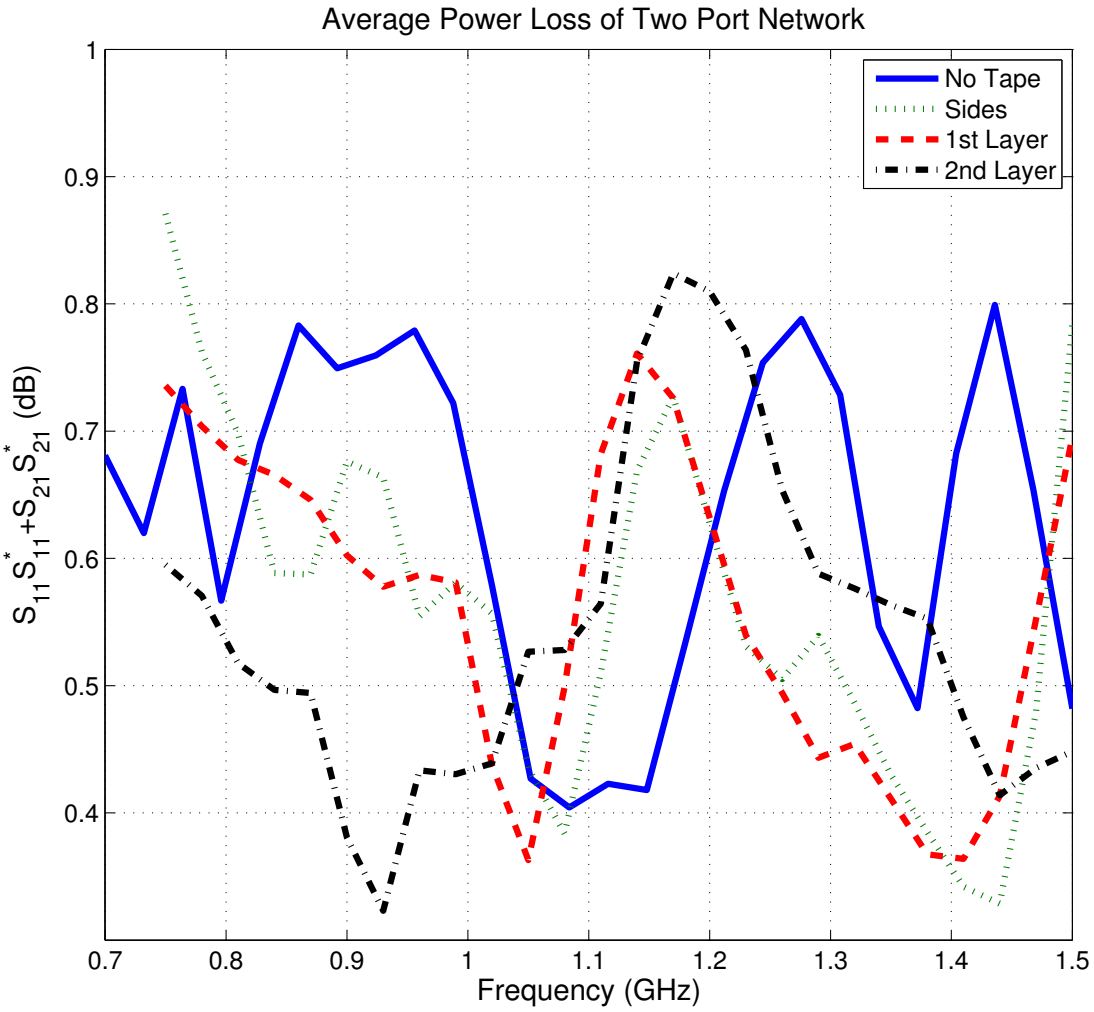

One can see that the self-structuring two-port network is on average very lossy. The best performance seen in the `5-20-21-2011-combine` dataset is a power balance of 94.6% at 1.244 GHz while the worst performance was 2.5% at 1.084 GHz.

It was unclear at this point in the research as to what loss mechanisms were playing the most significant roles.

4.4.4 Mitigation techniques

In order to increase the efficiency, and thereby, the usefulness of the self-structuring two-port network, various attempts were made to reduce the loss of the network. Because the design and construction of the network are similar to those of a patch SSA, it was thought that radiation was the primary loss mechanism. In order to reduce the radiated emissions from the network, copper tape was first applied to the edges of the board with the thought that the perimeter shorting posts were allowing the network to radiate. The maximum and minimum power balances for this case are plotted in Figure 4.17 and the average value plotted in Figure 4.18 as dotted green lines.

As the power loss was still very high, the shorting post pads and switches were insulated with electrical tape before the entire network was covered with a layer of copper tape. After measuring the losses, a second layer of tape was applied in an effort to close any gaps that might have existed in the first layer. Figure 4.19 shows the network after copper tape was applied. The maximum and minimum power balance for the first and second layer of tape are plotted as red, dash-dash lines and black, dash-dot lines, respectively, in Figure 4.17. The average values are plotted in Figure 4.18 using the same line styles.

Figures 4.17 and 4.18 suggest that the application of the copper tape does have some effect on the network; however, the effect is not a noticeable improvement with regards to the power balance of the network. This suggests that power is lost through a mechanism other than radiation.

Another possible source of power loss is common-mode current on the control cables.

Figure 4.19: Copper covered self-structuring two-port network.

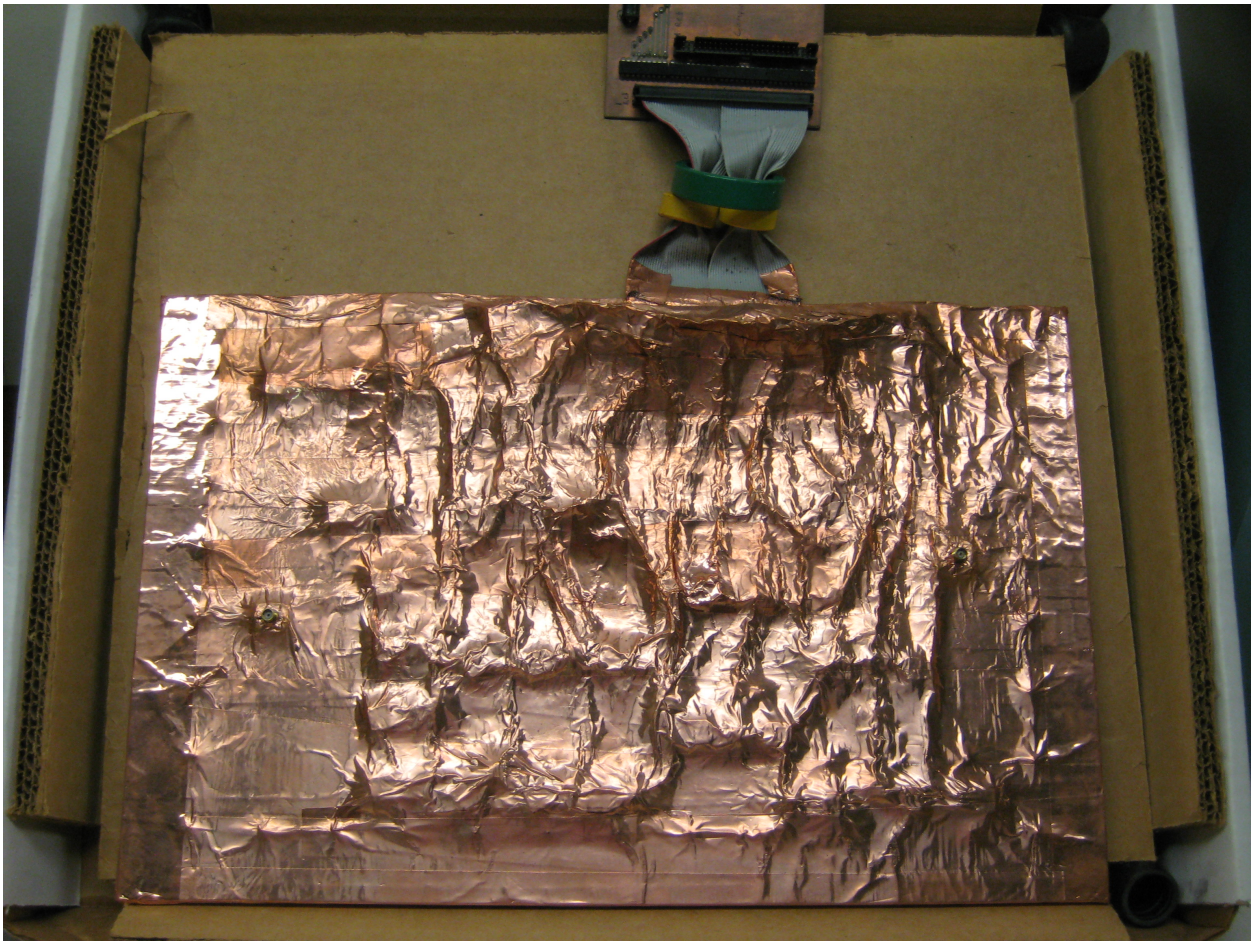

Three toroids were placed onto the control ribbon cable in order to reduce the common-mode current. The cable was split in half with a toroid placed around each half. The third toroid was placed around the entire ribbon cable. This setup can be seen at the top of Figure 4.19. Analysis of the power balance after application of the toroids did not show a significant reduction in power loss.

Given that the network is typically lossy, it is necessary to determine at what frequencies are associated with the highest loss and which are associated with the lowest loss. This was indirectly evaluated by finding the lowest reflection value ($min(\mathrm{S}_{11})$) and the highest transmission values ($max(\mathrm{S}_{21})$) at each frequency across all measured states. Figure 4.20 shows the best transmission and reflection values found in a random search, dataset `6-23-2010-090PM-v`. The difference between theses two values is shown in Figure 4.21. Values greater than 0 suggest that the network transfers more power than it reflects. The largest values tend to be below 3 GHz with two relatively wideband areas from 750 MHz to 1 GHz and 1.9 GHz to 2.2 GHz. These bands are most useful when transmission is a desirable characteristic of the two-port network.

4.5 Genetic Algorithm Based Search

Keeping in mind that the network is fairly lossy, several experiments were undertaken to optimize the self-structuring two-port network as a matching network with various loads and as an attenuator. The LabView based GA described in Section 4.3.3 was used. The parameters and results from the GA optimizations are shown in Table 4.2.

Figure 4.20: Best S_{21} and S_{11}.

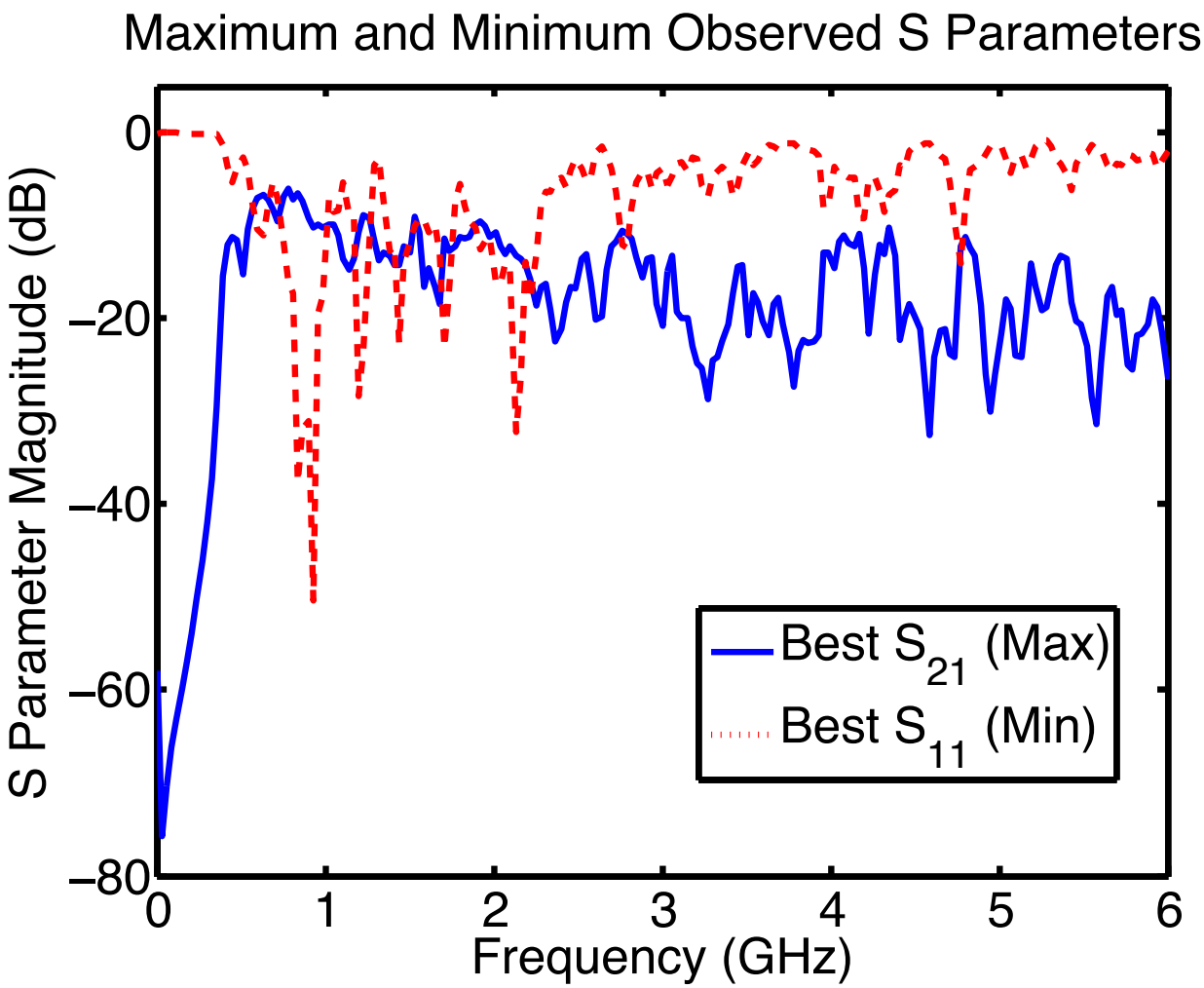

Figure 4.21: Difference between maximum transmission and minimum reflection.

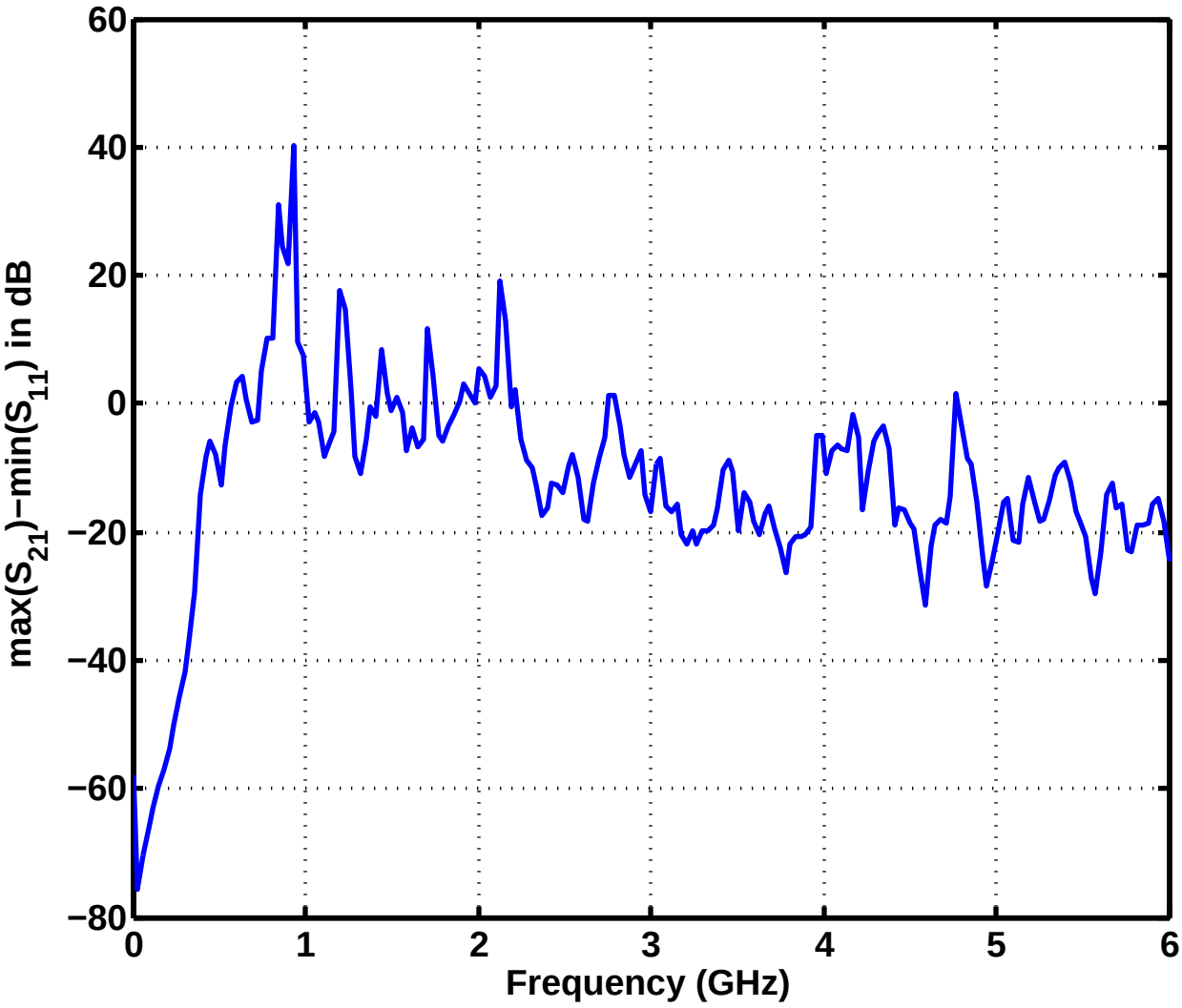

Table 4.2: Genetic algorithm search parameters and results.

Dataset	Best State	Cost	Mean, μ (dB)	St. Dev., σ (dB)	Minimum (dB)	Maximum (dB)	Freq (MHz)	Goal (dB)	Keep Top %	Mutation Prob.	Num. Evaluated
6-30-2010-950PM-v-config.txt	0xFED66FBE	96.67	-10.79	1.72	-13.16	-6.93	750-1000	-2	0.10	0.75	16174
7-1-2010-147AM-v-config.txt	0xCE299D61	100.59	-11.14	3.07	-16.14	-7.84	1400-1500	-2	0.10	0.75	16251
7-2-2010-231PM-v-config.txt	0x07BA1662	487.50	-46.32	2.71	-51.87	-43.50	1400-1500	-2	0.10	0.75	14773
7-2-2010-851PM-v-config.txt	0x87373662	484.45	-46.04	2.48	-51.05	-43.67	1400-1500	-2	0.15	0.80	14317
7-6-2010-1032AM-v-config.txt	0x5001C3DE	619.82	-58.35	5.47	-65.81	-48.63	1900-2200	-2	0.10	0.70	17401
7-8-2010-155PM-v-config.txt	0x86B8D4F2	636.14	-59.83	3.08	-64.45	-55.16	1400-1500	-2	0.10	0.70	16079
7-8-2010-613PM-v-config.txt	0x3F6D640A	8.35	-19.85	1.08	-21.57	-17.70	750-1000	-20	0.10	0.75	16293

- All GA searches were optimized at eleven, linearly spaced frequency points in the specified range.
- All GA searches used a population size of 250 individuals and a maximum of 200 generations.
- New individuals were created using random pairing, mutated one bit.
- The top 10% of the population was not mutated.
- All searches reached the maximum number of generations before reaching the goal cost.

4.5.1 Optimized transmission

To begin optimization, each port of the self-structuring two-port was connected to the network analyzer as shown in Figure 4.5. Two optimizations were performed, the first from 750 MHz to 1 GHz (dataset `6-30-2010-950PM-v`) and the second from 1.4 GHz to 1.5 GHz (dataset `7-1-2010-147AM-v`). A goal of -2 dB was set for all frequency points.

Figure 4.22 shows one of the lowest cost states, `0xFED66FBE`. This figure shows that the goal of -2 dB across the band was not met. As this state was found through optimization, this results suggests that the network will typically have about 10 dB of insertion loss. This particular state had an average insertion loss of $\mu = -10.79$ dB and a standard deviation of $\sigma = 1.72$ dB. A similar result is seen in Figure 4.23. This response shows a larger range of transmission values than in the lower frequency band; however, the general value of 10 dB remains ($\mu = -11.14$ dB, $\sigma = 3.07$ dB).

These results point to the manufactured self-structuring two-port network having an insertion loss of at least 10 dB for frequencies below 1.6 GHz. The author believes that when optimized as in these results, losses caused by changes in the states are reduced leaving only losses that result from the construction and physical properties of the network. This conclusion is supported by the random search results as shown in Figure 4.10. The lowest insertion loss found across the band during the random search was roughly 10 dB.

4.5.2 Spiral Antenna

In the previous section, the self-structuring two-port network was used to match 50 Ω loads on each port. In order to provide a more challenging and realistic experiment, a spiral antenna was connected to Port 2 of the network as shown in Figure 4.25. A picture of the spiral antenna used in this experiment is shown in Figure 4.24. Port 1 of the network analyzer was connected to Port 1 of the network while Port 2 of the analyzer was connected to the wideband horn antenna used in Section 4.4.2.

The solid blue lines in Figure 4.26 and Figure 4.27, show the transmission through the

Figure 4.22: Optimized transmission with 50 Ω loads, 750 MHz to 1.0 GHz, dataset `6-30-2010-950PM-v`.

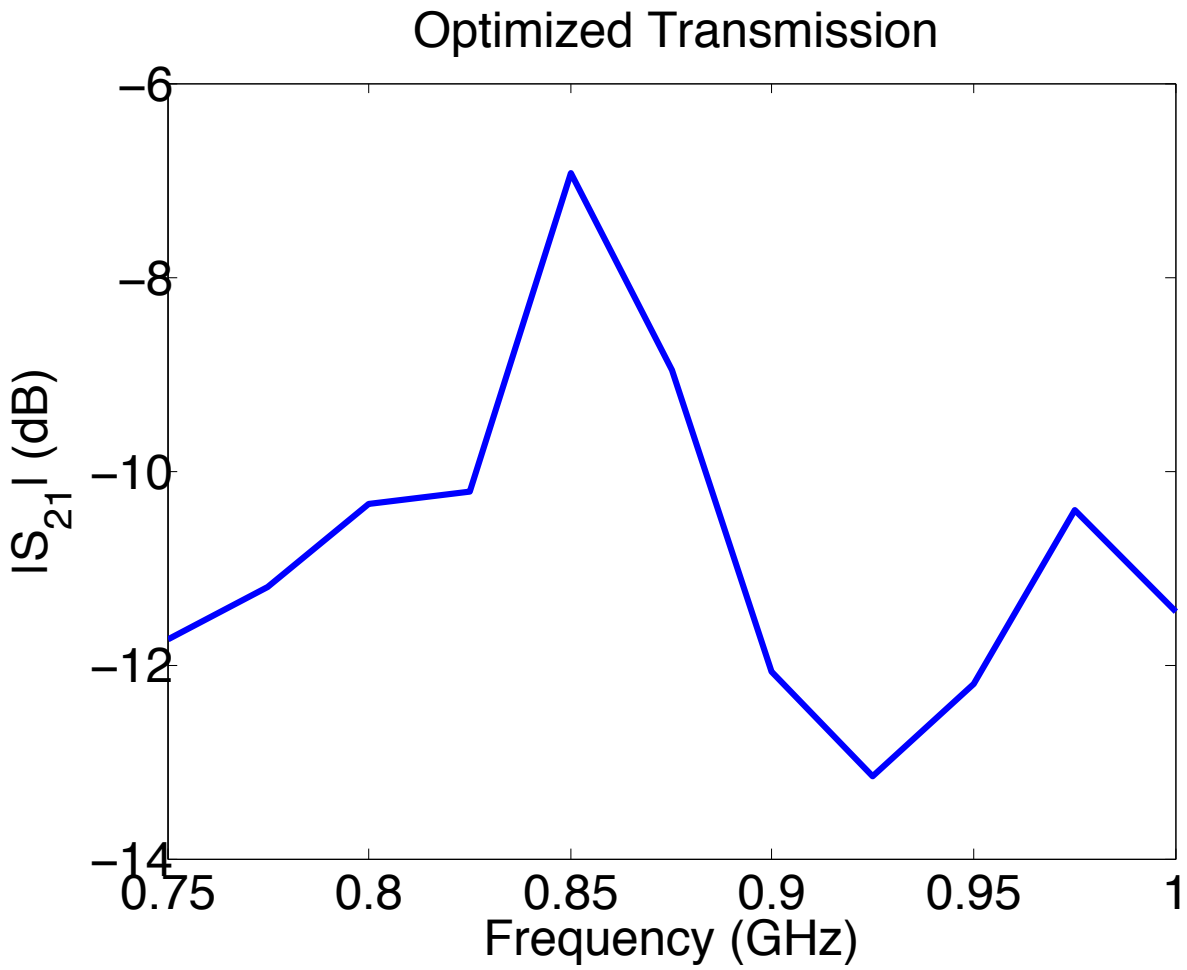

Figure 4.23: Optimized transmission with 50 Ω loads, 1.4GHz to 1.5 GHz, `7-1-2010-147AM-v`.

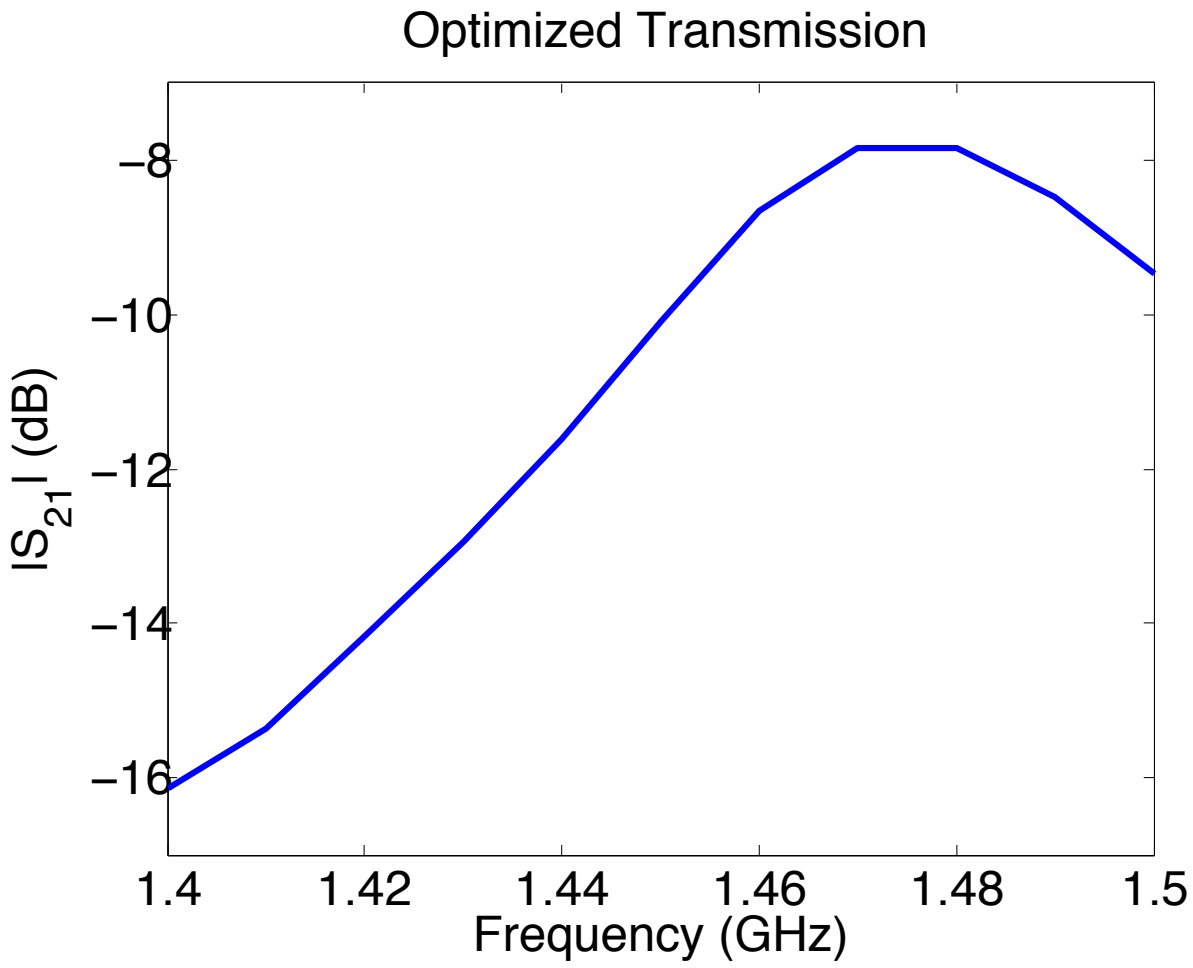

Figure 4.24: Spiral antenna used for input impedance matching experiments. Large numbers on the ruler are inches.

Figure 4.25: Experimental setup schematic for spiral antenna measurements and optimization.

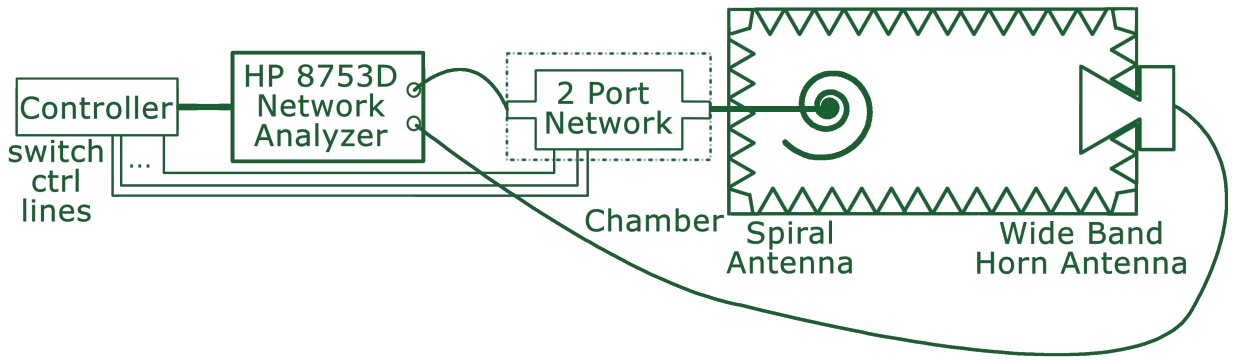

system when the spiral antenna was connected directly to the analyzer. The dashed lines in these figures show the transmission when the self-structuring two-port network was optimized for transmission. Figure 4.26 is from two different optimizations, dataset `7-2-2010-231PM-v` is Matching State 1 using state `0x07BA1662` and dataset `7-2-2010-851PM` is Matching State 2 using state `0x87373662`. Figure 4.27 uses `7-6-2010-1032AM-v` and shows the transmission for state `0x5001C3DE`. One can see that even after optimization, the insertion loss of the network is still relatively high.

4.5.3 Dipole Antenna Transmission

Further transmission testing was conducting using a dipole antenna. The experimental setup is similar to that used for the spiral antenna in Section 4.5.2 and is shown in Figure 4.28.

Results of the optimization at 1.4 to 1.5 GHz, dataset `7-8-2010-155PM-v`, are shown in Figure 4.29. As was seen before, the network exhibits an insertion loss of roughly 10 dB. The original transmission shape was closely followed. This is promising because it suggests that the network is able to be used as a matching network albeit with a fairly consistent insertion loss.

Figure 4.26: Spiral antenna transmission optimization results at 1.4 GHz to 1.5 GHz.

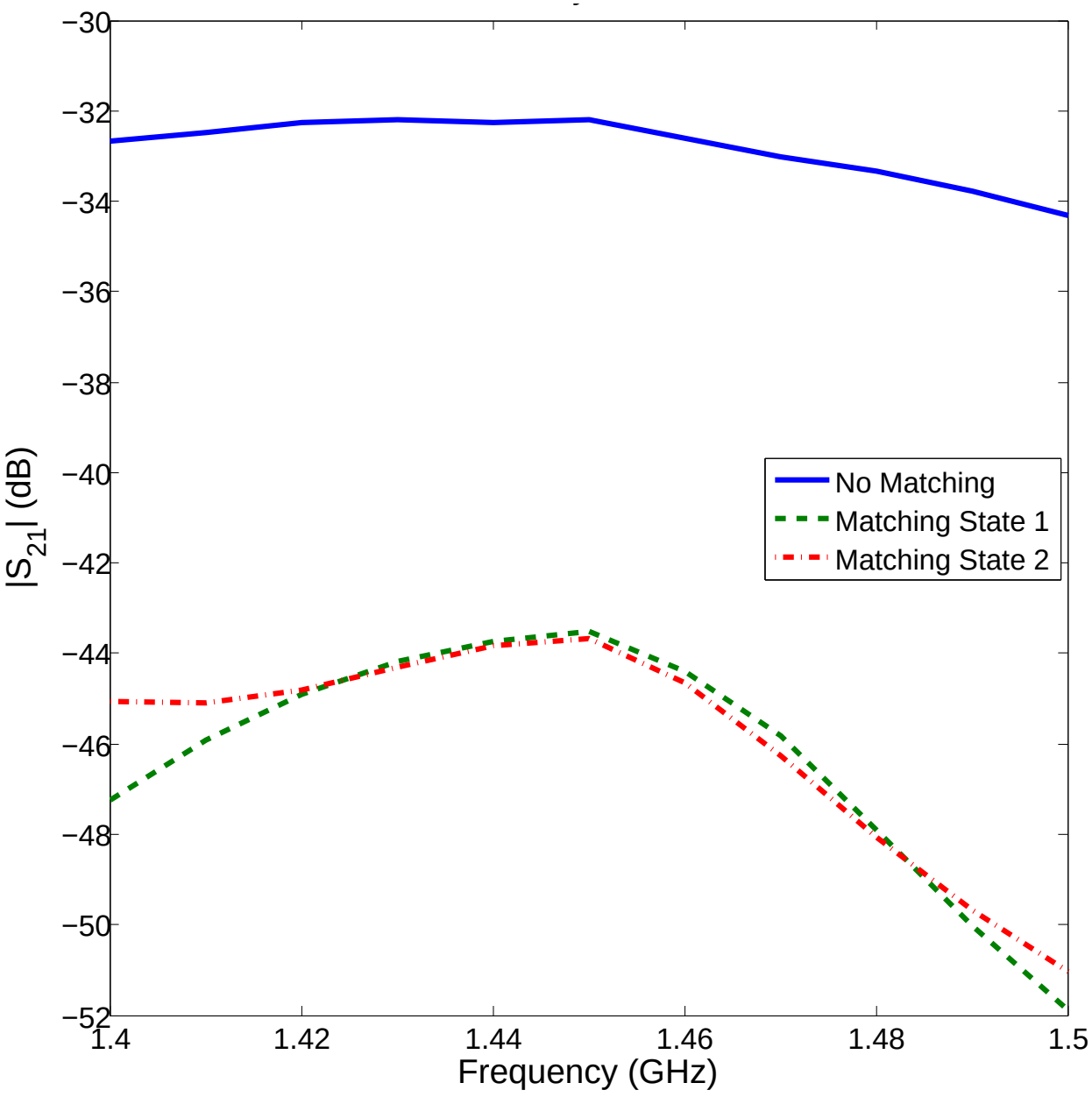

Figure 4.27: Spiral antenna system transmission, 1.9 GHz to 2.2 GHz, dataset `7-6-2010-1032AM-v`.

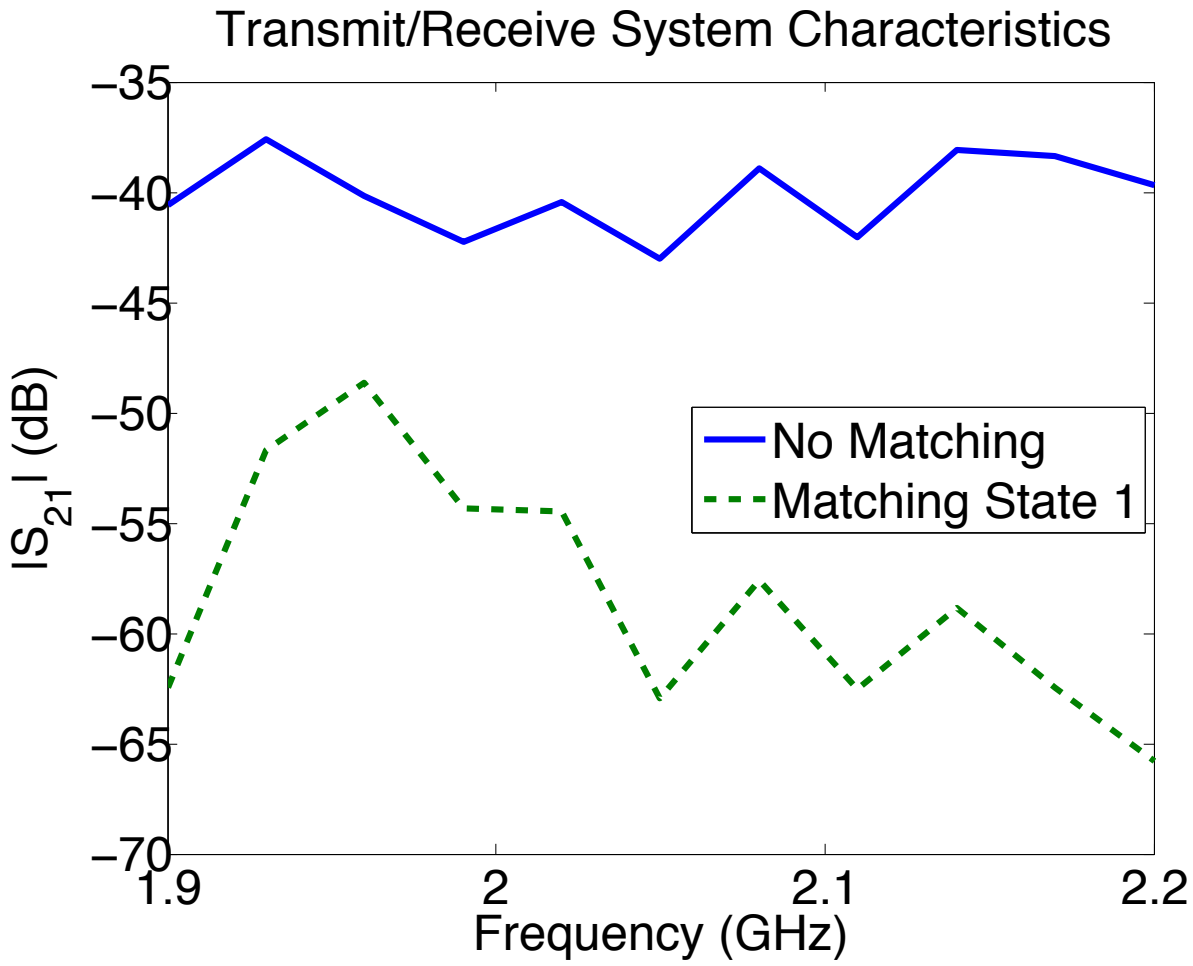

Figure 4.28: Experimental setup schematic for dipole antenna measurements and optimization.

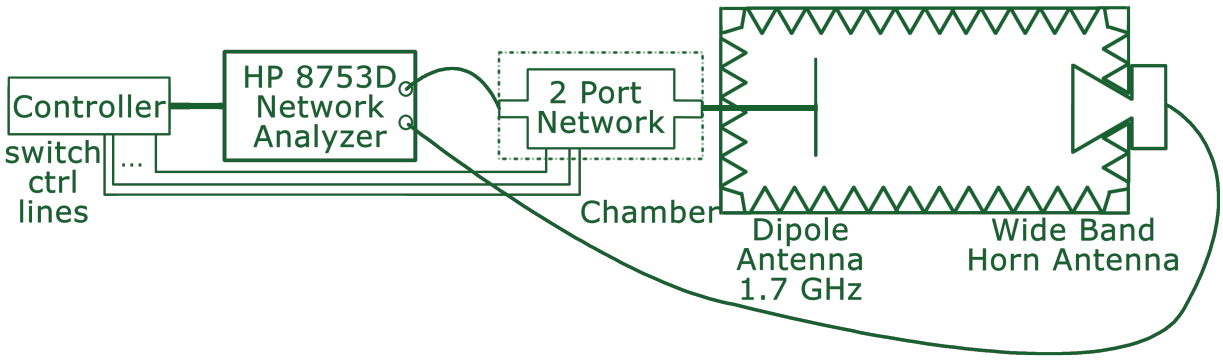

Figure 4.29: Dipole antenna throughput results, dataset `7-8-2010-155PM-v`.

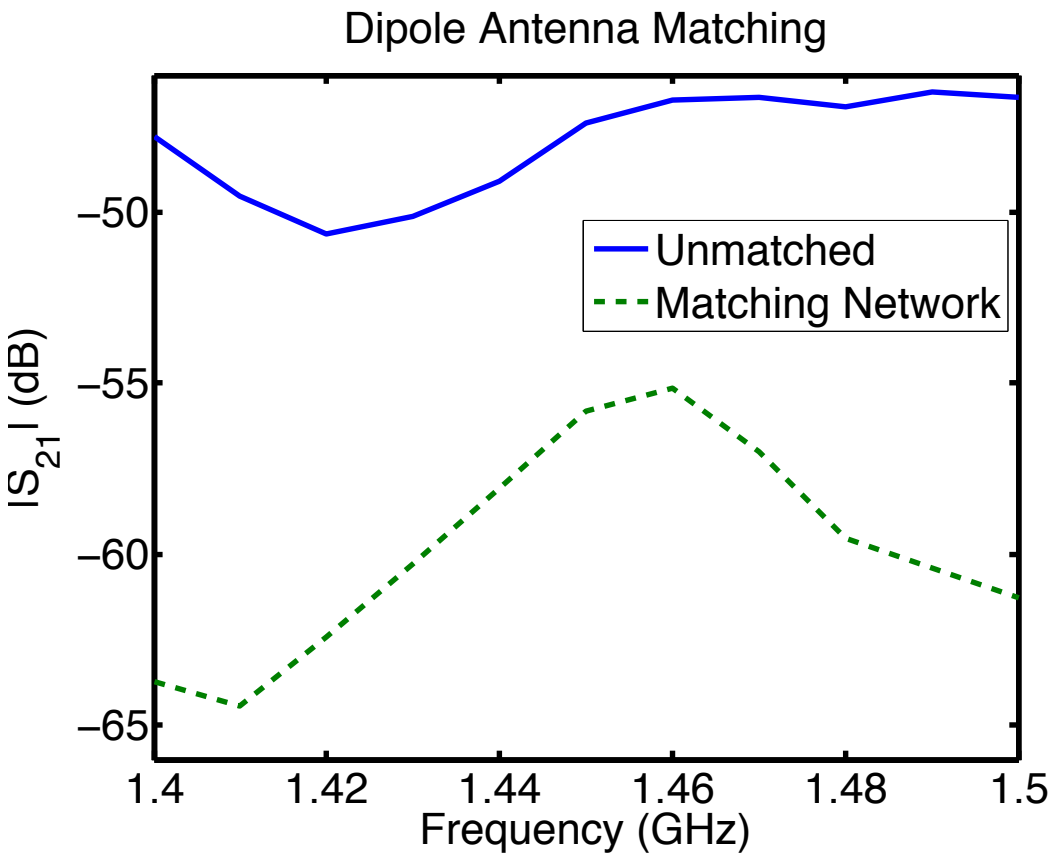

Figure 4.30: 20 dB attenuator optimization results.

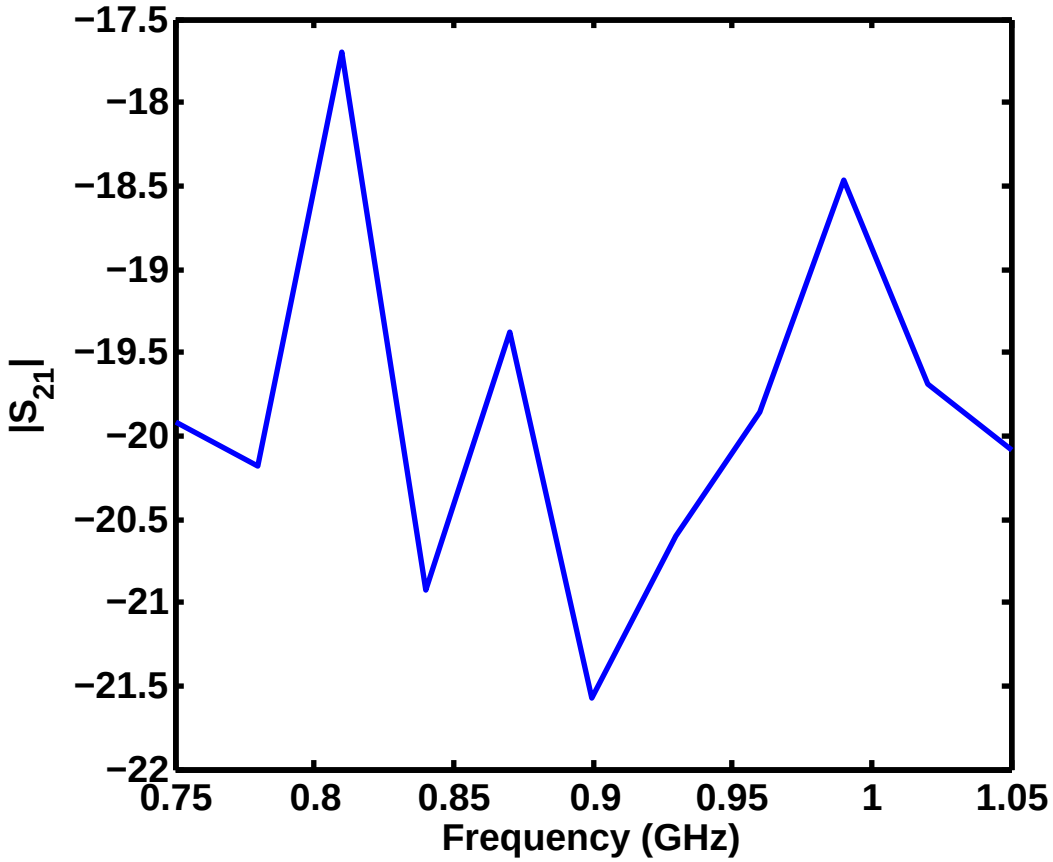

4.5.4 Attenuator

A self-structuring two-port network may be used to create other types of devices besides matching networks. The use as an adjustable attenuator was evaluated using the setup shown in Figure 4.5. An attenuation value of 20 dB was set as the goal. This value was selected because it was larger than the typical insertion loss of the self-structuring two-port network.

Figure 4.30 shows the final optimized state, `0x3F6D640A`. One can see that after optimization, an attenuator with 20±2 dB was created. In this frequency range, the average value is $\mu = 19.85$ dB with a standard deviation of $\sigma = 1.08$ dB.

Optimizations to create a filter were not carried out.

4.6 Switch Investigation

The high loss of power observed in experiments, even after mitigation attempts, dictated that further loss mechanisms be investigated. Simulations, as described in Section 3.2 were used for computational investigation. Experimentally, the power behavior of the Coto switches was investigated.

4.6.1 Individual Switch Properties

A 50 Ω microstrip line was manufactured to measure the S-parameters of the switches. The circuit board with the switch used for testing is shown in Figure 4.31. A +5 V_{DC} power supply was used to open and close the switch. The full two port S-parameters for the switch were measured in both open, Figure 4.32, and closed, Figure 4.32, states. The power balance for an open and closed switch is plotted in Figure 4.34.

These results suggest that a significant amount of power is being lost in the switch. It is believed that these losses come mostly from coupling into the control wires and into the relay coil inside the switch. As power loss is additive, the sum of these losses added across thirty-two switches has the potential to drastically effect the performance of the self-structuring, two-port network.

4.6.2 Switch Removal from Experiment

Due to the relatively high losses observed in the relay switches, the effect of these switches while connected to the network was investigated. First the copper covering was removed and the two port was measured in an all open state. These results are plotted in Figure 4.35. Next, the switches were disconnected from the shorting posts, but left connected to the control wires and the top side of the board. This configuration was then measured and the results are shown in Figure 4.36. The power balance from this experiment is shown in Figure 4.37. The difference between the unsoldered switches and the open state is shown in

Figure 4.31: Switch testing microstrip setup.

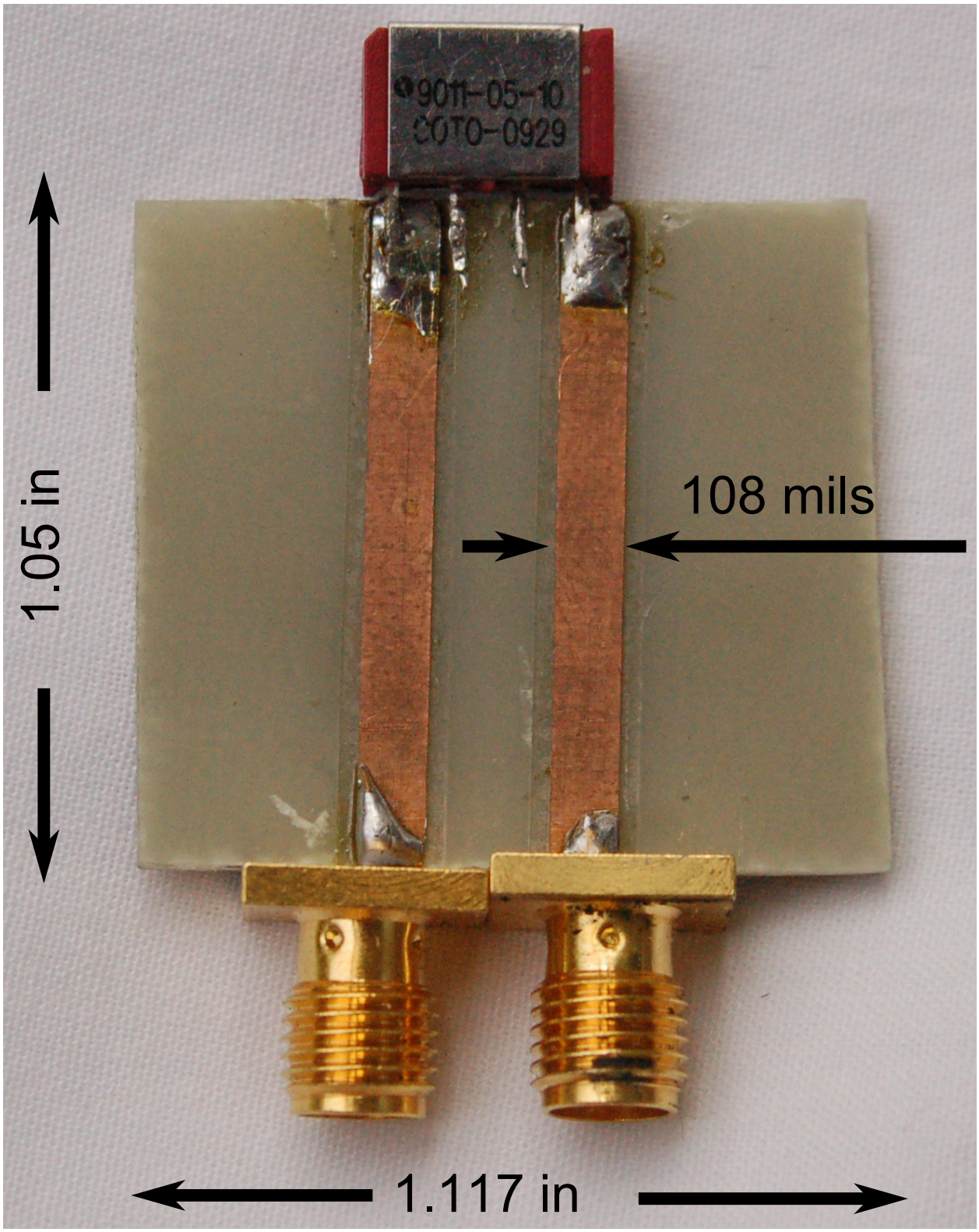

Figure 4.32: S-parameters of an opened relay switch.

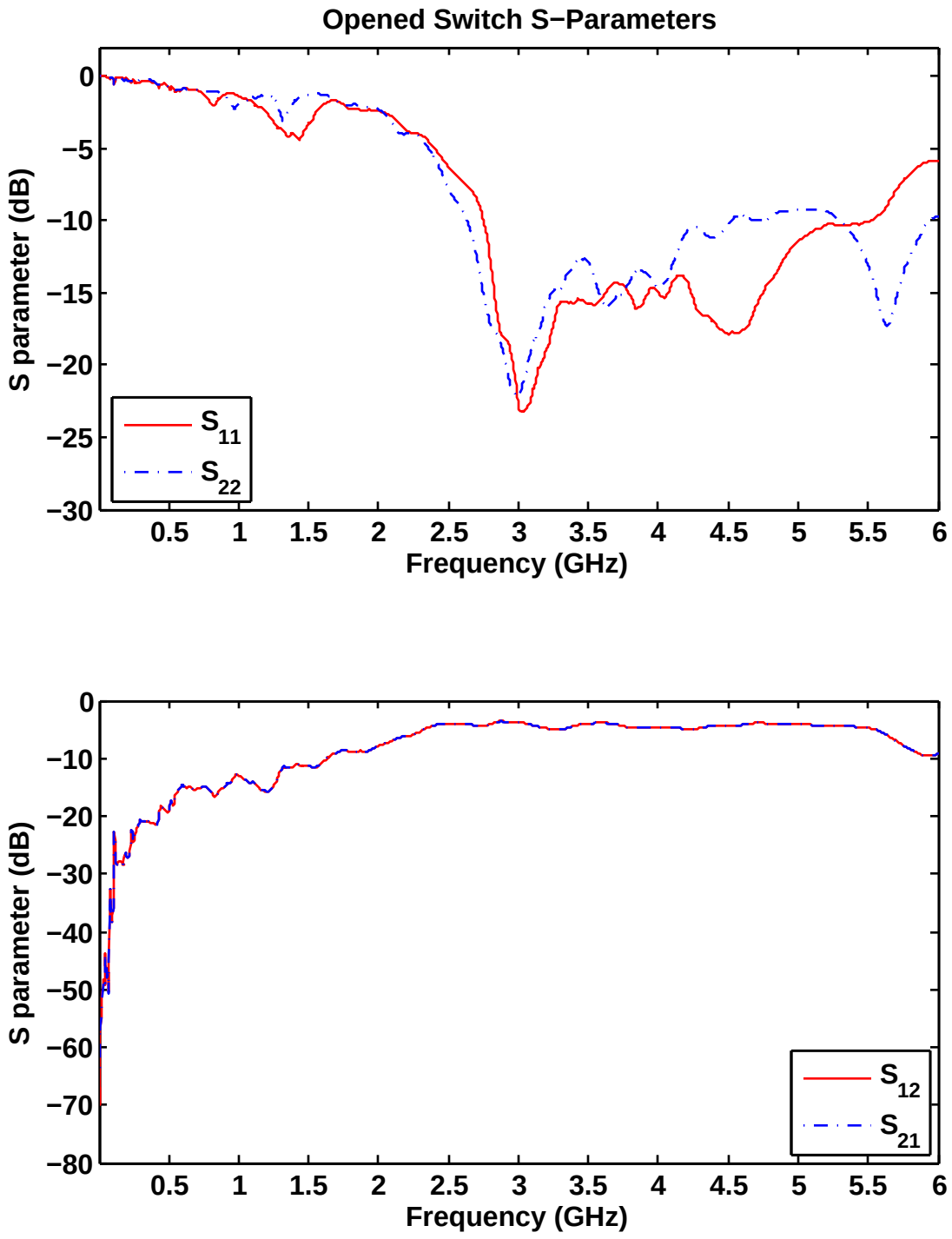

Figure 4.33: S-parameters of a closed relay switch.

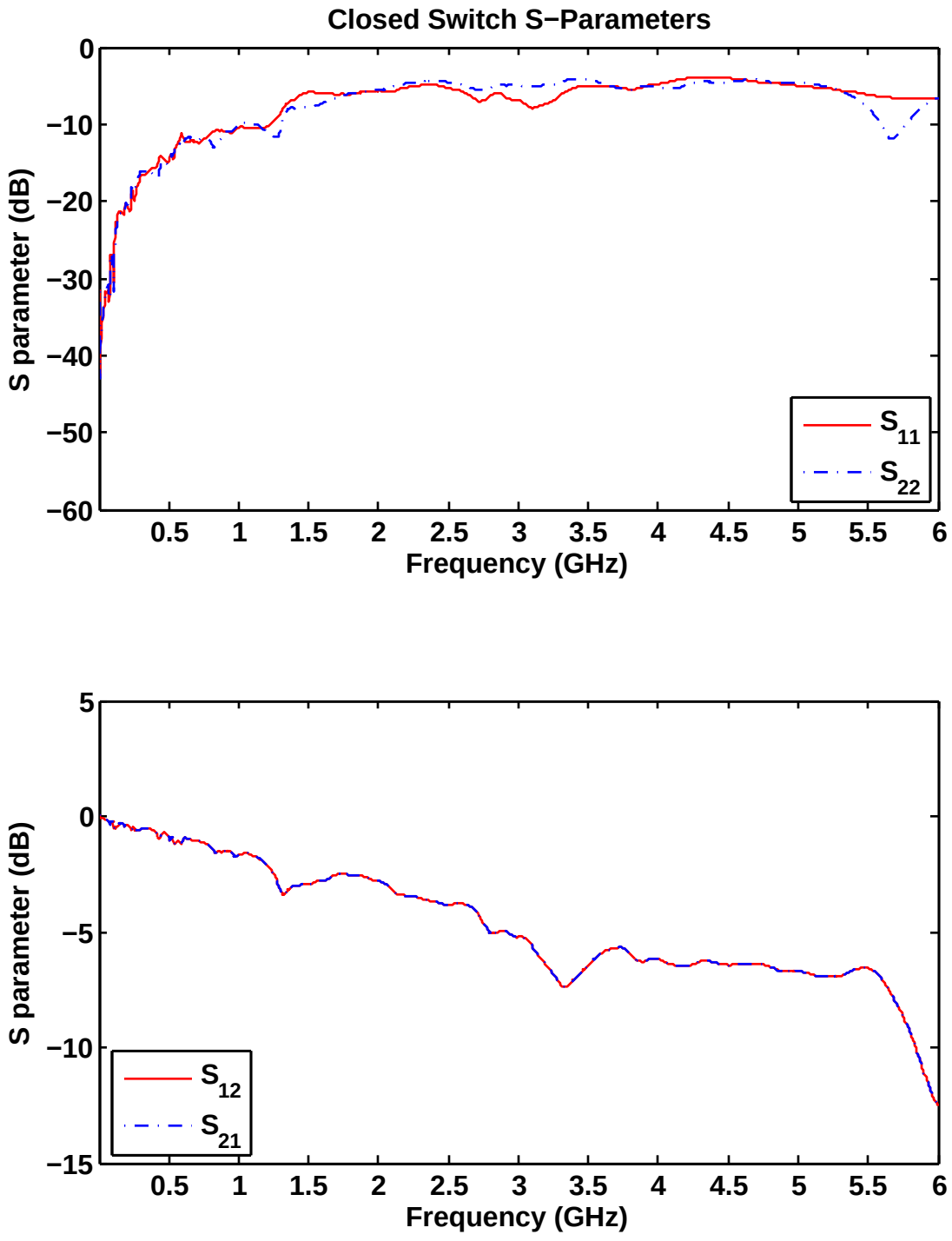

Figure 4.34: Power balance of a relay switch.

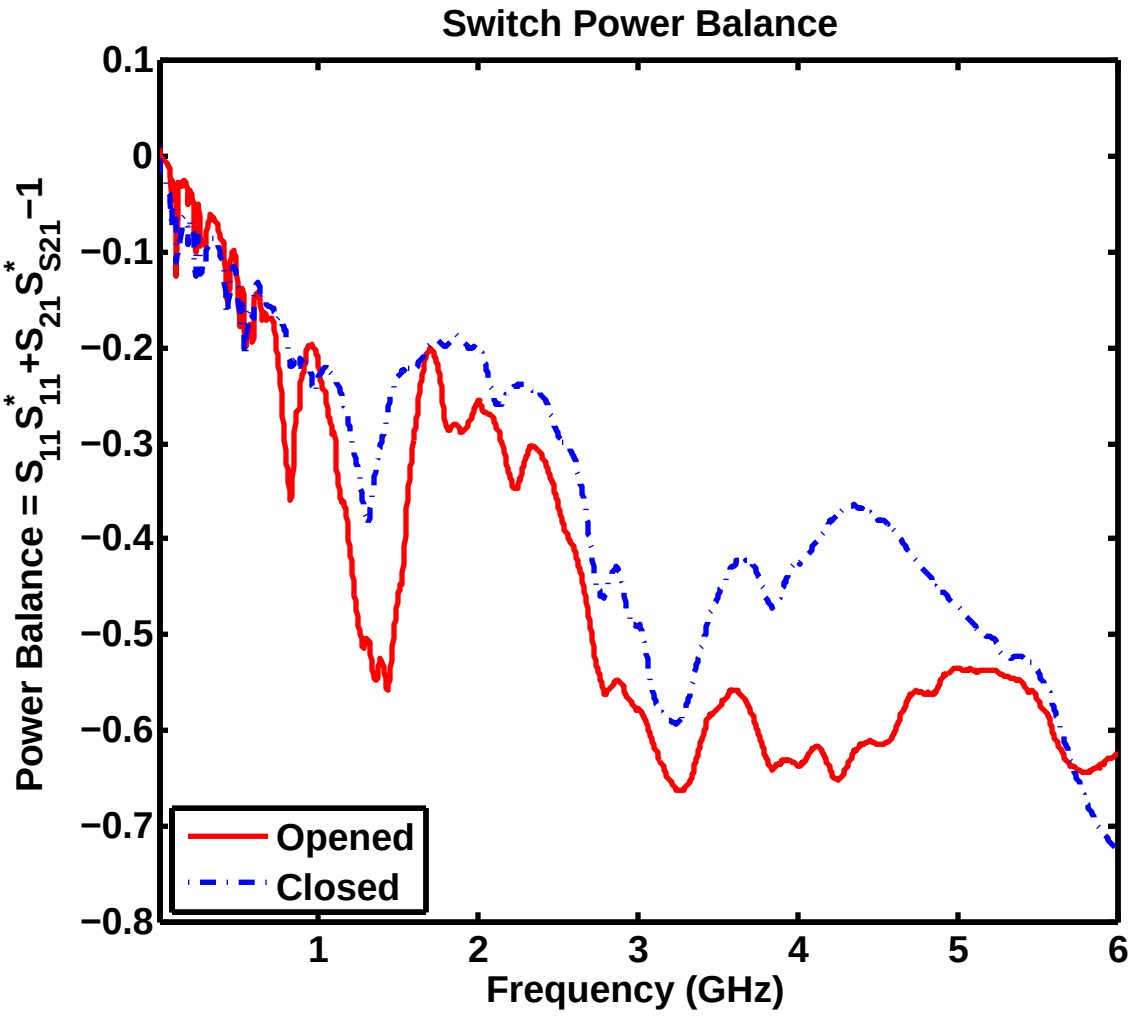

Figure 4.35: S-parameters for state 0x00000000.

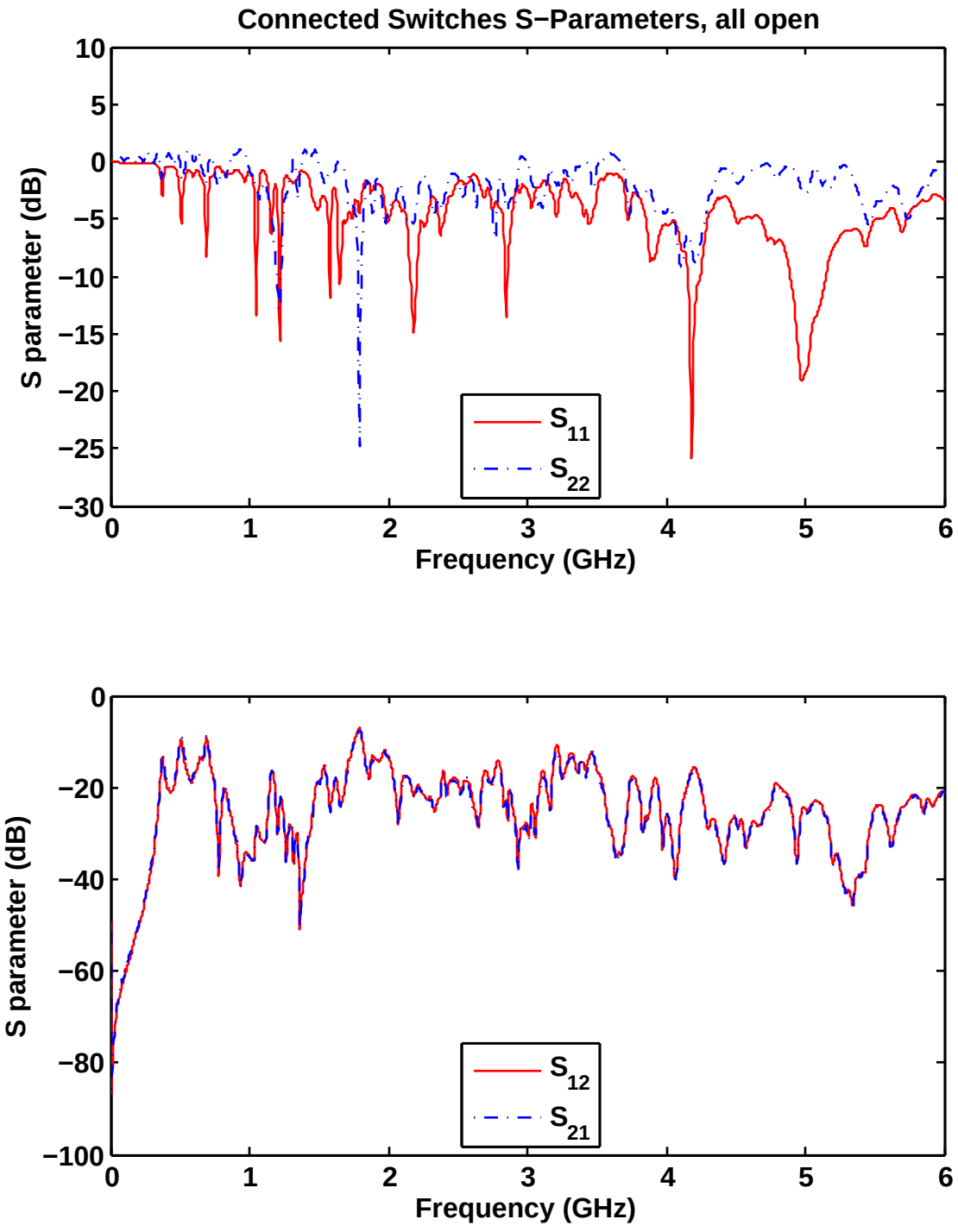

Figure 4.36: S-parameters with switches unsoldered from shorting posts.

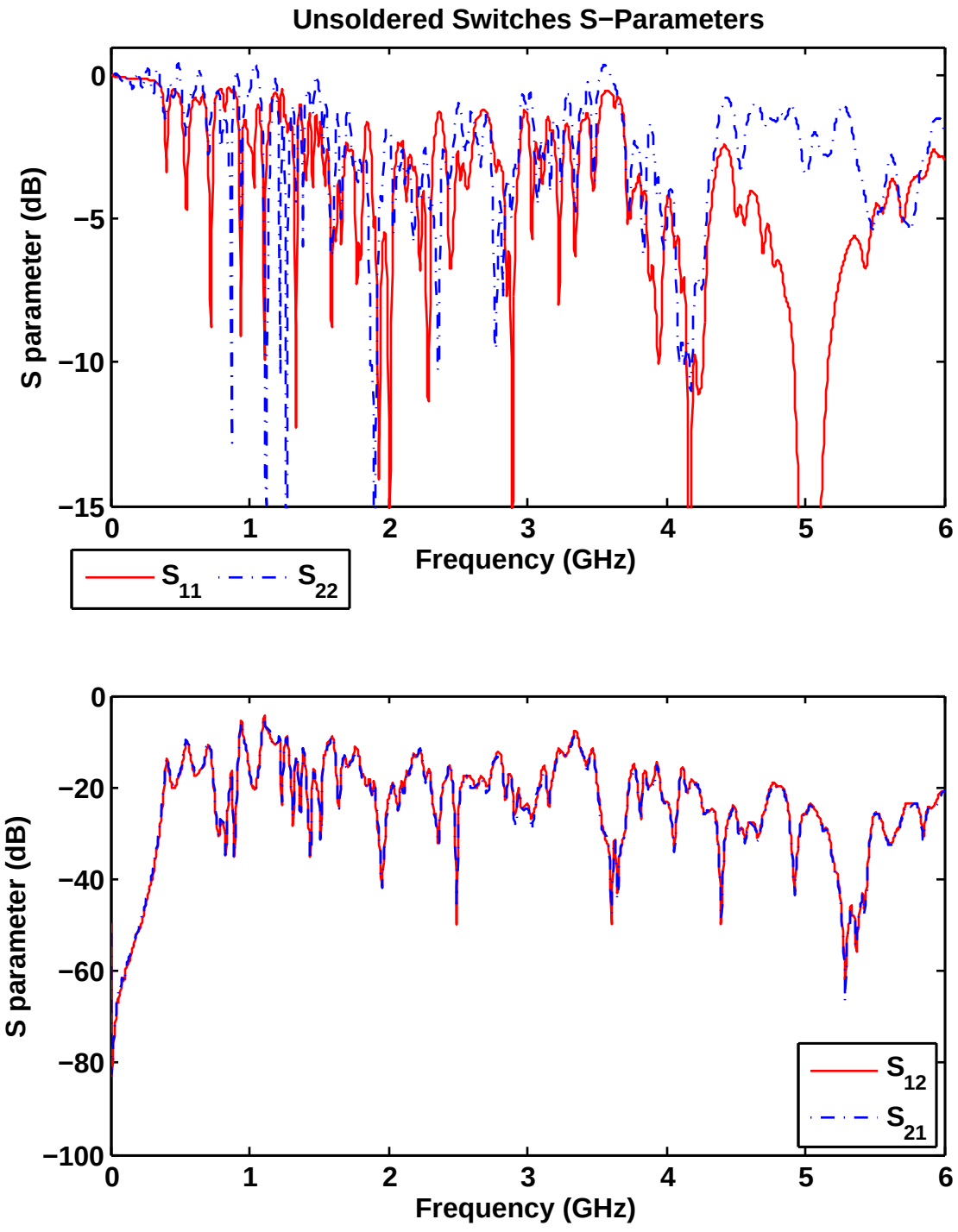

Figure 4.37: Power balance for switches unsoldered from shorting posts.

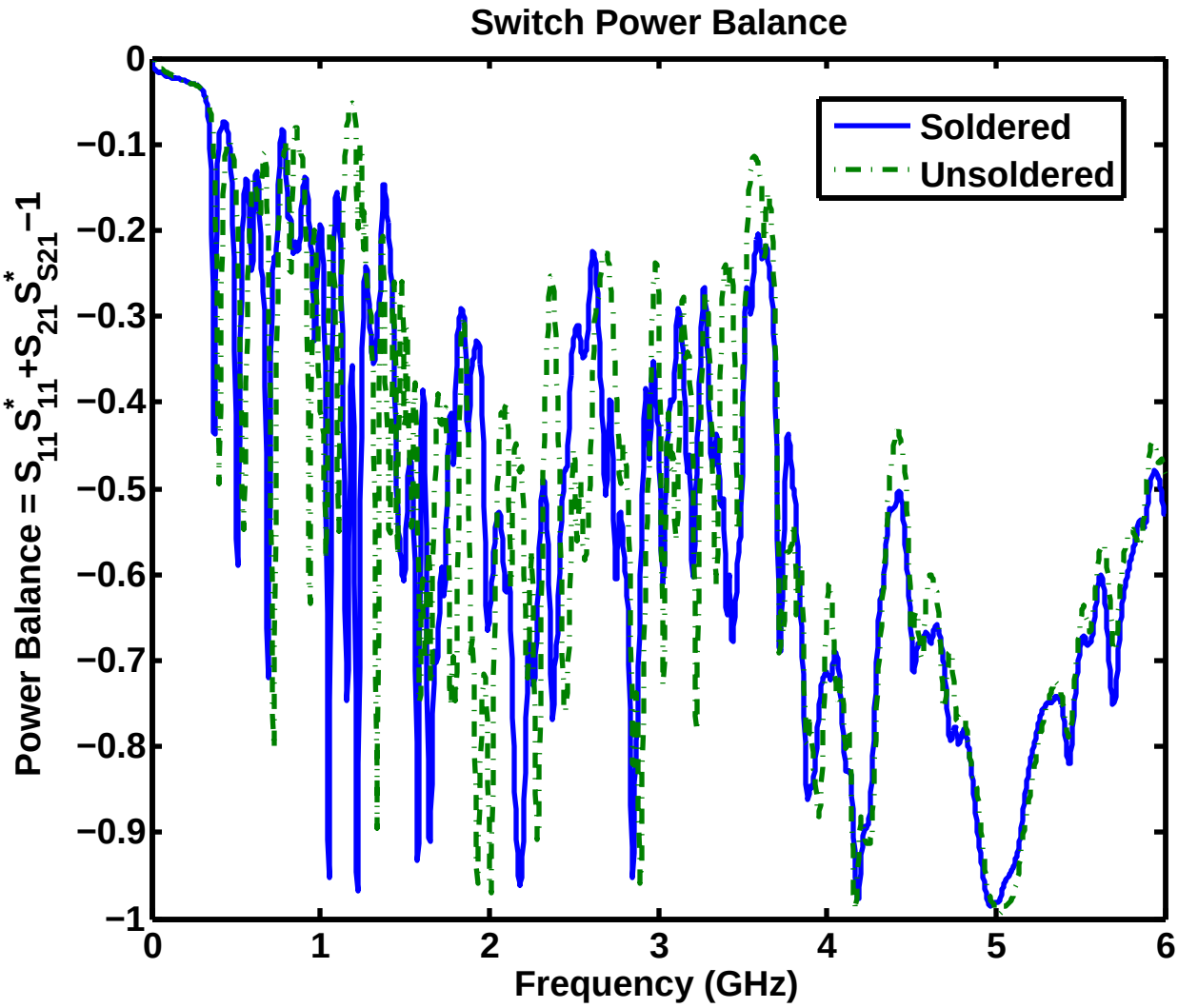

Figure 4.38 and with a limited frequency range of 700 MHz to 1.5 GHz in Figure 4.39. As can be seen in these figures, there seems to be no significant difference between having and not having the switches soldered to the shorting posts. This either means that power was not being lost through the switches or that power was coupling into the switches through the control wires and the other leg of the switch which had remained soldered to the top of the two-port.

To investigate further, the switches were completely removed (electrically) from the two-port. Control wires and most switches were disconnected from one another but remained on

Figure 4.38: Difference in power balance for between open state and unsoldered switches.

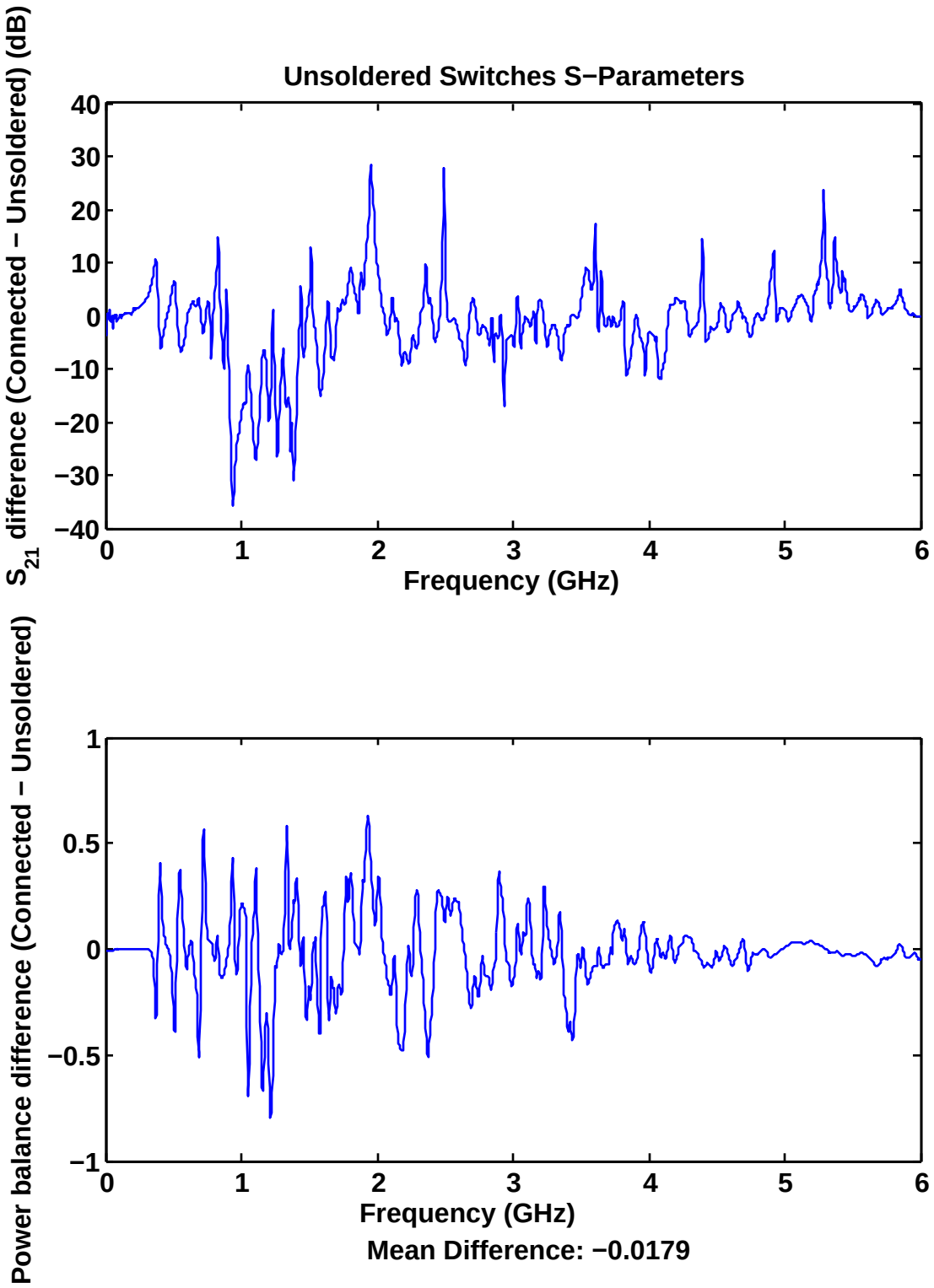

Figure 4.39: Limited frequency range for the difference in power balance for between open state and unsoldered switches.

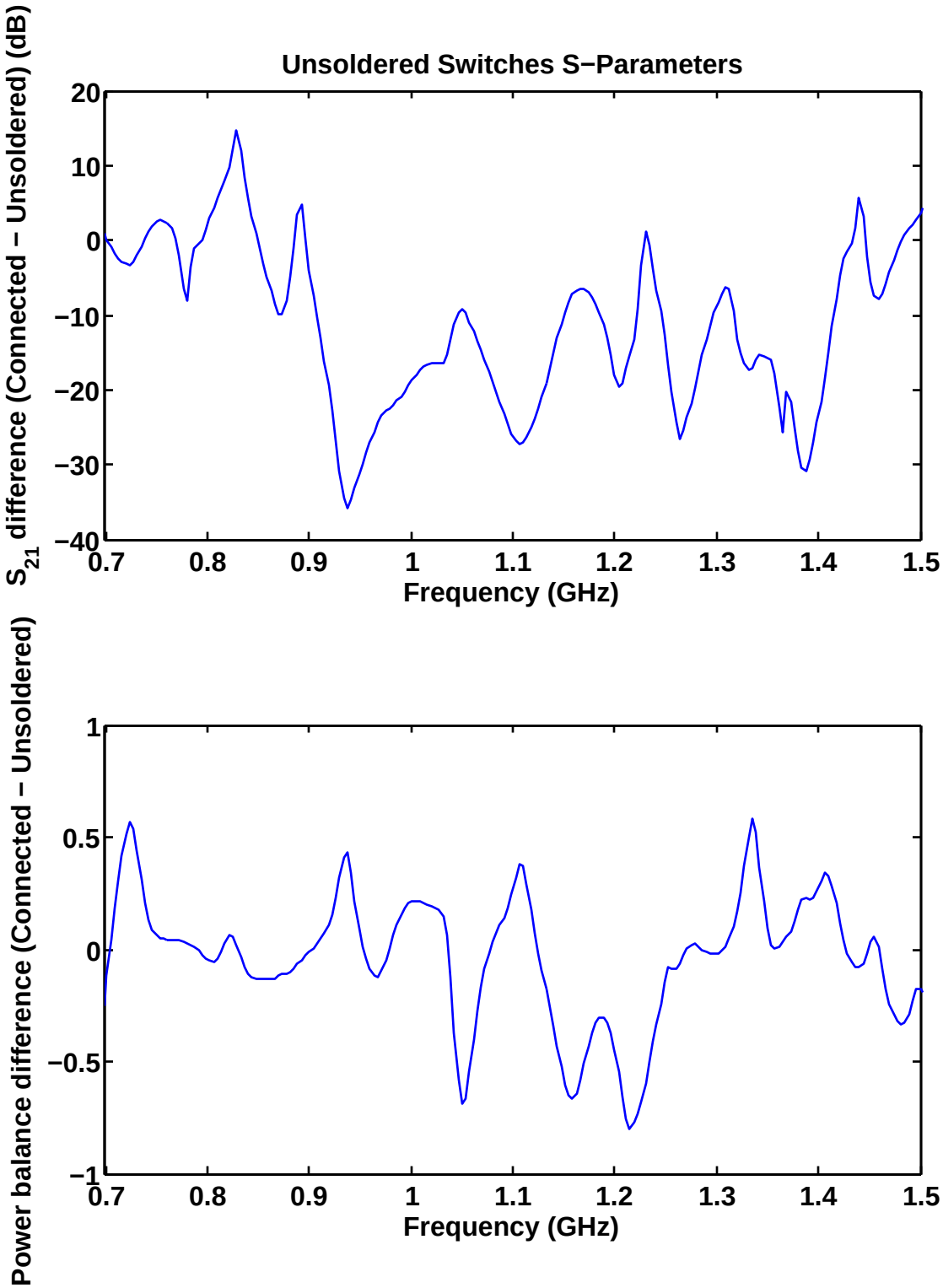

the board due to the potting used to secure them earlier in experiments. The S-parameters for this setup are shown in Figure 4.40 and the power balance for the network is shown in Figure 4.41. As is seen in the figure, there is still significant power loss even after the switches have been disconnected. This suggests that, while the switches may have been a sink for some power, the switches did not contribute significantly to the overall performance of the two port network.At this time, no one power loss mechanism has been identified as most significant. Instead, it is thought that a combination of various mechanisms leads to the high losses observed.

Figure 4.40: S-parameters with no switches connected to the two-port network.

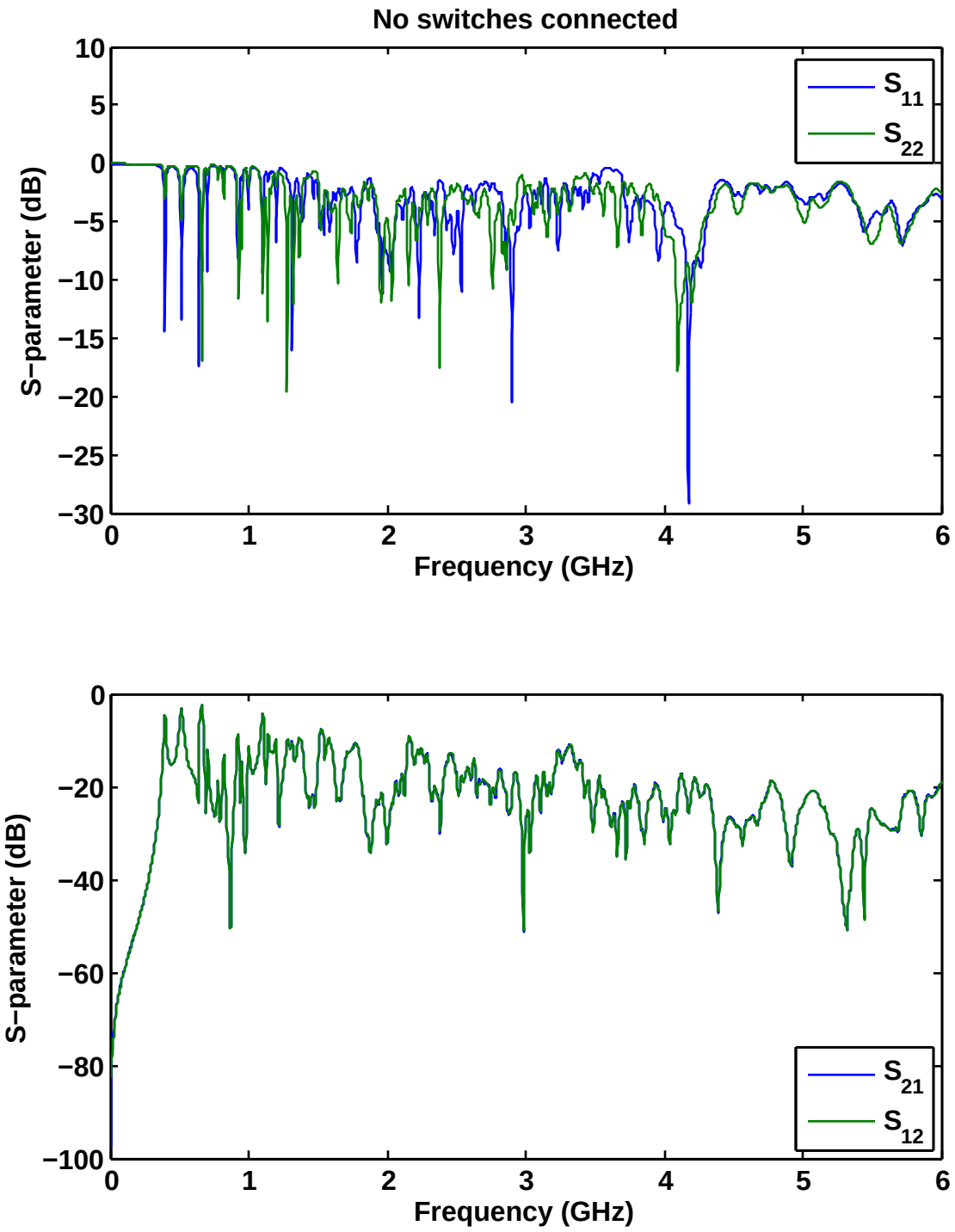

Figure 4.41: Power balance with no switches connected to the two-port network.

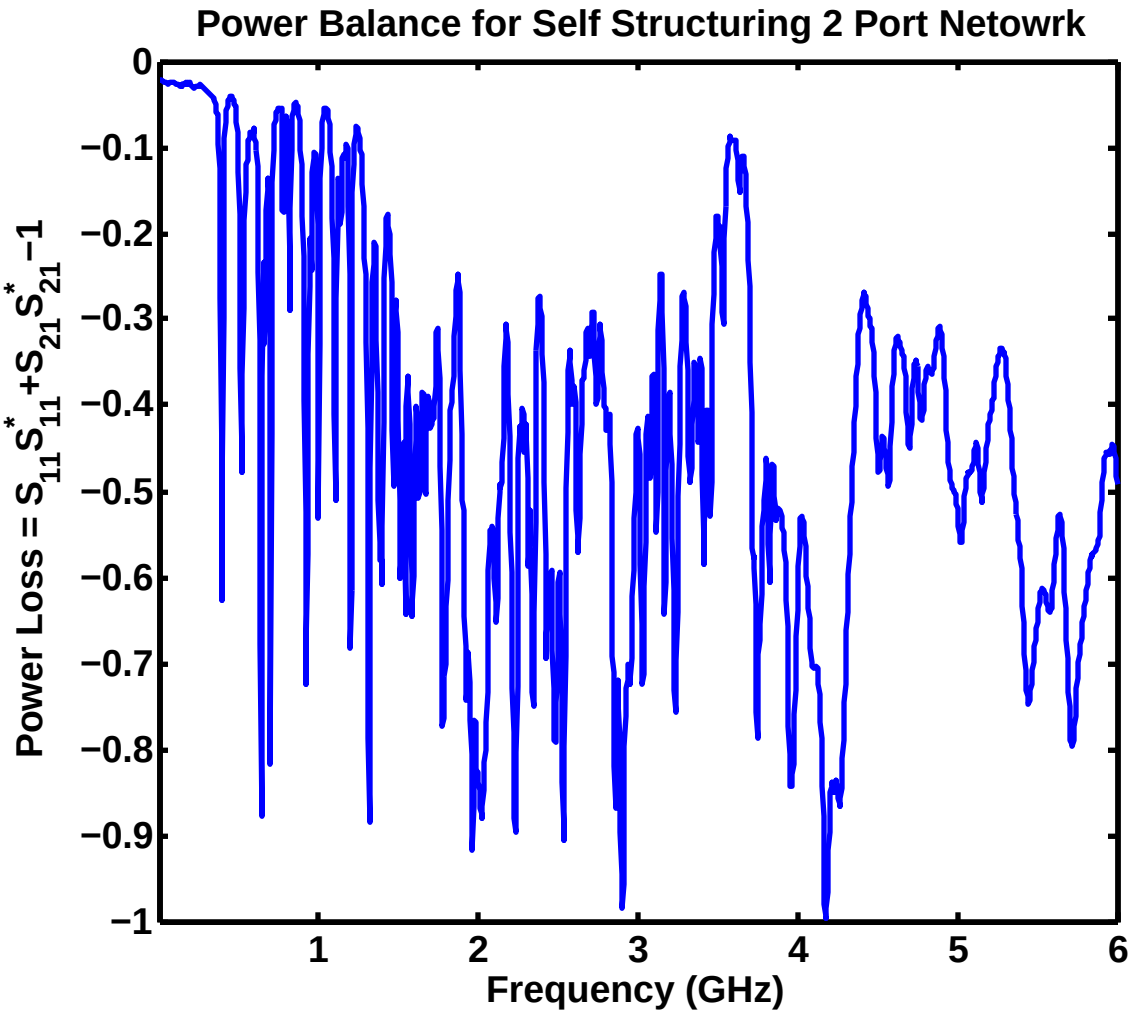

Chapter 5

Conclusion

5.1 Conclusion

This work has explored the capabilities of a self-structuring two-port network. A combination of simulations and experiments were carried out to characterize the network.

It was found that the constructed prototype exhibited significant loss of power. Research was undertaken to explore this topic further. While various loss mechanisms were identified, no one mechanism could be pinpointed as the most significant. Steps were taken in the experimental setup to mitigate the power lost with relatively little improvement.

Bearing in mind the lossy nature of the network, the capabilities of it were investigated using both random and genetic algorithm based searches. Results from the random search suggested that the lowest losses for the network are over the frequency range of approximately 750 MHz to 1.5 GHz. It was in this frequency range that most experiments were performed. Random search results suggested that switch combinations existed for matching various types of loads, given the insertion loss of the network. Results also pointed to the ability to vary the insertion loss to levels below that caused by power loss.

Using a genetic algorithm, select applications of the self-structuring two-port network were investigated. One such application was for the optimization of transmission through

the network. Accepting the system power loss, the network was fairly successful in matching arbitrary loads. The network was also used successfully to create an arbitrary attenuator with losses larger than normally observed in the network.

While the results obtained are promising, the actual performance of the manufactured two-port network is, overall, disappointing. Due to the high power loss observed in both simulations and in experiments, further research should be directed to creating a two-port network with lower losses. Doing so would allow for further exploration of this topic.

5.2 Contributions

This work has made various contributions to the scientific community. First, the work has been presented at the APS/URSI conference in 2009 and 2010 [64, 65]. It was also presented at the 2010 Graduate Academic Conference at Michigan State University [66]. and through numerous posters.

5.3 Topics and Suggestions for Future Study

After completing this work, it is the opinion of the author that the following items should be considered for, or when conducting, future work:

- Future investigations should consider using different connectors and control methods to reduce mechanical failures in experiments. If ribbon cables continued to be used, proper crimping tools should be purchased. Extreme care should always be exercised when connecting and disconnecting ribbon cables in order to extend their usable life.

- Any future prototype should consider redesigning how switches are connected to the control wires. Aspects of the design to be considered include switch orientation, methods of affixing the switch to the surface, methods of shorting the circuit under test, methods of connecting to the circuit under test, methods of connecting the control

wires to the switch pins, stress relief of control wires, and routing of the control wires. Designers should consider the harsh environment experienced in a laboratory setting including repeated stresses.

- The driver IC circuit should be updated to include a circuit that continually monitors and gives feedback on the condition of each output. An example of this is to have an LED that is one color when the output is within a given range to show that the switch is functioning; is another color in order to show that the output is staying high, i.e. the switch is not connected; and is a third color to show that there is a short in the control wires.

- When using SMA and N type connectors, a cal kit should be created from the Type N cal kit, HP 85032B, and the SMA cal kit, HP 85052D.

- Future investigations should consider using a substrate with different properties in an attempt to reduce the insertion loss.

- Future investigations should be considered that study how phase is effected by the network.

- Consideration should be given to constructing a self-structuring two-port network using MEMS techniques. This would considerably decrease the size of the network while hopefully decreasing losses.

- A very interesting potential application for a self-structuring two-port network is for power factor correction on the power grid. The power factor of a device is the ratio of the real power to the apparent power delivered to the device. The best performance is reached when the power factor is unity. For most consumers, the power factor of a device, or even their house, is not a major concern. For industrial customers the power factor is important. Often times such customers attempt to correct their power factor by installing what are essentially large capacitors or inductors.

Future research should consider creating a self-structuring two-port network capable of operating on the power grid.

- In the future a microstrip based self-structuring two-port network could be constructed. This may take the form of placing switches in a network of microstrip lines. These lines may be laid out out in a pattern similar to the templates used in early SSA's [1, 2].

Appendix

HP 85052D Economy Mechanical Calibration Kit, DC to 26.5 GHz, 3.5 mm

This appendix outlines procedures for editing and downloading the definitions for the HP 85052D Calibration Kit to the HP 8753D Network Analyer. This procedure is done using `VNA Cal Kit Manager` [61] and is written for version 2.10. The procedure can be adopted to define any calibration kit for the network analyzer such as a combined SMA and N type kit. Refer to the user manual of the cal kit [67] for more information and calibration tables.

1. Open `VNA Cal Kit Manager`
2. Open the 85053D calibration kit definition from the `Agilent_85052D.ckm` file found in the same directory as the VNA Cal Kit Manager program
   (default location: `C:/Program Files/VNA Cal Kit Manager 2/Agilent_85052D.ckm`)
3. Save the file under a new name: `File->Save As...`
4. Go to the `Standard Definitions` tab
5. In the `Standard Type` column of the table, select `none` for standards #5 through #8
6. Copy the entries for standards #9, #11, and #13 to standards #3 through #5

7. Select `none` for standards #9, #11, and #13
8. Select the `Class Assignments` tab
9. Select `8753D/E` from the `VNA` menu at the top of the program window
10. In Column A of the Class Assignments table, enter 2, 1, 3, 2, 1, 3, 5,5,5,5, 3, 3 for rows `S11A` through `Response & Isolation`
11. Under the `Cal Kit Properties` tab, enter a label for the calibration kit definition and update the description
12. After make sure the 8753D is turned on, select `Check GPIB` from the `GPIB` menu. A window saying `GPIB Check Passed` and `HEWLETT PACKARD,8573D,0,6.14` should be displayed. Click OK. If it is not, ensure that the GPIB interface between the computer and the analyzer is properly setup.
13. Select `Send Kit to VNA` from the `GPIB` menu. This can also be done using the button on the toolbar.
14. A success window should show up after transfering the cal kit to the VNA. Click OK
15. On the 8753D, select the `SAVE USER KIT` soft key
16. Press the `CAL` button on the front of the 8753D
17. Select `CAL KIT`
18. Select `SELECT CAL KIT`
19. Select `USER KIT`
20. Press the `CAL` button on the front of the 8753D
21. The Cal Kit Label entered in the definition should now be displayed under the `CAL KIT` soft key item

22. Calibrate using the standard procedures

Bibliography

Bibliography

[1] Coleman, C.M. and Rothwell, E.J. and Ross, J.E., "Self-structuring Antennas," in *Antennas and Propagation Society International Symposium, 2000. IEEE*, vol. 3, pp. 1256 –1259 vol.3, 2000.

[2] Coleman, C.M. and Rothwell, E.J. and Ross, J.E. and Nagy, L.L., "Self-structuring Antennas," *Antennas and Propagation Magazine, IEEE*, vol. 44, pp. 11 – 23, June 2002.

[3] Perry, B.T. and Coleman, C.M. and Basch, B.F. and Rothwell, E.J. and Ross, J.E., "Self-structuring Antenna for Television Reception," in *Antennas and Propagation Society International Symposium, 2001. IEEE*, vol. 1, pp. 162 –165 vol.1, 2001.

[4] Coleman, Christopher, *Self-Structuring Antennas*. Ph.d. dissertation, Michigan State University, May 2002.

[5] Perry, Bradley, *A Self-Structuring Antenna Prototype*. M.s. thesis, Michigan State University, August 2002.

[6] Coleman, C.M. and Rothwell, E.J. and Ross, J.E., "Investigation of Simulated Annealing, Ant-Colony Optimization, and Genetic Algorithms for Self-Structuring Antennas," *Antennas and Propagation, IEEE Transactions on*, vol. 52, pp. 1007 – 1014, April 2004.

[7] Yumei Guo and Yingzeng Yin and Huili Zheng and Jingli Guo, "Self-Structuring Antenna for Multi-Band Operation," in *Microwave, Antenna, Propagation and EMC Technologies for Wireless Communications, 2005. MAPE 2005. IEEE International Symposium on*, vol. 1, pp. 350 – 353 Vol. 1, August 2005.

[8] Jessberger, Joachim, *Investigation of the Near-Field Properties of the Self-Structuring Antenna*. M.s. thesis, Michigan State University and Studienarbeit, Kaiserslautern University, October 2005.

[9] Perry, B.T. and Rothwell, E.J. and Nagy, L.L., "Analysis of Switch Failures in a Self-Structuring Antenna System," *Antennas and Wireless Propagation Letters, IEEE*, vol. 4, pp. 68 – 70, 2005.

[10] Greetis, L.M. and Rothwell, E.J., "A Self-Structuring Patch Antenna," in *Antennas and Propagation Society International Symposium, 2008. AP-S 2008. IEEE*, pp. 1 –4, July 2008.

[11] Greetis, Lynn, *A Self-Structuring Patch Antenna*. M.s. thesis, Michigan State University, May 2008.

[12] Ouedraogo, R.O. and Rothwell, E.J., "Self-Tuning Cavity Resonator," in *Antennas and Propagation Society International Symposium, 2008. AP-S 2008. IEEE*, pp. 1 –4, July 2008.

[13] Ouedraogo, Raoul Ouatagom, Jr., *A Self Tuning Electromagnetic Shutter*. M.s. thesis, Michigan State University, August 2008.

[14] Greetis, L. and Ouedraogo, R. and Greetis, B. and Rothwell, E.J., "A Self-Structuring Patch Antenna: Simulation and Prototype," *Antennas and Propagation Magazine, IEEE*, vol. 52, pp. 114 –123, February 2010.

[15] Ouedraogo, R.O. and Rothwell, E.J. and Shih-Yuan Chen and Greetis, B.J., "An Automatically Tunable Cavity Resonator System," *Microwave Theory and Techniques, IEEE Transactions on*, vol. 58, pp. 894 –902, April 2010.

[16] Ouedraogo, R.O. and Rothwell, E.J. and Shih-Yuan Chen and Temme, A., "A Self-Tuning Electromagnetic Shutter," *Antennas and Propagation, IEEE Transactions on*, vol. 59, pp. 513 –519, February 2011.

[17] Songnan Yang and Chunna Zhang and Helen Pan and Fathy, A. and Nair, V., "Frequency-Reconfigurable Antennas for Multiradio Wireless Platforms," *Microwave Magazine, IEEE*, vol. 10, pp. 66 –83, February 2009.

[18] Schaubert, D. and Farrar, F. and Sindoris, A. and Hayes, S., "Microstrip antennas with frequency agility and polarization diversity," *Antennas and Propagation, IEEE Transactions on*, vol. 29, pp. 118 – 123, January 1981.

[19] Lan, G. and Sengupta, D.L., "Frequency Agile Circular Microstrip Antennas," in *Microwave Symposium Digest, 1985 IEEE MTT-S International*, pp. 693 –695, June 1985.

[20] Chakravarty, T. and De, A., "Design of Tunable Modes and Dual-band Circular Patch Antenna Using Shorting Posts," *Microwaves, Antennas and Propagation, IEE Proceedings*, vol. 146, pp. 224 –228, June 1999.

[21] Bonefacic, D. and Bartolic, J. and Germ, M., "Shorted Patch Antenna with PIN Diode Operating Band Switching," in *Microwave Conference, 2006. 36th European*, pp. 862 –865, September 2006.

[22] Zhong, S.S. and Lo, Y.T., "Single-element Rectangular Microstrip Antenna for Dual-Frequency Operation," *Electronics Letters*, vol. 19, pp. 298 –300, April 1983.

[23] Bao Wang and Yuen Lo, "Microstrip Antennas for Dual-Frequency Operation," *Antennas and Propagation, IEEE Transactions on*, vol. 32, pp. 938 – 943, September 1984.

[24] Waterhouse, R., "Small Microstrip Patch Antenna," *Electronics Letters*, vol. 31, pp. 604 –605, April 1995.

[25] Waterhouse, R.B. and Targonski, S.D. and Kokotoff, D.M., "Design and Performance of Small Printed Antennas," *Antennas and Propagation, IEEE Transactions on*, vol. 46, pp. 1629 –1633, November 1998.

[26] Kan, H.K. and Waterhouse, R.B., "A Small Printed Antenna for Wireless Communication Handset Terminals," in *Microwave Conference, 2000 Asia-Pacific*, pp. 723 –726, December 2000.

[27] Shackelford, A.K. and Sang-Yick Leong and Kai-Fong Lee, "Simulation of a Probe-fed Notched Patch Antenna with a Shorting Post," in *Antennas and Propagation Society International Symposium, 2001. IEEE*, vol. 2, pp. 708 –711, July 2001.

[28] Kan, H.K. and Waterhouse, R.B. and Lee, A.Y.J. and Pavlickovski, D., "Variations of the Shorted Patch Antenna," in *Antennas and Propagation Society International Symposium, 2005 IEEE*, vol. 2B, pp. 230 – 233, July 2005.

[29] Zavosh, F. and Aberle, J.T., "Improving the Performance of Microstrip-patch Antennas," *Antennas and Propagation Magazine, IEEE*, vol. 38, pp. 7 –12, August 1996.

[30] Jun Zhao and Raman, S., "Design of "chip-scale" patch antennas for 5-6 GHz wireless microsystems," in *Antennas and Propagation Society International Symposium, 2001. IEEE*, vol. 2, pp. 6 –9, July 2001.

[31] Shaojun Fang and Jun Zheng and Xiuzhen Luan, "A Novel Multi Arc Slot Antenna for WLAN Applications," in *Antenna Technology: Small Antennas and Novel Metamaterials, 2005. IWAT 2005. IEEE International Workshop on*, pp. 209 – 212, March 2005.

[32] Hunter, I.C. and Rhodes, J.D., "Electronically Tunable Microwave Bandpass Filters," *Microwave Theory and Techniques, IEEE Transactions on*, vol. 30, pp. 1354 –1360, September 1982.

[33] Casini, F. and Gatti, R.V. and Perrone, V. and Sorrentino, R., "A New Approach to the Analysis and Synthesis of Lossy Reconfigurable Matching Networks," in *Microwave Conference, 2009. EuMC 2009. European*, pp. 1235 –1238, October 2009.

[34] Qin Shen and Barker, N.S., "Distributed MEMS Tunable Matching Network using Minimal-Contact RF-MEMS Varactors," *Microwave Theory and Techniques, IEEE Transactions on*, vol. 54, pp. 2646 –2658, June 2006.

[35] Unlu, M. and Topalli, K. and Atasoy, H.I. and Temocin, E.U. and Istanbulluoglu, I. and Bayraktar, O. and Demir, S. and Civi, O.A. and Koc, S. and Akin, T., "A Reconfigurable RF MEMS Triple Stub Impedance Matching Network," in *Microwave Conference, 2006. 36th European*, pp. 1370 –1373, September 2006.

[36] Vaha-Heikkila, T. and Rebeiz, G.M., "A 20-50 GHz Reconfigurable Matching Network for Power Amplifier Applications," in *Microwave Symposium Digest, 2004 IEEE MTT-S International*, vol. 2, pp. 717 – 720 Vol.2, June 2004.

[37] Vähä-Heikkilä, Tauno and Rebeiz, Gabriel M., "A 4–18-GHz Reconfigurable RF MEMS Matching Network for Power Amplifier Applications," *International Journal of RF and Microwave Computer-Aided Engineering*, vol. 14, no. 4, pp. 356–372, 2004.

[38] Domingue, F. and Fouladi, S. and Mansour, R.R., "A Reconfigurable impedance Matching Network Using Dual-Beam MEMS Switches for an Extended Operating Frequency Range," in *Microwave Symposium Digest (MTT), 2010 IEEE MTT-S International*, pp. 1552 –1555, May 2010.

[39] Domingue, F. and Fouladi, S. and Kouki, A.B. and Mansour, R.R., "Design Methodology and Optimization of Distributed MEMS Matching Networks for Low-Microwave-Frequency Applications," *Microwave Theory and Techniques, IEEE Transactions on*, vol. 57, pp. 3030 –3041, December 2009.

[40] Karim, MF. and Ai-Qun Liu and Alphones, A. and Aibin Yu, "A Reconfigurable Micromachined Switching Filter Using Periodic Structures," *Microwave Theory and Techniques, IEEE Transactions on*, vol. 55, pp. 1154 –1162, June 2007.

[41] Q. Shen and N. Barker, "Reconfigurable Matching with a 10-30 GHz Distributed RF-MEMS Tuner," in *Microwave Conference Proceedings, 2005. APMC 2005. Asia-Pacific Conference Proceedings*, vol. 4, p. 4 pp., December 2005.

[42] Fouladi, S. and Akhavan, A. and Mansour, R.R., "A Novel Reconfigurable Impedance Matching Network Using DGS and MEMS Switches for Millimeter-Wave Applications," in *Microwave Symposium Digest, 2008 IEEE MTT-S International*, pp. 145 –148, June 2008.

[43] Domingue, F. and Fouladi, S. and Mansour, R. R., "A Reconfigurable impedance Matching Network Using Dual-Beam MEMS Switches for an Extended Operating Frequency Range," in *Microwave Symposium Digest (MTT), 2010 IEEE MTT-S International*, p. 1, May 2010.

[44] Yumin Lu and Peroulis, D. and Mohammadi, S. and Katehi, L.P.B., "A MEMS reconfigurable matching network for a class AB amplifier," *Microwave and Wireless Components Letters, IEEE*, vol. 13, pp. 437 – 439, October 2003.

[45] Draskovic, D. and Budimir, D., "Optically Reconfigurable Matching Networks," in *Microwave Photonics, 2008. Jointly held with the 2008 Asia-Pacific Microwave Photonics Conference. MWP/APMP 2008. International Topicsl Meeting on*, pp. 135 –137, October 2008.

[46] Draskovic, D. and Christodoulou, C. and Budimir, D., "Optically Reconfigurable RF circuits," in *Antennas and Propagation (EuCAP), 2010 Proceedings of the Fourth European Conference on*, pp. 1 –3, April 2010.

[47] Malmqvist, R. and Samuelsson, C. and Rantakari, P. and Vaha-Heikkila, T. and Smith, D. and Varis, J. and Baggen, R., "RF MEMS and MMIC Based Reconfigurable Matching Networks for Adaptive Multi-Band RF Front-Ends," in *RF Front-ends for Software Defined and Cognitive Radio Solutions (IMWS), 2010 IEEE International Microwave Workshop Series on*, pp. 1 –4, February 2010.

[48] Hong, J.S. and Lancaster, M.J., "Microstrip Bandpass Filter Using Degenerate Modes of a Novel Meander Loop Resonator," *Microwave and Guided Wave Letters, IEEE*, vol. 5, pp. 371 –372, November 1995.

[49] Abbaspour-Tamijani, A. and Dussopt, L. and Rebeiz, G.M., "Miniature and tunable filters using MEMS capacitors," *Microwave Theory and Techniques, IEEE Transactions on*, vol. 51, pp. 1878 – 1885, July 2003.

[50] Cen Ong and Okoniewski, M., "MEMS-Switchable Coupled Resonator Microwave Bandpass Filters," *Microwave Theory and Techniques, IEEE Transactions on*, vol. 56, pp. 1747 –1755, July 2008.

[51] Peng Wen Wong and Hunter, I.C., "A New Class of Low-Loss High-Linearity Electronically Reconfigurable Microwave Filter," *Microwave Theory and Techniques, IEEE Transactions on*, vol. 56, pp. 1945 –1953, August 2008.

[52] Perruisseau-Carrier, Julien and Pardo-Carrera, Pablo, "Recent Developments on Reconfigurable Band-Filtering Antennas," in *Antennas and Propagation (EuCAP), 2010 Proceedings of the Fourth European Conference on*, pp. 1 –4, April 2010.

[53] Xiaoguang Liu and Katehi, L.P.B. and Chappell, W.J. and Peroulis, D., "High-Q Tunable Microwave Cavity Resonators and Filters Using SOI-Based RF MEMS Tuners," *Microelectromechanical Systems, Journal of*, vol. 19, pp. 774 –784, August 2010.

[54] Karim, M.F. and Liu, A.Q. and Alphones, A. and Yu, A.B., "A Novel Reconfigurable Filter Using Periodic Structures," in *Microwave Symposium Digest, 2006. IEEE MTT-S International*, pp. 943 –946, June 2006.

[55] Yi-Ming Chen and Sheng-Fuh Chang and Cheng-Yu Chou and Kun-Hsing Liu, "A Reconfigurable Bandpass-Bandstop Filter Based on Varactor-Loaded Closed-Ring Resonators [Technical Committee]," *Microwave Magazine, IEEE*, vol. 10, pp. 138 –140, February 2009.

[56] Naglich, E.J. and Juseop Lee and Peroulis, D. and Chappell, W.J., "A Tunable Bandpass-to-Bandstop Reconfigurable Filter With Independent Bandwidths and Tunable Response Shape," *Microwave Theory and Techniques, IEEE Transactions on*, vol. 58, pp. 3770 –3779, December 2010.

[57] Ramo, Simon and Whinnery, John R. and Van Duzer, Theodore, *Fields and Waves in Communication Electronics*. John Wiley and Sons, Inc., 3^{rd} ed., 1994.

[58] EM Software & Systems-S.A. (Pty) Ltd., "FEKO - EM Simulation Software." http://www.feko.info/.

[59] Jack Ross and Associates, LLC., "GA-Suite." http://www.johnross.com/gasuite.html.

[60] Coto Technology, "9011, 9012 & 9117 Miniature SIP Relays." http://www.cotorelay.com/9011__9012___9117.pdf.

[61] Barry Brown and Agilent, "VNA Help - Microwave Network Analyzer Measurement Information." http://na.tm.agilent.com/vnahelp/.

[62] National Instruments, "NI LabView." http://www.ni.com/labview/.

[63] Randy L. Haupt and Sue Ellen Haupt, *Practical Genetic Algorithms*. New York : Wiley, Second Ed. ed., 2004.

[64] Andrew Temme and Chien-Hsien Lee and Raoul Ouedraogo and Shih-Yuan Chen and Brian J. Greetis and Edward J. Rothwell, "A Self-Structuring 2-Port Network," *2009 USNC/URSI National Radio Science Meeting*, June 2009.

[65] Andrew K. Temme and Edward J. Rothwell, "Optimization of a Self-Structuring Two-Port Network for Use as a Wideband RF Matching Network," *2010 USNC/URSI National Radio Science Meeting*, July 2010.

[66] Andrew K. Temme, "A Self-Structuring Two-Port Network," *2010 Graduate Academic Conference Michigan State University*, March 2010.

[67] Agilent, "Agilent Technologies 85052D 3.5mm Economy Calibration Kit." User's and Service Guide, September 2007.